UNIVERSITY OF CALIFORNIA
SANTA CRUZ

OPTIMAL ELECTRICAL ENERGY SLEWING FOR REACTION WHEEL SPACECRAFT

A dissertation submitted in partial satisfaction of the
requirements for the degree of

DOCTOR OF PHILOSOPHY

in

APPLIED MATHEMATICS & STATISTICS

by

Harleigh Christian Marsh

March 2018

The Dissertation of Harleigh Christian Marsh is approved:

Professor Qi Gong, Chair

Professor Mark Karpekno

Professor Hongyun Wang

Professor Daniele Venturi

Tyrus Miller
Vice Provost and Dean of Graduate Studies

Table of Contents

List of Figures

List of Tables

Abstract

Optimal Electrical Energy Slewing for Reaction Wheel Spacecraft

by

Harleigh Christian Marsh

The results contained in this dissertation contribute to a deeper level of understanding to the energy required to slew a spacecraft using reaction wheels. This work addresses the fundamental manner in which spacecrafts are slewed (eigenaxis maneuvering), and demonstrates that this conventional maneuver can be dramatically improved upon in regards to reduction of energy, dissipative losses, as well as peak power.

Energy is a fundamental resource that effects every asset, system, and subsystem upon a spacecraft, from the attitude control system which orients the spacecraft, to the communication subsystem to link with ground stations, to the payloads which collect scientific data. For a reaction wheel spacecraft, the attitude control system is a particularly heavy load on the power and energy resources on a spacecraft. The central focus of this dissertation is reducing the burden which the attitude control system places upon the spacecraft in regards to *electrical energy*, which is shown in this dissertation to be a challenging problem to computationally solve and analyze.

Reducing power and energy demands can have a multitude of benefits, spanning from the initial design phase, to in-flight operations, to potentially extending the mission life of the spacecraft. This goal is approached from a practical standpoint apropos to an industry-flight setting. Metrics to measure electrical energy and power are developed which are in-line with the cost associated to operating reaction wheel based attitude control systems. These metrics are incorporated

into multiple families of practical high-dimensional constrained nonlinear optimal control problems to reduce the electrical energy, as well as the instantaneous power burdens imposed by the attitude control system upon the spacecraft. Minimizing electrical energy is shown to be a problem in L^1 optimal control which is nonsmooth in regards to state variables as well as the control. To overcome the challenge of nonsmoothness, a method is adopted in this dissertation to transform the nonsmooth minimum electrical energy problem into an equivalent smooth formulation, which then allows standard techniques in optimal control to solve and analyze the problem.

Through numerically solving families of optimal control problems, the relationship between electrical energy and transfer time is identified and explored for both off-and on-eigenaxis maneuvering, under minimum dissipative losses as well as under minimum electrical energy. A trade space between on-and off-eigenaxis maneuvering is identified, from which is shown that agile near time optimal maneuvers exist within the energy budget associated with conventional eigenaxis maneuvering. Moreover, even for conventional eigenaxis maneuvering, energy requirements can be dramatically reduced by maneuvering off-eigenaxis. These results address one of the fundamental assumptions in the field of optimal path design verses conventional maneuver design.

Two practical flight situations are addressed in this dissertation in regards to reducing energy and power: The case when the attitude of the spacecraft is predetermined, and the case where reaction wheels can not be directly controlled. For the setting where the attitude of spacecraft is on a predefined trajectory, it is demonstrated that reduced energy maneuvers are only attainable though the application of null-motions, which requires control of the reaction wheels. A computationally light formulation is developed minimizing the dissipative losses

through the application of null motions. In the situation where the reaction wheels can not be directly controlled, it is demonstrated that energy consumption, dissipative losses, and peak-power loads, of the reaction-wheel array can each be reduced substantially by controlling the input to the attitude control system through attitude steering. It is demonstrated that the open loop trajectories correctly predict the closed loop response when tracked by an attitude control system which does not allow direct command of the reaction wheels.

This simple body of work is dedicated to God, who Is Love, and to my wife Joanna Ruth Marsh whom I love.

Acknowledgments

"To learn one must be humble.
But life is the great teacher."

James Joyce
Ulysses

Truly I could not be here today without the support of those about me. I am thankful to have the opportunity to be able to acknowledge the following; to be able to say how much you have influenced my life in a positive manner, and to acknowledge that I have received so much from so many. It is an ardent hope that I will be able encourage and support like what I have received.

Thank you God, for all is by Your Grace. Your Hands have shaped this clay, and I am so thankful for this day which You made.

Thank you my dear wife, you truly lift me Up and humble me ever so: I am so thankful, ever so thankful to God and you, to be on this Journey with you!

Thank you ma! Being a single mom couldn't, and certainly was not easy. I couldn't be here without all of your support. Ya done good!

Academically, many have given me the motivation, support and guidance to reach this stage: First and foremost are professors Qi Gong and Mark Karpenko, the results of this work are truly through the help and positive reinforcement from you both; Michael Ross from the Naval Postgraduate School in Monterey California. Professors from Modesto Junior College pivotal to the start of this journey; notable mentions are: Dr. Xiang-Dong Ye of the mathematics department, Mr. Brian Larson of the computer science department, and Dr. Joseph Monast of the philosophy department. Professors in the Mathematics Department the University of California Polytechnic University, San Luis Obispo; notable mentions: Dr. Shapiro, Dr. Mark Stankus, and Dr. Anton Kaul. The Applied Mathematics and Statistics department at the University of California, Santa Cruz: For being such an excellent and supportive department, fostering both academics and social health (e.g. morning bagels and coffee): To David Draper, giving that thoughtful advice of patience and stamina: "Harleigh, a PhD is a marathon, not a sprint".

And, those I have the honor of knowing as my friends-like-family: James Skorupski, Jeffrey Bergamini, Ryan Panos, William Taylor, Michael Roberts, Garrett Grohl, and Chris Phelps.

Chapter 1

Introduction

"No problem can withstand the assault of sustained thinking."

Voltaire

A significant effort has been made, in attitude control, regarding minimizing the transfer time to perform a slew using reaction wheels. A culmination of such research was the first ever flight implementation of a set of time-optimal (reaction wheel) slews, which were performed upon NASA's Transition Region And Coronal Explorer (TRACE) spacecraft.[1,5,6] Minimizing the transfer time of a slew is efficacious under a number of goals (e.g. faster slews, hence more imaging, therefore more utility of the imaging satellite, thereby reducing the monetary cost associated to imaging[7]). Minimum-time slews are synonymous with off-eigenaxis maneuvers, because a well known fact to the attitude control community is that eigenaxis maneuvers are not time optimal. It is through the means of off-eigenaxis maneuvering which allows the angular velocities of all three body axes to be built simultaneously, which thereby maximizes the agility of a spacecraft. While reducing transfer time through maximizing the agility of the spacecraft is clearly important, *power* as well as *energy* play equally important role. Conventional wisdom associates minimum time slews with large effort. What if the batteries

are depleted upon the spacecraft? What happens to the spacecraft when electrical power decreases and demand exceeds supply? In such a case power loads (e.g. scientific instruments) must be shut off one-by-one, as seen with Voyager I.[8–10] In comparison to the body of literature associated to agility, comparatively little has been done with regards to minimum energy slewing. It is partially due to the fact that the minimum energy problem is a challenging nonsmooth and nonlinear optimal control problem. This dissertation is aimed at attaining and understanding minimum energy maneuvers for reaction wheel spacecraft under a variety of operational scenario apropos to an industry-strength flight setting.

The rest of the introduction is organized as follows: Section 1.1 briefly presents background information most-relevant to this dissertation. The focus of this dissertation, its aims, and its goals (along with motivation to these goals) are presented in Section 1.2. In the subsequent section that follows, the organization of the dissertation is outlined, and a brief synopsis for each chapter is provided which includes a small note concerning how each chapter meets the aims and goals of this dissertation. Section 1.4 outlines the results obtained by, and contributions from, this dissertation.

1.1 Background Information

As the focus of this dissertation is upon the attitude control of a spacecraft, this section serves to briefly outline various basics of attitude control in relation to spacecraft. This section begins with a brief and general introduction to attitude control in relation to spacecraft and next defines eigenaxis and off-eigenaxis slewing-strategies.

1.1.1 Introduction to Attitude Control

The *attitude* of an object, such as a missile, plane, crane, spacecraft or sensor upon a spacecraft, describes the *orientation* of the object relative to some reference frame. Attitude control, referrers to controlling the orientation of a spacecraft through some from of actuator. The (sub)system upon a spacecraft, whose primary purpose is to orient (i.e. point) a payload (e.g. sensor) to a desired location, is the Attitude Control System (ACS). Common reasons to reorient the spacecraft include primary mission objective of scientific data collection, such as orienting a sensor to a point of interest, as well as *housekeeping* duties required to keep the mission active. Examples of such housekeeping duties the ACS performs include such objectives as orienting solar panels at the sun to generate electrical power, aiming its communication antennas to download and upload to and from a ground station, as well as pointing thermal radiators to the non sun-side to allow heat to dissipate off of the spacecraft.[11] Slew is a very common term in the vernacular of the attitude control field: "Slewing a spacecraft", or "To *slew* a spacecraft" referrers to altering the attitude of a spacecraft by application of torque (be it internal or external). A common slew maneuver is one where the spacecraft begins and ends at rest, and such maneuver is referred to as a rest-to-rest maneuver (or rest-to-rest slew).

Methods for controlling the attitude of a spacecraft, while numerous, may be categorized as either *passive* or *active*. Passive methods, which are also known as environmental methods, use external environmental torques such as gravity gradient, solar radiation, atmospheric or magnetic to modify the orientation of the spacecraft.[12] These methods do not require any fuel nor energy source. Concerns of passive methods include: *i*) These passive methods typically can not grantee three-axis stabilization; *ii*) Pointing accuracy of passive methods is limited, when

compared to non-passive methods; *iii*) Passive methods, by their very nature, can only be used where the environmental torque exits. For example, because magnetorquers are reliant on an external magnetic field, they may only be applied in Low Earth Orbit (LEO). Similarly, atmospheric torques may only be utilized while in LEO,[12] and the use of atmospheric torques speeds up the decay of the spacecraft's orbit.

Active methods can guarantee three axis stabilization, and may be categorized into *external torque* propellant consuming thrusters and *internal torque* momentum exchange devices (MEDs) which consume electrical power (so named as these actuators exchange the angular momentum between themselves and the spacecraft). Thrusters consume a non-renewable fuel source, whereas MEDs consume a renewable source of energy due to the advent of solar panels which are capable of generating electrical energy. Two commonly utilized MEDs are Reaction Wheels (RWs) and Control Moment Gyros (CMGs). Both RWs and CMGs rely on the conservation of angular momentum and operate based on the principal of Newton's third law to perform attitude control; both are able to achieve very accurate pointing, and both require momentum dumping in order to avoid saturation. Reaction wheels spin about a fixed axis and exert a torque upon the spacecraft by changing the angular velocity of the reaction wheel (hence changing the angular momentum, hence torque). Generally, at least three reaction wheels are required to be able to orient to any location. If a spacecraft uses four or more reaction wheels to perform a slew, the spacecraft is said to have a "*redundant*" number of reaction wheels. It is quite common that four or more reaction wheels are mounted in the reaction wheel array. The reason for this redundancy is that if one wheel fails, arbitrary pointing in three-space is still feasible. CMGs, while not the a focus of this work, differ from reaction wheels in that a CMG spins at

a constant speed, and the change in angular momentum (i.e. torques) is achieved by rotating its spin axis (an operation known as "gimbaling"). This dissertation focuses on the attitude control of a spacecraft equipped with a redundant number of reaction wheels. Another system, whose primary purpose is to dump accumulated momentum is known as the Momentum Management System (as external torques always exist, and these external torques are absorbed by the MEDs, and hence over time the accumulated momentum in the MEDs need to be purged–this process is called momentum dumping).

1.1.2 Slewing A Spacecraft: Canonical & State of the Art Slewing

This section briefly presents two slewing strategies which are studied throughout this dissertation. One specific manner of slewing a spacecraft has the distinction of being known as the industry standard and is used onboard current spacecraft.[1] This canonical method of slewing is called an *eigenaxis* maneuver (EAM). An eigenaxis maneuver is when all of the rotational motion of the spacecraft is constrained about an axis which is fixed to both the spacecraft and inertial frame throughout the entire duration of the slew. During an EAM, the boresight (i.e. the sensor of interest–think of the center of the optical viewfinder to a camera) traces the shortest angular path between the two orientations, resulting with the shortest circular arc connecting the two orientations. Figure 1.1 shows an EAM for a 90 degree rotation about the spacecraft z-axis; the boresight is seen to trace the shortest circular arc between the initial and final orientation.

Shortest-time maneuvers, recently spanning out from theory and into application by being implemented in flight,[1,5,6] are time-optimal attitude maneuvers based on optimal control theory. Characterized by building up the body-rates

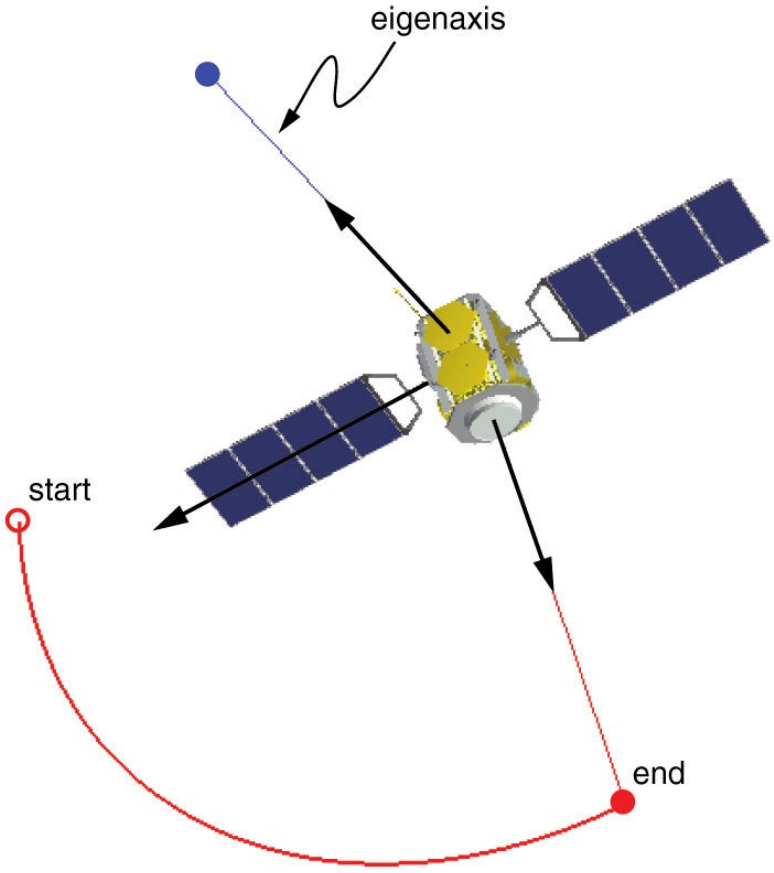

Figure 1.1: 90 degree conventional eigenaxis slew.[1]

of all three spacecraft body axes simultaneously, STMs maximize the agility of a spacecraft by taking full-advantage of the inertia ellipsoid, nonlinear rotational dynamics, and the operational constraints imposed upon the nonlinear rotational dynamics. Figure 1.2 shows a typical for a 90 degree rotation about the spacecraft z-axis; off-eigenaxis maneuvers (the z-axis is the eigenaxis for this maneuver) are seen by the trace of the boresight deviating from the shortest circular arc seen in Figure 1.1. Contrary to intuition, a shorter transfer time is obtained by traveling a longer path! This result is similar to the counterintuitive solution to the Brachistochrone problem, where the shortest path (a straight line) is not the time optimal solution.[13]

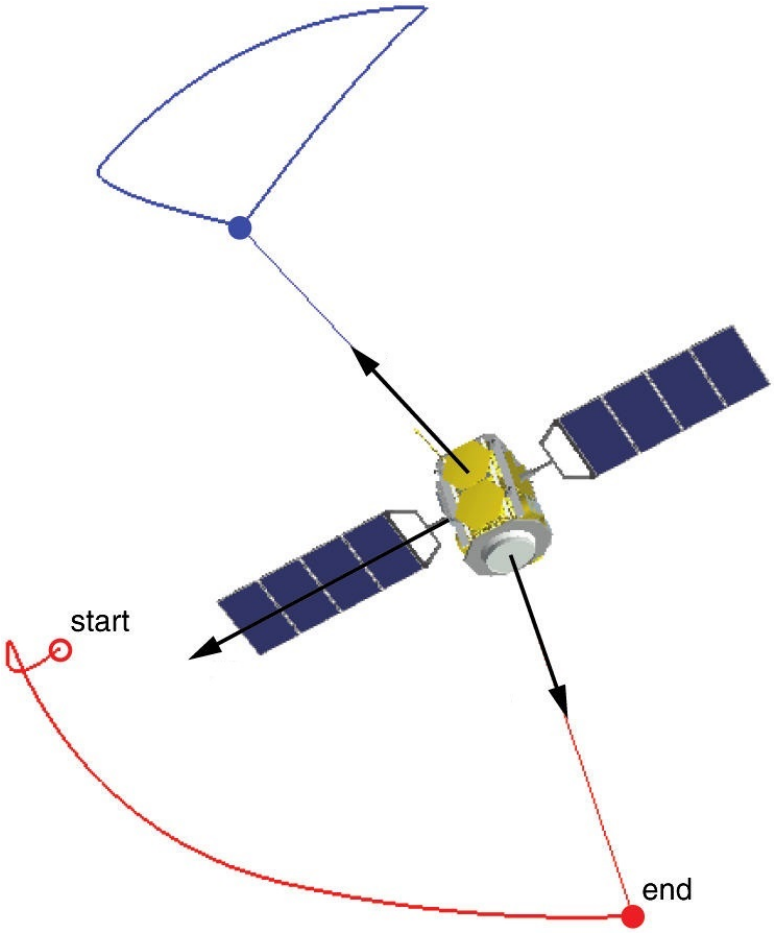

Figure 1.2: Off-eigenaxis shortest time maneuver of a 90 degree maneuver.[1]

1.2 Dissertation Aims, Motivation, and Focus

As mentioned in the previous section, eigenaxis maneuvering, which is the industry standard to slewing a spacecraft,[1] is not time optimal.[14] Rather, it was through off-eigenaxis maneuvering that transfer time could be reduced. The initial motivational idea that started the research process, was to follow these results between off-and on-eigenaxis maneuvering concerning transfer time, but in regards to "energy": Could energy be saved by maneuvering off eigenaxis, just as time is saved by off-eigenaxis maneuvering? Does constraining a spacecraft to maneuver only about an eigenaxis severely increase energy consumption? What

(in regards to energy) of the entire band of transfer times in-between time optimal shortest-time maneuvering and not time optimal eigenaxis maneuvering? The preceding questions gave the underlying aim and initial focus of this dissertation, and the foundation which all content of this body is connected: The minimization of energy required to slew a *reaction wheel* spacecraft. The means unto which the optimized trajectories (w.r.t. minimum energy) are obtained, is through the use of computational methods from the field of optimal control.

Another aim which arches across this entire body of work is to be as close as possible to an operational (e.g. flight) scenario. Therefore, operational requirements which arise in a practical scenario, are considered in this dissertation. The first practical concern is obtaining an energy metric that is in line with the operation of a reaction wheel attitude control system. Since the actuator performing the attitude adjustments is from the operation of a reaction wheel, understanding energy consumed by this device is *key* to obtaining *minimum energy* maneuvers. The torque from a reaction wheel comes from the spin motor,[15] and this motor is an electric motor.[15,16] Therefore, from a practical setting, the objective is to minimize the *electrical* energy of the reaction wheel motors. Additionally, the following practical constraints must be considered:

- Actuator constraints: each reaction wheel can only spin so fast, and can only generate so much torque. Therefore actuator limits must be imposed upon the spacecraft. Otherwise, the optimization may generate trajectories infeasible to a flight scenario (e.g. apply infinite torque for a minimum time problem).

- Saturation concerns upon the rate gyros: Rate gyros are used to measure the attitude of the spacecraft, and saturation of these could result in the loss of control to the spacecraft.

- Reaction Wheel Speed Bias: Being able to attain the desired pointing vector (i.e orientation) of the boresight and being able to place the spacecraft at rest is not enough from a practical point of view. A constraint demanded in an industry-strength flight setting is that the spacecraft should perform the rest-to-rest slew with all reaction wheels beginning, and ending, at a specified rate. The reason for this, is the reaction wheel array is to normally operate at a speed well away from zero in order to avoid imprecise torque that occurs at zero speed.[15] By nominally operating reaction wheels away from zero speed (i.e. 0 revolutions per minute) issues of stiction[17] and jitter, which occur near zero speeds and result with undesirable vibrations occurring throughout the body.

Keeping along the trend of practicality, this dissertation considers situations which gain relevancy when interfacing with the attitude and control guidance system of the spacecraft. These considerations constitute and allows an exploration of minimum energy maneuvers under a variety of settings amenable to a flight-setting:

(S_1) How, if at all, can energy be reduced when the attitude of the spacecraft predetermined (and may *not* be modified); in this situation is it possible to reduce the energy required to slew?

(S_2) How, if at all, can energy be reduced when the reaction wheels *can not* be directly controlled?

It is a goal of this dissertation to explore minimum energy maneuvers under the preceding situations S_1, S_2, as well as the absence of these situations (which is the setting of complete freedom to design the attitude profile, and controllability of the reaction wheels). First though, this introduction provides motivation to these situations and of when, where and why these situations might occur in an industry setting.

Concerning situation S_1: There exists scenarios in which the attitude of the spacecraft may not be freely chosen, but rather, it is fixed (i.e. predefined or prechosen) by some logic onboard the spacecraft, housed in the attitude control system. For instance, a flight-scenario may require that the maneuver between two desired orientations must be performed as an eigenaxis maneuver. In this setting, an obtained minimum energy solution which does not satisfy the attitude constraint (e.g. by maneuvers off-eigenaxis) would not be a feasible (and hence not a flyable) solution.

Situation S_2, is the case when the reaction wheels may not be directly controlled. This occurs in a setting where the spacecraft implements its own control allocation scheme, which is usually least squares.[18] In this case, direct control of the reaction wheels is not possible, as the spacecraft has a predefined algorithm in which to allocate the reaction wheel torques. Additionally, such a feedback system lacks a feedforward term. In this setting, a minimum energy maneuver must be able to work about the control allocation scheme. Therefore, for the setting where the spacecraft implements its own allocation scheme (which is usually least squares[18]) a work around is required to achieve a minimum energy profile.

To place these two situations (S_1 and S_2) into better context, the attitude control and guidance system of a spacecraft may be considered.[19] Figure 1.3 shows a block diagram to an Attitude Control System for a reaction wheel spacecraft, and consists of a combination of an outer-loop, as well as an inner-loop portion. The components which comprise the attitude control system in Figure 1.3 is a Slew Generator block, a Quaternion Error Feedback block, Control Allocation block, and a block for the spacecraft plant, as well as a high level task. The *task* is the driving goal of the entire system, and is often chosen by a human (though this higher-decision making could also be automated; for a discussion on artificial

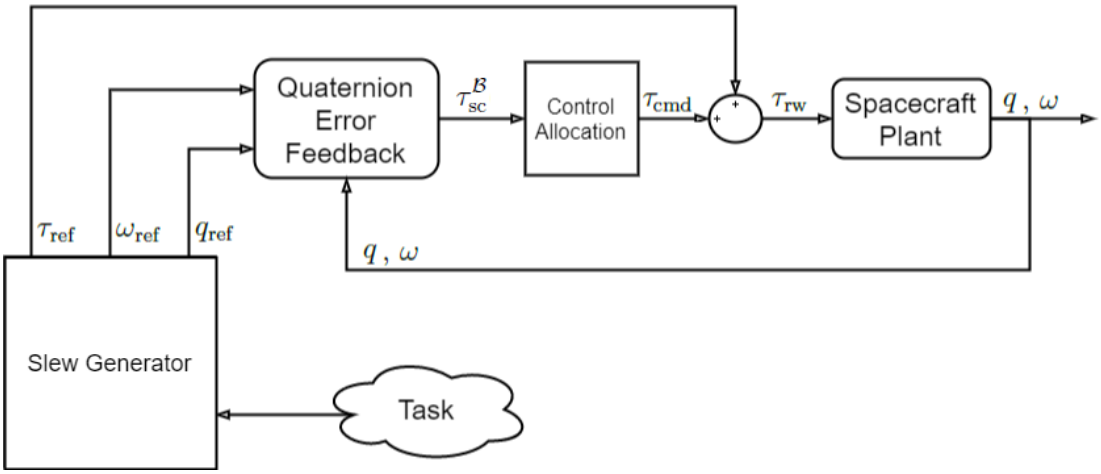

Figure 1.3: A general structure of an Attitude Control System where the outer loop (Slew Generator) interfaces with an inner loop (Quaternion Error Feedback Law) block.

intelligence and its relationship as well as application to optimal control, see Ross in Ref. [20]). The task may be considered colloquially as a simple command to change the attitude of the spacecraft which would be requested to observe an area for scientific collection, or perhaps to point an antennae to a ground station for communications operations scenario. The Slew Generator comprises the outer-loop portion of the attitude control system, and from a given task, outputs feedforward terms for reaction wheel control torque, $\tau_{\text{ref}} \in \mathbb{R}^{N_{\text{rw}}}$, spacecraft body velocity ω_{ref}, and attitude q_{ref}. The slew generator block can be as complex as returning an *optimal* state control solution to the specified task, or it could be as simple as outputting an eigenaxis maneuver for the quaternion error feedback block to execute.[21,22] The quaternion error feedback block comprises the inner-portion of the ACS, and serves to track the attitude profile provided by the slew generator portion of the attitude control system through an efficient and (pretty surprisingly simple) means;[23] this block outputs a commanded body torque profile $\tau_{\text{sc}}^{\mathcal{B}} \in \mathbb{R}^3$ to alter the attitude of the spacecraft. The control allocation block outputs commanded reaction wheel motor torques $\tau_{\text{cmd}} \in \mathbb{R}^{N_{\text{rw}}}$ which is

able to generate the commanded body torque profile $\tau_{\text{sc}}^{\mathcal{B}}$ (e.g. with L^2 allocation, $\tau_{\text{cmd}} = A^{+}\tau_{\text{sc}}^{\mathcal{B}}$, so $A\tau_{\text{cmd}} = \tau_{\text{sc}}^{\mathcal{B}}$). The most common form of control allocation is L^2 allocation, also known as Least Squares allocation, also known as Moore-Penrose allocation, and also known as Pseudoinverse allocation.[24,25] The reason for the control allocation block is to be produce $N_{\text{rw}} \geq 3$ reaction wheel motor torques that produce the body torque $\tau_{\text{sc}}^{\mathcal{B}} \in \mathbb{R}^3$. The spacecraft plant executes the reaction wheel motor torques τ_{rw}, outputting the produced body velocity and attitude.

To summarize, the focus of this dissertation is the study of minimum energy maneuvers for reaction wheel spacecraft which considers various limiting scenarios all of which cast in a practical industry-strength setting. These settings span from the complete freedom to design a maneuver (i.e. off-eigenaxis maneuvers allowable, and direct access to the reaction wheels is available) to constrained settings such as the attitude profile is fixed (e.g. attitude constrained to be an eigenaxis maneuver), as well as consideration to the case when the reaction wheel themselves can not be directly controlled. Table 1.1 lists the cases explored in this body of work relating to minimum electrical energy slewing for reaction wheel spacecraft, and where they might be found in this dissertation.

Table 1.1: The four cases which explore reduced energy expenditure for attitude slews of a reaction wheel spacecraft. Metrics for modeling the electrical energy and power expenditure associated to reaction wheel is detailed in Chapter 2.

Case	Attitude Profile	Reaction Wheel Torque Allocation	Electrical Energy Situation	Chapter Focus
I	free	free	Complete Freedom	4, 5
II	free	fixed	Attitude Steering	6
III	fixed	free	Null Motions	4, 5
IV	fixed	fixed	Unable to Effect Energy Profile	–

The numerical approach taken in this dissertation, is that optimal control is applied to generate the minimum energy trajectories, hence generating open loop commands. Before a candidate state-control pair can be considered a solution

to the optimal control problem, it must pass a very important *verification and validation* (V&V) stage. In this stage, the candidate state-control pair is tested for *feasibility*, which consists of propagating the candidate-control through the dynamics to check sure it does not drive the system to violate any constraints (e.g. boundary conditions or path constraints). Then, in the second stage of V&V the candidate state-control solution is checked to see if it meets (to a user-defined tolerance) the necessary conditions of optimality as given by Pontryagin's Minimum Principle. Only a state-control pair which successfully passes the V&V stage, may be considered for flight. The open loop optimal trajectories serve a very important and relevant roles in industry. These roles are fulfilled as references to track, as well as for planning purposes (e.g. get a lower bound on the transfer time). To implement these optimized (open-loop) trajectories in practice, is typically most effective when used as an open-loop feedforward for a feedback controller to track,[15] just as in Figure 1.3. This numerical approach taken in this dissertation is the same approach that has already been successfully implemented in space flight applications; see Refs. [1, 5, 6, 26–29].

1.3 Thesis Outline and Organization

Derivations for the spacecraft model and electrical energy metrics, which are used throughout this body of work, are presented in Chapter 2. Both the spacecraft and the collection of electrical energy metrics are integral portions to this body of work, for they constitute the dynamics and cost functionals to the optimal control problems *created* throughout this dissertation.

In Chapter 3 the relationship between electrical energy and transfer time for a reaction wheel spacecraft is explored for both eigenaxis and off-eigenaxis maneuvering under minimum dissipative losses. The tradespace between on-and

off-eigenaxis maneuvering is identified and analyzed in this chapter. Null-motions are utilized to demonstrate that reduced-electrical energy solutions can exist in the situation where the attitude is fixed, and are used to show that shortest time maneuvers are not unique with respect to (electrical) energy, thereby addressing situation S_1.

Chapter 4 focuses on the nonsmooth energy metric. An augmentation method is applied which generates an equivalent smooth formulation. This method lifts the formulation through the addition of ancillary controls and path constraints upon the controls. Using this technique, the relationship between electrical energy and transfer time is revisited under minimum electrical energy (as apposed to minimizing dissipative losses only) within this chapter, and the results are compared to the reduced energy maneuvers minimizing dissipative losses found in Chapter 3.

Chapter 5 considers minimizing electrical energy maneuvers in the situation where the reaction wheels can not be directly controlled. The results in this chapter show that the electrical energy may be substantially reduced by altering the steering the attitude of the spacecraft (which conceptually may be considered as steering the path of the boresight). Last words and concluding remarks concerning this body of work are constituted in Chapter 6.

Appendix A contains the simulation parameters used to populate the optimal control problem formulations developed all throughout this body of work. Maximal effort has been made to design the optimal control problems as close to an operational scenario as possible. This much vested effort has been made in regards to using realistic parameters within the optimal control problems throughout this dissertation. Lastly, Appendix B contains a listing of published works, posters, talks which formed the synthesis of this dissertation.

Pseudospectral methods of optimal control implemented in the software package DIDO are applied to obtain solutions to the optimal control problems developed throughout the body of this work. An attractive feature of pseudospectral optimal control theory is the ability to generate adjoint variables from the numerical solutions via the Covector Mapping Theorem.[30–32] This enables the verification of the optimality of numerical solutions against Pontryagin's Minimum Principle. While there are a tremendous amount of numerical methods for optimal control,[33] the choice for DIDO was made because the problems considered in this dissertation are high-dimensional, nonlinear, and host a number of state, control, and mixed state and control path constraints. DIDO, which is a MATLAB optimal control toolbox, has a long history of successful solutions implemented in many NASA and DoD missions.[1,5,6,26–29,34] Such industrial-strength problems include, achieving successful ground tests [34], to the landmark achievements of both the Zero & Optimal Propellant Maneuvers flown International Space Station [26–29], to the first flight-implementation of time optimal slews [1, 5, 6].

1.4 Contributions of the Dissertation

This dissertation focuses upon minimum energy maneuvering. Dynamic optimization is performed with respect to the minimization of electrical energy, whereas literature has focused mainly upon the minimization proxies associated to only mechanical energy. The main contributions from this body of work, collected in this dissertation, is presented in this section.

Firstly, the research in this dissertation demonstrates results analogous to the work that eigenaxis is not time optimal, by showing that eigenaxis maneuvering is not energy optimal for reaction wheel spacecraft. This dissertation showes that the industry standard eigenaxis slew can be dramatically improved upon,

with regards to reduced energy, by maneuvering off eigenaxis. It is demonstrated that agile maneuvers exist within the energy budget of conventional eigenaxis maneuvering. The nonlinear relationship between electrical energy and transfer time is revealed for both eigenaxis and off-eigenaxis maneuvering under minimum dissipative losses and under minimum electrical energy. By studying this nonlinear relationship, two main results are arrived upon which may be significant to mission planning, operations, and design: *i*) There exists a band of near time optimal maneuvers which require substantially less energy as their shortest time maneuver counterpart and *ii*) Eventually there exists diminishing returns on energy savings. The nonlinear relationship between energy and transfer time is first identified under minimum dissipative losses associated to operating the electrical motors, thereby reducing the thermal stresses upon the reaction wheels, and hence potentially increasing the longevity of the reaction wheel actuators. Minimizing *dissipative losses* is quite pertinent in regards to small spacecraft (e.g. cubeSat and smaller), since due to their small size, they have difficulty in rejecting excess heat incurred from dissipative losses.[24,35] From identifying the relationship between electrical energy and transfer time *for both* on-and off-eigenaxis maneuvering, a tradespace was identified between the two maneuvering types. It is this tradespace that demonstrates that off-eigenaxis maneuvers completely dominate conventional eigenaxis maneuvering in regards to energy as well as transfer time. Another contribution from this dissertation is from focusing directly upon the case when the attitude of the spacecraft can not be altered. In such situation, null motions are crucial to ameliorate the energy expenditure whilst slewing. A computational efficient method of performing null motions has been developed in this dissertation. This method results in a fast and reliable way of generating reduced energy solutions that can be incorporated into a feedback solution in the

setting where the attitude of the spacecraft can not be altered. This method has also presented specialized necessary condition for optimality associated to minimum energy maneuvers, which is computationally light enough to be done in real time onboard the spacecraft (hence providing an additional verification and validation of a maneuver before–and during–flight).

In this dissertation, the minimum electrical energy problem is shown to be a constrained high-dimensional L^1 optimal control which is nonsmooth with *both state and control*. To overcome the challenge of nonsmoothness, a method is adopted that allows the minimization of electrical energy, or applications which require the positive-only (or negative-only) portion of a continuous function to be minimized (thereby opening the door for many applications). The relationship between electrical energy and transfer time for both off-eigenaxis maneuvering and eigenaxis maneuvering, which was identified in this dissertation under minimum dissipative losses, is shown to hold for minimum electrical maneuvers; the tradespace between off-eigenaxis maneuvering and eigenaxis maneuvering holds as well. These results demonstrate that agile maneuvering can indeed be performed within the budget of *minimum energy* eigenaxis maneuvering.

Many of the approaches to reduce electrical energy of the attitude control system to perform a slew in literature require *direct access* to the reaction wheels. Null-motions, a very popular means to reduce energy, requires direct access to the reaction wheels. A major contribution to this dissertation is identifying situations when direct access to the reaction wheels is not possible, and showing that even in such situations the electrical energy required to slew a spacecraft *can be reduced*. This dissertation demonstrates the amount of electrical energy and power consumed to perform a slew may be reduced by performing *minimum energy attitude steering* when the reaction wheels can not be directly controlled.

This method also is shown to reduce the peak power, reduce average power, and drive the peak to average power ratio closer to unity (as compared to conventional eigenaxis maneuvering). From these results, accurate energy budgeting is attainable for systems, such as heritage attitude control systems, which might not have the capability to allow direct control over the reaction wheels.

Synthesizing the entire dissertation, into one single response, is that the results contribute a deeper level of understanding to minimum energy slewing for reaction wheel spacecraft.

Chapter 2

Dynamic Modeling

> "This most beautiful system of the sun, planets and comets, could only proceed from the counsel and dominion of an intelligent and powerful Being."
>
> *Isaac Newton*

In this section, the rotational dynamics of the spacecraft, and the metrics for electrical energy and power are derived. In the following chapters, these derived models are subsequently incorporated in optimal control problem formulations, for the purpose of minimizing the electrical energy of a spacecraft performing a slew.

2.1 Spacecraft Model

The spacecraft model is composed of two portions: (i) The rotational dynamics (about the center of mass) of the spacecraft, and (ii) The rotational kinematics of the spacecraft. The spacecraft is modeled as a ridged body, and therefore the equations of motion which describe the evolution of the continuous motion of the spacecraft are derived by application of ridged body mechanics. This field is often reference as Eulerian Mechanics, as the field is governed by Euler's equation of

motion[2] which, in colloquial terms, states that the rate of change of the angular momentum of a ridged body (about its center of mass or the inertial coordinate frame origin) is equal to the external torque acting on the body (about it's center of mass) (i.e. $\dot{\mathbf{H}} = \mathbf{T}$, where $\mathbf{H} \in \mathbb{R}^3$ is the vector of angular momentum of the ridged body and T is the external torque acting on the body). The rotational kinematics (sometimes referred to as rigid body kinematics) serves to describe the orientation of a ridged body (e.g. a spacecraft) relative to some reference frame.

2.1.1 Rotational Dynamics

The rotational dynamics of a spacecraft for attitude control, may be derived from first principals, by considering the conservation of angular momentum in the inertial frame $\mathcal{N}$:

$$\mathrm{H}^{\mathcal{N}}_{\mathrm{tot}}(t) = \int_0^t \tau^{\mathcal{N}}_{\mathrm{ext}}(s)\, ds + \mathrm{H}^{\mathcal{N}}_{\mathrm{tot}}(0),$$

where $\mathrm{H}^{\mathcal{N}}\mathrm{tot}(t) \in \mathbb{R}^3$ is the total angular momentum, at time t, of the spacecraft expressed in the inertial frame $\mathcal{N}$, and $\tau^{\mathcal{N}}_{\mathrm{ext}}(t)$ is the vector representing the total external torque (e.g.: solar, atmospheric, magnetic) acting upon the spacecraft. The rate of change of the spacecraft with respect to the body frame is given by an application of the transport theorem [2]

$$\tau^{\mathcal{N}}_{\mathrm{ext}}(t) = \frac{\mathrm{d}}{\mathrm{d}t}\mathrm{H}^{\mathcal{N}}_{\mathrm{tot}}(t) = \frac{\mathrm{d}}{\mathrm{d}t}\mathrm{H}^{\mathcal{B}}_{\mathrm{tot}}(t) + \omega(t) \times \mathrm{H}^{\mathcal{B}}_{\mathrm{tot}}(t), \tag{2.1}$$

where $\mathrm{H}^{\mathcal{B}}_{\mathrm{tot}}(t), \omega(t) \in \mathbb{R}^3$ are time varying vectors of the angular momentum and angular velocity of the spacecraft represented in the body frame $\mathcal{B}$ respectfully, and the cross product term is resultant to the relative motion between the two frames. The total angular momentum of the spacecraft in the body frame may be decomposed into the individual contributions from the spacecraft body and from

the reaction wheels:

$$\mathrm{H}^{\mathcal{B}}_{\mathrm{tot}}(t) = \mathrm{H}^{\mathcal{B}}_{\mathrm{sc}}(t) + \mathrm{H}^{\mathcal{B}}_{\mathrm{rw}}(t), \tag{2.2}$$

where $\mathrm{H}^{\mathcal{B}}_{\mathrm{sc}}(t) \in \mathbb{R}^3$ is the total angular momentum of the spacecraft, $\mathrm{H}^{\mathcal{B}}_{\mathrm{rw}}(t) \in \mathbb{R}^3$ is the total angular momentum of the reaction wheels in the body frame. The total angular momentum of the spacecraft may be expanded as

$$\mathrm{H}^{\mathcal{B}}_{\mathrm{sc}}(t) = J_{\mathrm{sc}}\omega(t), \tag{2.3}$$

where $J_{\mathrm{sc}} \in \mathbb{R}^{3\times 3}$ is the spacecraft inertia tensor. The total angular momentum of the reaction wheels may be expressed as:

$$\mathrm{H}^{\mathcal{B}}_{\mathrm{rw}}(t) = Ah_{\mathrm{rw}}(t), \tag{2.4}$$

where $A = [a_1|\cdots|a_{N_{\mathrm{rw}}}] \in \mathbb{R}^{3\times N_{\mathrm{rw}}}$ is the matrix which projects from the reaction wheel actuator frame $\mathcal{A}$ onto the spacecraft body frame. Each a_i gives the orientation of the i-th reaction-wheel spin axes in relation to the spacecraft body frame. The quantity $h_{\mathrm{rw}}(t) \in \mathbb{R}^{N_{\mathrm{rw}}}$ is the angular momentum of each reaction wheel relative to its spin axis (notation "$h^{\mathcal{A}}_{\mathrm{rw}}(t)$" to represent the actuator frame is avoided due to clarity; the actuator frame is assumed to be rigidly attached to the spacecraft, so the relative angular velocity between the spacecraft body and the reaction wheel housing is null). Therefore, using Eqs. (2.3) and (2.4), the total angular momentum of the spacecraft in the body frame may be expand as

$$\mathrm{H}^{\mathcal{B}}_{\mathrm{tot}}(t) = J_{\mathrm{sc}}\omega(t) + Ah_{\mathrm{rw}}(t). \tag{2.5}$$

The rate of change of the spacecraft with respect to the body frame is given as

$$\frac{\mathrm{d}}{\mathrm{d}t}H^{\mathcal{B}}_{\mathrm{tot}}(t) = \frac{\mathrm{d}}{\mathrm{d}t}(J_{\mathrm{sc}}\omega(t) + Ah(t)) = J_{\mathrm{sc}}\dot{\omega}(t) + A\dot{h}(t),$$

under the assumption that J_{sc} and A are time invariant, and noting that the relative motion between the reaction wheel actuator frame and the spacecraft body is null. Therefore Eq. (2.1) may be expanded as

$$\tau_{\mathrm{env}}(t) + \tau_{\mathrm{mms}}(t) = J_{\mathrm{sc}}\dot{\omega}(t) + A\dot{h}_{\mathrm{rw}}(t) + \omega(t) \times (J_{\mathrm{sc}}\omega(t) + Ah_{\mathrm{rw}}(t)), \tag{2.6}$$

where the external torque acting upon the spacecraft, $\tau^{\mathcal{N}}_{\mathrm{ext}}(t)$, has been decomposed into environmental torques, as well as torque from the spacecraft momentum management system (MMS). A reasonable assumption upon the rotational dynamics model, is that total external torques in Eq. (2.6) may be taken as null during the course of a slewing maneuver. This assumption is quantified as reasonable because the MMS is only used for momentum dumping and is generally not active during a slew. Moreover, the magnitude of the environmental torques acting upon the spacecraft are typically quite small during the course of a slewing maneuver.

Turning attention to the reaction wheel dynamics, the angular momentum of each reaction wheel is modeled by the following equation:

$$h_{\mathrm{rw}}(t) = J_{\mathrm{rw}}\Omega_{\mathrm{rw}}(t) - J_{\mathrm{rw}}A^{\intercal}\omega(t), \tag{2.7}$$

where J_{rw} is a diagonal matrix with N_{rw} entries along the main-diagonal, whose i-th entry is the inertia of the i-th reaction wheel, which is assumed to be time invariant with respect to the spacecraft body frame. The vector $\Omega_{\mathrm{rw}}(t) \in \mathbb{R}^{N_{\mathrm{rw}}}$ is comprised of the angular rates of the reaction wheels about their respective spin

axes. The angular momentum increment resulting from the spacecraft relative to the wheels is described by $J_{\text{rw}}A^{\intercal}\omega(t)$. Because reaction wheels are normally operated at a bias rate, $\Omega_{\text{rw},i}(t) \gg a_i^{\intercal}\omega(t)$. Because of this, Eq. (2.7) may be reasonably approximated as

$$h_{\text{rw}}(t) = J_{\text{rw}}\Omega_{\text{rw}}(t). \tag{2.8}$$

Noting that the reaction wheel control torque is given as

$$\tau_{\text{rw}}(t) = \dot{h}_{\text{rw}}(t) = J_{\text{rw}}\dot{\Omega}_{\text{rw}}(t), \tag{2.9}$$

the equations as derived in this section, along with the reasonable assumptions made in this section, may be coalesced:

$$\begin{aligned}
0 &= \tau_{\text{ext}}^{\mathcal{N}}(t) \\
&= \frac{\mathrm{d}}{\mathrm{d}t}\mathrm{H}_{\text{tot}}^{\mathcal{N}}(t) \\
&= \frac{\mathrm{d}}{\mathrm{d}t}\mathrm{H}_{\text{tot}}^{\mathcal{B}}(t) + \omega(t) \times \mathrm{H}_{\text{tot}}^{\mathcal{B}}(t) \\
&= J_{\text{sc}}\dot{\omega}(t) + A\dot{h}_{\text{rw}}(t) + \omega(t) \times (J_{\text{sc}}\omega(t) + Ah_{\text{rw}}(t)) \\
&= J_{\text{sc}}\dot{\omega}(t) + A\tau_{\text{rw}}(t) + \omega(t) \times (J_{\text{sc}}\omega(t) + AJ_{\text{rw}}\Omega_{\text{rw}}(t))
\end{aligned}$$

Synthesizing derivations made in this section, the equations of rotational motion of a spacecraft with N_{rw} reaction wheels can be written in the following matrix form:

$$\begin{bmatrix} \dot{\omega}(t) \\ \dot{\Omega}_{\text{rw}}(t) \end{bmatrix} = \begin{bmatrix} J_{sc}^{-1}(-A\tau_{\text{rw}}(t) - \omega(t) \times (J_{sc}\omega(t) + AJ_{\text{rw}}\Omega_{\text{rw}}(t))) \\ J_{\text{rw}}^{-1}\tau_{\text{rw}}(t) \end{bmatrix}. \tag{2.10}$$

2.1.2 Kinematics

To complete the spacecraft model, the attitude of the spacecraft is represented using a quaternion parameterization. The choice of quaternions is by virtue of being free of singularities or discontinuities inherit to three-parameter representations.[36] The quaternion parameterization is taken as

$$q = \left[e_1 \sin\left(\frac{\Phi}{2}\right),\ e_2 \sin\left(\frac{\Phi}{2}\right),\ e_3 \sin\left(\frac{\Phi}{2}\right),\ \cos\left(\frac{\Phi}{2}\right) \right]^{\mathsf{T}} \in \mathbb{R}^4, \tag{2.11}$$

where $e = [e_1, e_2, e_3]^{\mathsf{T}}$ is the eigenaxis and Φ is the rotation angle about the eigenaxis. With regards to the representation of rotations, quaternions are quite intuitive: $e \in \mathbb{R}^3$ may be composed of the direction cosines that orient the eigenvector, and Φ gives the amount of rotation about the eigenaxis. The four-dimensional parameterization of attitude given in Eq. (2.11) has further intuitive geometric meanings that arises from the Euler's rotational theorem[37] which states that a rigid body can be brought from an arbitrary initial orientation to an arbitrary final orientation by a *single* rigid rotation, through a principal angle Φ about the principal axis $\boldsymbol{e}$ which is fixed in both the initial and final orientation; Figure 2.1 is a visual depiction of Euler's rotational theorem.

The quaternion parameterization given in Eq. (2.11) is a left-handed representation; for a discussion on quaternion conventions, the reader is directed to reference [38]. The quaternion kinematic differential equations are described by the following system [25]:

$$\dot{q} = \frac{1}{2}\mathcal{Q}(\omega)q, \tag{2.12}$$

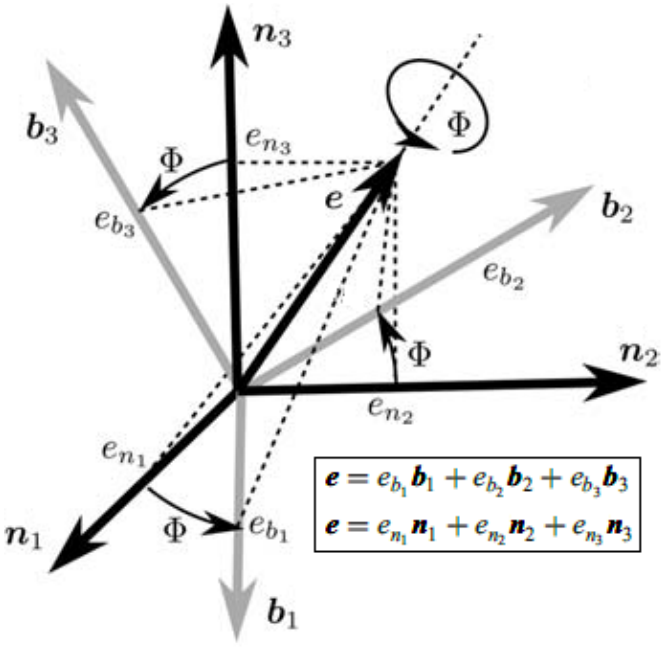

Figure 2.1: Geometric description of the representation of attitude using a quaternion parameterization: $\mathcal{N}$ may be rotated to $\mathcal{B}$ by rotating about the eigenaxis $\boldsymbol{e}$, by the amount of Ψ; image adapted from Ref. [2], pp. 96.

where $\mathcal{Q}(\omega)$ is a skew-symmetric matrix given as

$$\mathcal{Q}(\omega) \triangleq \begin{bmatrix} 0 & \omega_3 & -\omega_2 & \omega_1 \\ -\omega_3 & 0 & \omega_1 & \omega_2 \\ \omega_2 & -\omega_1 & 0 & \omega_3 \\ -\omega_1 & -\omega_2 & -\omega_3 & 0 \end{bmatrix}.$$

Quaternions are a redundant attitude parameterization, and so increase the dimension of the system's state by one when compared to non-redundant three-parameter attitude representations. Because quaternions are, however, free of singularities or discontinuities inherit to three-parameter representations,[36] and so are well-suited for arbitrary large-angle slews. Moreover, since no trigonometric relations appear in the kinematic differential equations described in Eq. (2.12), rather only products, quaternions are befitting for on-board real-time computa-

tion,[25] and have been implemented in spacecrafts such as Galileo,[21] HEAO (High Energy Astronomy Observatory),[39] the space shuttle,[21] as well as in TRACE.[1] While quaternions are free of singularities, quaternions (i.e. *unit quaternions* used for rotation) in Eq. (2.11), do have a quadratic norm constraint which must be satisfied for valid rotations:[25]

$$1 = q_1^2 + q_2^2 + q_3^2 + q_4^2 \tag{2.13}$$

2.2 Electrical Energy Modeling and Electrical Metrics

An optimal-control problem formulation, which is composed of a cost functional, the dynamics and boundary conditions of the underlying application, and for practical problems consideration must be made concerning constraints upon the state and control variables (e.g., saturation limits on the rate gyros and motor torques), which take the form of *path constraints*. One of the *keystones* developing the problem formulation is the *choice* of the performance index (i.e. cost functional) in which to minimize over the entire maneuver trajectory. The motivation of why to consider electrical energy models, is the minimization of the electrical energy of a spacecraft performing a rest-to-rest slew. The manner in which the spacecraft's attitude is altered, is through the use of reaction wheels. Therefore, the cost functional should be tied, as close as possible, to the underlying physics and industry-knowledge of the application at-hand. Practical industry knowledge gives that reaction wheels are inherently *electric* motors, driven by brushless direct current (DC) motors.[3,16,40,41]

2.2.1 Derivation of an Electric Model

From the standpoint of minimizing the energy consumption of the reaction wheels to perform a slew, the electric motors which drive the reaction wheels are modeled as direct current (DC) motors in steady state [3]. By this model choice, inductive losses are assumed to be small compared to the DC power loss in the windings. An electric motor is a device which converts electrical energy into mechanical energy. A schematic depicting the equivalent electronic circuit of a DC motor is shown in Figure 2.2. The armature circuit is given by a resistance (R) in series with an inductance (I) as well as an induced voltage (V_{emf}) that apposes the voltage source V. The induced voltage V_{emf} is called the back electro-motor force (EMF), and occurs due to the armature conductors turning through a magnetic field (and therefore inducing an EMF).

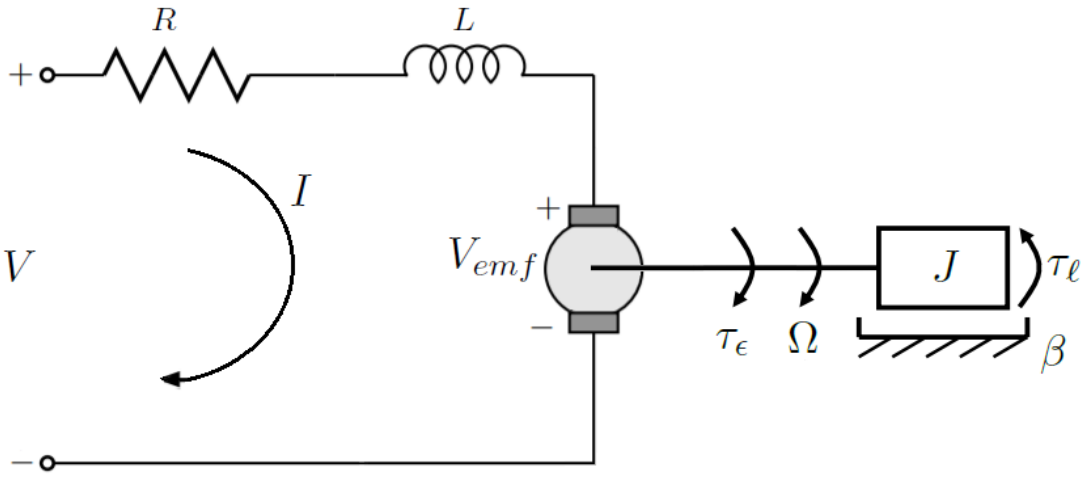

Figure 2.2: Equivalent armature circuit of a DC motor, along with the mechanical load of a reaction wheel (inertia J) under a drag torque, modeled linearly with a viscous friction term β.

The dynamics of a DC motor consists of an electrical component (derived by an application of Kirchoff's law) as well as a mechanical component (derived by Newton's second law for rotational systems). Kirchhoff's Voltage Law (KVL) gives

that the sum of all voltages around the electrical loop must equal zero. Applying KVL to the circuit in Figure 2.2 gives

$$0 = V_R + V_L + V_{emf} - V, \tag{2.14}$$

where $V_R = IR$ is the voltage across the resistor, found by an application of Ohms Law. Next,

$$V_L = L\frac{\mathrm{d}I}{\mathrm{d}t},$$

is the voltage across the inductor, and is proportional to the change in armature current through the coil with respect to time. The back EMF, according to Faraday's Law of Inductance, is proportional to the speed of the motor (which is taken as the speed of the reaction wheel Ω):

$$V_{emf} = K_V\Omega,$$

where $K_V \in \mathbb{R}$ is a velocity constant is a given parameter, determined by i) the flux density of the permanent magnets, ii) reluctance of iron core loss of armature, iii) the number of turns of armature windings. Therefore Eq. (2.14) gives

$$V = IR + L\frac{\mathrm{d}I}{\mathrm{d}t} + K_V\Omega \tag{2.15}$$

Defining J as the inertia of the reaction wheel, and β as a viscous friction coefficient, the mechanical equation of the DC motor is arrived-upon via an application of Newton's second law:

$$J\dot{\Omega} = \tau_\epsilon - \beta\Omega - \tau_\ell. \tag{2.16}$$

where τ_ϵ is the electromagnetic torque exerted by the motor, which is proportional

to armature current:

$$\tau_\epsilon = K_\tau I$$

The scalar K_τ is based on the same three conditions as K_V; in SI units $K_V = K_\tau$ (Nm/A for K_τ, V/(rad/s) for K_V). The term $\beta\Omega$ is a drag torque which has been modeled linearly as a viscous friction term, which acts opposite to the direction of the torque exerted by the motor, and the term τ_ℓ is the torque of the mechanical load. In the subsection to follow, this derived model is expanded to generate very useful metrics which serve to measure instantaneous power consumption, and energy consumption over a finite time horizon.

2.2.2 Electrical Power and Energy Metrics

From the derivations given in Eqs.(2.15) and (2.16), the electric motor of a reaction wheel is modeled as a direct-current (DC) motor in steady state. The average current I flowing through the armature in steady state must is taken as the commanded torque ($\tau_{\text{rw}} = J\dot{\Omega}$) and a viscous friction term ($\beta\Omega$):

$$I(t) = \frac{1}{K_\tau}(\tau_{\text{rw}}(t) + \beta\Omega(t)). \tag{2.17}$$

where it is clear from Eq. (2.17) that the drag torque is modeled linearly with a viscous friction term $\beta\Omega$. The equation which describes the supply voltage to the DC motor in steady state is given as

$$V_{\text{s}}(t) = I(t)R + K_{\text{V}}\Omega(t) \tag{2.18}$$

As in the derivations of the electrical and mechanical equations of a DC motor, in the above equations, V is armature voltage, I is the armature current, R is the

armature resistance, K_V is the back electromotive force (EMF) constant, K_τ is the torque constant, β is the viscous friction coefficient. For SI units we note that $K_\tau = K_V$. When determining the electrical power at any instant in time, which is done by expanding the electrical power input equation $\mathcal{P}(t) = I(t)V_{\mathrm{s}}(t)$ three terms appear: an armature copper-loss term which represents power lost as heat in the windings, a mechanical power term, and a term representing the amount of power loss due to friction:

$$\mathcal{P}(t) = V_{\mathrm{s}}(t)I(t) = I^2(t)R + K_V\Omega(t)I(t), \tag{2.19}$$

$$= \underbrace{\frac{R}{K_\tau^2}(\tau_{\mathrm{rw}}(t) + \beta\Omega(t))^2}_{\text{Copper Loss}} + \overbrace{\tau_{\mathrm{rw}}(t)\Omega(t)}^{\text{Mechanical Power}} + \underbrace{\beta\Omega^2(t)}_{\text{Friction Loss}}. \tag{2.20}$$

The copper-loss term represents power lost as heat in the windings, and is proportional to the amount of torque effort requested. The friction-loss term represents the loss incurred to overcome wheel drag, and is proportional to the magnitude of the angular velocity of the reaction wheel. Both the copper loss and the friction loss term in the electric power-input equation in Eq. (2.19) are known as *dissipative* losses.

During the course of a maneuver, each motor which drives a reaction wheel may alternate between acting as a load ($\mathcal{P}_i(t) > 0$) or acting as a source ($\mathcal{P}_i(t) < 0$). In a system which implements a *regenerative* scheme, energy can be restored to the system when the motor is acting as a source.[24,42,43] In practice, regenerative methods are typically not implemented for a spacecraft, so when a motor acts as a source, the power it generates is shunted to ground via a ballast resistor.[3] Because bus power is only being utilized by the reaction wheels when $\mathcal{P} > 0$,the

total electric power-input to an array of N_{rw} reaction wheels is given as:

$$\mathcal{P}_{\text{array}}(t) = \sum_{i=1}^{N_{\text{rw}}} \{V_i(t) I_i(t)\}^+ = \sum_{i=1}^{N_{\text{rw}}} \{\mathcal{P}_i(t)\}^+, \tag{2.21}$$

where $\{\cdot\}^+$ is defined as

$$\{f(t)\}^+ = \begin{cases} f(t) & \text{if } f(t) > 0 \\ 0 & \text{if } f(t) \leq 0 \end{cases}. \tag{2.22}$$

Integrating Eq. (2.21) represents the total electrical-energy required by the reaction wheel array to perform a slew over the transfer time $[0, T]$:

$$\mathcal{E} = \int_0^T \mathcal{P}_{\text{array}}(t)\, dt. \tag{2.23}$$

Although $\mathcal{E}$ represents the electrical energy consumed when performing a maneuver, taking $\mathcal{E}$ as the cost functional in an optimal control problem poses both *significant* numerical as well as theoretical challenges, in that $\mathcal{P}$ is a non-smooth function with respect to *both* the reaction wheel motor torque and wheel-speed. Indeed, a substantial contribution from this collection of research is working with Eq. (2.23) (through a metric which will define electrical dissipative losses) and developing a method to minimize Eq. (2.23) in an optimal control problem formulation.

The following section expands upon why Eq. (2.23) poses such a challenge. The positive-only portion of the reaction wheel power-input equation of Eq. (2.23) is fundamentally tied to an L^1 norm, demonstrated by the following relation:

$$\{\mathcal{P}_i(t)\}^+ = \frac{1}{2}(\mathcal{P}_i(t) + |\mathcal{P}_i(t)|) \quad \text{for each } i = 1, \ldots, N_{\text{rw}}. \tag{2.24}$$

Therefore the total electrical energy consumed on the time interval $[0, T]$, may be expanded as

$$\begin{aligned}
\mathcal{E} &= \int_0^T \mathcal{P}_{\text{array}}(t)\, dt, \\
&= \int_0^T \sum_{i=1}^{N_{\text{rw}}} \{\mathcal{P}_i(t)\}^+ \, dt, \\
&= \int_0^T \sum_{i=1}^{N_{\text{rw}}} \{V_i(t) I_i(t)\}^+ \, dt, \\
&= \frac{1}{2} \int_0^T \left\{ \sum_{i=1}^{N_{\text{rw}}} \mathcal{P}_i(t) + \sum_{i=1}^{N_{\text{rw}}} |\mathcal{P}_i(t)| \right\} dt. \qquad (2.25)
\end{aligned}$$

Along with Eq. (2.21), which describes the total amount of energy consumed by the reaction wheel array, another useful energy metric is the cumulative amount of dissipated energy by the reaction wheel array. Being able to measure dissipative losses is valuable metric, for dissipative losses are rejected as heat. By being able to reduce dissipative losses, would reduce induced thermal stresses in wheel drive electronics and wheel bearing/lubrication systems.[44] Additionally, small spacecrafts are limited in how much heat they may reject,[24] so being able to measure (and hence potentially minimize) dissipative losses offers potential benefit to attitude control. The metric measuring the total dissipation loss incurred throughout the course of the slewing maneuver is defined as the total amount of copper and frictional losses incurred by the motors over the course of a slewing maneuver:

$$\mathcal{E}_{total}^{loss} \triangleq \sum_{i=1}^{N_{\text{rw}}} \mathcal{C}_{\text{loss},i} + \sum_{i=1}^{N_{\text{rw}}} \mathcal{F}_{\text{loss},i}, \qquad (2.26)$$

where, for each $i = 1, \ldots, N_{\text{rw}}$,

$$\mathcal{C}_{\text{loss},i} \triangleq \int_0^T I_i^2(t) R \, dt \tag{2.27}$$

$$\mathcal{F}_{\text{loss},i} \triangleq \int_0^T \beta_{\text{v}} \Omega_{\text{rw},i}^2(t) \, dt. \tag{2.28}$$

Equations (2.27) and (2.28) represent the cumulative electric-energy lost in the motor windings, $\mathcal{C}_{loss}$, and cumulative electric-energy lost due to friction incurred by the reaction wheel motors, $\mathcal{F}_{loss}$, over the course of a slew.

$\mathcal{E}$, a new metric is instead considered which measures the electrical power under the assumption of a 100 percent regenerative scheme. This regenerative-scheme metric is simply given as the summation of the individual electrical powers:

$$\mathcal{P}_{total}^{rgn}(t) = \sum_{i=1}^{N_{\text{rw}}} V_i(t) I_i(t). \tag{2.29}$$

The motivation for Eq. (2.29) comes from reference [24], in which the following cost functional was considered that considers power metric based off of a 100 percent regenerative mechanical power scheme:

$$\mathcal{P}_{mech}^{rgn}(t) = \sum_{i=1}^{N_{\text{rw}}} \tau_{\text{rw},i}(t) \Omega_{\text{rw},i}(t). \tag{2.30}$$

From the relationship of the torque generated about each reaction wheel about its spin axis, $\tau_{\text{rw}} = J_{\text{rw}} \dot{\Omega}_{\text{rw}}$, the following relation is arrived upon by an application of integration by parts:

$$\int_0^T \sum_{i=1}^{N_{\text{rw}}} \tau_{\text{rw},i}(t) \Omega_{\text{rw},i}(t) \, dt = \sum_{i=1}^{N_{\text{rw}}} \frac{J_{\text{rw},i}}{2} \left(\Omega_{\text{rw},i}^2(T) - \Omega_{\text{rw},i}^2(0) \right), \tag{2.31}$$

where $J_{\text{rw},i}$ is the inertia of the i-th reaction wheel. When the starting and ending wheel speeds are fixed for each maneuver, Eq. (2.31) is a fixed constant. Due to

jitter associated to stiction, resultant when operating a reaction wheel near a zero-angular velocity,reaction wheels are typically held at a constant nominally away from zero between slews and in practice, zero-crossings are typically minimized in order to prolong the life expectancy of reaction wheels.[44] Therefore from a practical flight setting, the spacecraft is flown with a fixed starting and ending wheel bias. Integrating Eq. (2.29) in the situation where a slew begins and ends with the same wheel bias (i.e. all reaction wheels start and end at the same speed) yields the following simplified energy metric:

$$\begin{aligned}
\mathcal{E}^{rgn} &= \int_0^T \mathcal{P}^{rgn}(t)\,dt \qquad (2.32)\\
&= \int_0^T \sum_{i=1}^{N_{\mathrm{rw}}} V_i(t) I_i(t)\,dt \\
&= \int_0^T \sum_{i=1}^{N_{\mathrm{rw}}} \left(\frac{R}{K_\tau^2} (\tau_{\mathrm{rw},i}(t) + \beta_{\mathrm{v}} \Omega_{\mathrm{rw},i}(t))^2 + \beta_{\mathrm{v}} \Omega_{\mathrm{rw},i}^2(t) \right) dt \\
&= \int_0^T \sum_{i=1}^{N_{\mathrm{rw}}} \frac{R}{K_\tau^2} (\tau_{\mathrm{rw},i}(t)\,dt + \beta_{\mathrm{v}} \Omega_{\mathrm{rw},i}(t))^2 + \int_0^T \sum_{i=1}^{N_{\mathrm{rw}}} \beta_{\mathrm{v}} \Omega_{\mathrm{rw},i}^2(t)\,dt \\
&= \int_0^T \sum_{i=1}^{N_{\mathrm{rw}}} I_i^2(t) R\,dt + \int_0^T \sum_{i=1}^{N_{\mathrm{rw}}} \beta_{\mathrm{v}} \Omega_{\mathrm{rw},i}^2(t)\,dt. \\
&= \sum_{i=1}^{N_{\mathrm{rw}}} \mathcal{C}_{\mathrm{loss},i} + \sum_{i=1}^{N_{\mathrm{rw}}} \mathcal{F}_{\mathrm{loss},i} \\
&= \mathcal{E}_{total}^{loss} \qquad (2.33)
\end{aligned}$$

Equation (2.32) is the energy required to perform a slew under a 100 percent electric-regenerative scheme under the assumption of a matching starting and ending bias for each wheel. But, $\mathcal{E}^{rgn}$ serves as a secondary metric as well, measuring the cumulative amount of energy lost as heat occurring in the windings and energy lost as heat due to overcoming friction. This is seen from Eq. (2.32), as $\mathcal{E}^{rgn}$ is the summation of the copper-loss and friction-loss term for each reaction wheel motor. Therefore, while an ideal motor which can achieve 100% regenerative motor

is idealistic and can not exist in practicality, this metric can answer a very *important* question on whether regenerative methods should be implemented. Earlier in this chapter it was mentioned that regenerative methods upon spacecraft are rarely implemented in practice, if at all. The regenerative metric in Eq. (2.29) could be used to determine an upper bound on the maximum amount of possible energy regeneration, if a regenerative system was implemented on a spacecraft. Additionally, due to this research avenue discussed in the preceding paragraphs, the following observation can be made concerning the minimization of energy for reaction wheel slews and that, if not careful in the selection of the components of an optimal control formulation, an ill-posed problem may result.

In a practical setting, where the reaction wheels start and end at a fixed wheel-bias, integrating Eq. (2.30) results with a value of zero, as seen in Eq. (2.31). Hence there is noting to optimize if the running cost is taken as Eq. (2.30). Therefore, attempting to use Eq. (2.30) for the application where the reaction wheels are set to begin and end at a bias results with an ill-posed problem in dynamic optimization.

In the setting where the starting and ending reaction wheels speeds are not fixed, then Eq. (2.31) depicts that the only way to minimize energy when the running cost is Eq. (2.30), is to modify either the starting or ending speeds of the reaction wheels.

Chapter 3

The Relationship between Electrical Energy and Transfer Time Under Minimum Dissipative Losses

> "The longest way round is the shortest way home."
>
> *James Joyce*
> *Ulysses*

The dichotomy between minimum time and minimum effort is well known. Minimum time solutions are synonymous with large effort, whereas minimum effort solutions imply large time horizons. Shortest-time attitude maneuvers are minimum time slews for agile reorientation of space vehicles. Intuition and experience would suggest that such maneuvers are expensive in terms of effort. In this chapter, we show that this is not the case: agile maneuvers exist within the energy budget associated with conventional attitude control systems. Moreover, even for conventional slew strategies (such as eigenaxis) energy requirements can

be reduced. The energy savings are realized via a re-allocation of the control effort by exploiting null motions within the control space, while shaping the velocity profile of the spacecraft over the maneuver trajectory. We develop a cost functional for minimum energy slews that is in-line with true energy cost associated to reaction wheel-based attitude control systems. This energy metric is incorporated into a family of constrained nonlinear optimal control formulations whose solutions present a relationship between transfer time and energy. Both agile (off-eigenaxis) slews and conventional (eigenaxis) slews are studied. A trade space between transfer time and energy is identified, which can be exploited for mission operations, planning and design.

3.1 Introduction

Minimum time attitude maneuvers have been widely studied in the literature. The survey paper by Scrivener and Thompson[45] describes the state of the art up to 1994. The early work, which focused largely on kinematic motion planning (under the assumption of a spherical inertia tensor), showed that the slew time improvement was typically small (less than 1% for a 30 deg maneuver).[14] Later, Shen and Tsiotras,[46] and Proulx and Ross[47] studied minimum-time maneuvering for the cases of axisymmetric and non-symmetric rigid bodies, respectively. In their work, higher performance was obtained by considering the full dynamics of the spacecraft. Fleming[48] and Fleming et al. in Refs. [49–52] further advanced the analysis to the more realistic cases of spacecraft equipped with various actuators, from magnetic torquers to reaction wheels and control moment gyros (CMGs). In 2010, flight tests on the TRACE spacecraft showed that shortest-time maneuvers – slews designed to exploit the spacecraft dynamics – can indeed enhance the performance of practical space systems.[1,6]

In the body of work described in the preceding paragraph, the primary focus was on enhancing spacecraft agility by reducing maneuver time. Experience and intuition would suggest that the price to be paid for a reduction in slew time is a significant increase in the energy that must be expended in order to execute the slew. Energy is a fundamentally-limited resource of a spacecraft: directly affecting its utility and mission life. With this in mind, operational implementation of intuitively "inefficient" agile maneuvers may seem contrary to the stringent requirements on the size, weight and power of a satellite attitude control system. The goal of this chapter is to explore the relationship between maneuver time and energy for reaction wheel attitude control in order to determine the boundaries of the energy budget for agile attitude control. In order to accomplish this task, it is necessary to identify suitable energy metrics for measuring the consumption of agile maneuvering schemes. Existing research on minimum energy attitude maneuvers for reaction wheel spacecraft has been approached from a variety of perspectives concerning the way in which reaction wheel power is modeled, and whether energy consumption is minimized instantaneously – a local approach – or over an entire trajectory – a global approach.

The local approach minimizes the instantaneous reaction wheel power by static optimization. In the literature, various proxies for instantaneous reaction wheel power have been employed. In Refs. [24, 35], solutions were developed that minimize the reaction wheel mechanical power for a spacecraft with a redundant actuator array. This was done by allocating the body frame control torques determined by a given attitude control law to the individual reaction wheels. In Ref. [35] the L^2 norm of reaction wheel mechanical power, $\tau\Omega$, was minimized, whereas in Ref. [24] mechanical power was minimized under the assumption that mechanical energy may be extracted when braking a wheel. The instantaneous

L^1 norm of mechanical power was considered in Ref. [53] as a part of a dissipative power reduction allocation scheme.

The global approach minimizes the energy over the entire maneuver trajectory, i.e. the integral of the instantaneous power, by constructing and solving an optimal control problem.[54–56] For example in Ref. [54], the cost functional was constructed to minimize the integrated reaction wheel copper-loss, I^2R, the current-squared times winding resistance. Reaction wheel friction losses were not considered so minimizing the copper loss was analogous to minimizing the L^2 norm of the reaction wheel motor torque, τ. Global optimization using a quadratic performance index based on reaction wheel mechanical power was considered in Ref. [55] for a single wheel slew and in Ref. [56] for a three wheel array. In reality, a model for reaction wheel power consumption is more complicated than the simplified models based on mechanical power or copper-loss would suggest. Three terms should be considered simultaneously: the copper-loss, friction loss, and the mechanical power. A complication, however, is that such a model additionally requires that only the positive part of the reaction wheel power be considered since energy is only consumed when a wheel motors act as a load. Energy generated when the wheel motors act as sources, the negative part of the power equation, is typically shunted to ground. The resulting non-smooth optimal control problem can be challenging to solve, thus motivating the use of proxies for power as described above.

In this chapter, the relationship between maneuver time and energy for a practical reaction wheel attitude control system is studied for both on-and off-eigenaxis maneuvering under minimum dissipative losses. The total amount of energy consumed to complete a slew is computed by identifying, at each instant of time, whether a motor is acting as a consumer or a generator and integrat-

ing only the positive part of the reaction wheel power equations. It is observed that for a zero-net bias momentum control system where the reaction wheels are operated about a nominally fixed bias rate, the reaction wheel electrical power input equation can be reduced to a quadratic form comprising only dissipative terms. Thus, a smooth cost functional can be written based on the cumulative dissipative losses. This energy metric is incorporated into a constrained nonlinear optimal control problem formulation that is solved using Pseudospectral optimal control theory.[20] The constructed optimal control problem formulation directly considers the nonlinear dynamics of the rotating spacecraft, along with state and control constraints pertinent to an operational environment, for example reaction wheel speed bias, limits on achievable-torque and momentum, as well as saturation of the rate-gyros. The relationship between transfer time and energy is determined by solving a series of fixed-time problems for both agile (off-eigenaxis) slews and conventional (eigenaxis) slews. The results indicate a a counterintuitive result, that agile maneuvers can, in fact, be performed within the energy budget associated with a conventional attitude control system. Moreover, energy requirements for conventional slew strategies (such as eigenaxis) can be reduced. The dichotomy between minimum time and minimum effort is addressed via the additional degrees-of-freedom associated with the redundant reaction wheel array. In particular, the results show that the energy savings are realized via a re-allocation of the control effort by exploiting null motions within the control space while simultaneously shaping the spacecraft angular velocity profile. Thus, a trade space between transfer time and energy exists which can be exploited for mission operations, planning and design.

The remainder of this chapter is organized as follows. In section 3.2.2, a set of optimal control problems are formulated to minimize the energy required to per-

form a rest-to-rest maneuver under various constraints in line with an operational setting. Section 3.3 analyzes the minimum energy maneuvers, and elaborates on the mechanism for energy reduction by an analysis of the reaction wheel null space. Section 3.4 presents the results on the nonlinear relationship between transfer time and energy required to perform a maneuver for both agile (off-eigenaxis) and conventional (eigenaxis) slews. The trade space between energy and transfer time between for various maneuver types is identified and explored. Lastly, conclusions are given in section 3.5.

3.2 The Development of Minimum Dissipative Losses Problem Formulations

This section presents the development of a family of constrained high dimensional nonlinear (time fixed) optimal control formulations for the minimization of (electrical) dissipative losses. This family consists of a formulation for off-eigenaxis maneuvering, and a formulation which enforces on-eigenaxis (or rather, just "eigenaxis") maneuvering. This section will go over the details of the development of an optimal control problem. The development of a problem formulation is *iterative*; it is also a very creative process. What follows is a brief discussion on what constitutes an optimal control problem formulation. A problem formulation first begins, *always*, with a word problem; some problem whose solution is desired. The entirety of this dissertation tackles the problem of minimizing the energy associated with performing a slew for a reaction wheel spacecraft. Based upon the direction given by the word problem, the dynamics is the next step. For this dissertation, "Reaction wheel spacecraft" is the portion of the word problem which dictates the direction for the dynamics, (which were derived in Chapter 2).

Concerning the dynamics, there is a very important choice to the level of fidelity of the dynamical model as well as the coordinate system. Often engineering applications will have a *truth model*, as well as an *optimization model* (for example, a six degrees of freedom model for the truth model, and a three degrees of freedom for the optimization model). The truth model is usually of the highest fidelity possible. This fidelity does not often (if ever) lend itself well being model upon which optimization is performed (i.e. the optimization model). For example, in this work, an approximation was made in Eq. 2.8 because the small addition of angular momentum resulting from the spacecraft relative to the wheels is so small that its presence does not effect the solutions to the optimal control problem. Along with the dynamics of the system, the word problem also states the practical constraints pertinent to the environment. These constraints take the form of path constraints in the problem formulation, as well as the boundary conditions: Because the application is a rest-to-rest slew, under a specified starting and ending wheel bias, there shall be a starting and ending attitude (in the form of a quaternion parameterization), starting and ending angular velocity of the spacecraft body of zero, and a starting and ending reaction wheel speeds. Now, with the dynamics, boundary conditions and path constraints the cost functional is the last portion to obtain an optimal control problem formulation. Once again it is the word problem which dictates the direction for the choice to the cost functional. For the application and aims of this dissertation, the cost functional is to minimize the energy of the spacecraft.

This chapter is organized as follows: In the first section, problem formulations are constructed for both off-eigenaxis and on-eigenaxis maneuvering (in Section 3.2.2). In the section that follows, the necessary conditions for optimality are derived for the off-eigenaxis formulation by application of Pontryagin's Minimum

Principle. A minimal dissipative losses maneuver which has the same transfer time as the shortest-time maneuver is demonstrated to satisfy the necessary conditions of optimality. This maneuver will be compared to the solved shortest time maneuver in Section 3.3.1 to demonstrate that shortest time maneuvers are not unique in regards to energy.

3.2.1 Selection of Cost Functional

This section defines the selection of a cost functional which minimizes the dissipative losses incurred by the reaction wheel motors.Chapter 2 developed the base energy metrics for the electrical power input equation, electrical energy, and the dissipative loss metric. While $\mathcal{E}$ represents the energy consumed to perform a maneuver, taking $\mathcal{E}$ as the cost functional in an optimal control problem poses a numerical challenge since $\mathcal{P}^+$ is a non-smooth function, as discussed in chapter 2, which involves the L^1 norm of both state and control. It will be shown in Chapter 4, that a new method in the field of optimal control theory had to be invented to solve the minimum the minimum electrical energy formulation. Alternatively to directly minimizing $\mathcal{E}$, for each reaction wheel, we may write $\mathcal{P}^+ = \frac{1}{2}(\mathcal{P} + |\mathcal{P}|) \leq \frac{1}{2}(\tau_{rw}\Omega + |\tau_{rw}\Omega| + 2\mathcal{D}_{loss})$ where $\mathcal{D}_{loss}$ is the instantaneous dissipative loss in Eq. (2.19). Integrating this equation term by term (to evaluate energy consumption over a slew) gives

$$\begin{aligned}\mathcal{E}(T) \leq\ & \frac{J_{rw}}{4}\left(\Omega_{rw}^2(T) - \Omega_{rw}^2(0)\right) \\ & + \int_0^T \left(\frac{|\tau_{rw}(t)\Omega_{rw}(t)|}{2}\right)dt + \int_0^T \left(\frac{R}{K_T^2}(\tau_{rw}(t) + \beta\Omega_{rw}(t))^2 + \beta\Omega_{rw}^2(t)\right)dt.\end{aligned} \tag{3.1}$$

If it is assumed that each slew begins and ends with the same wheel bias, the first term in Eq. (3.1) is null leaving

$$\mathcal{E}(T) \leq \int_0^T \left(\frac{|\tau_{rw}(t)\Omega_{rw}(t)|}{2} \right) dt + \int_0^T \left(\frac{R}{K_T^2} (\tau_{rw}(t) + \beta\Omega_{rw}(t))^2 + \beta\Omega_{rw}^2(t) \right) dt, \tag{3.2}$$

which may be further decomposed into the following relationship

$$\mathcal{E}(T) \leq \int_0^T \left(\frac{|\tau_{rw}(t)\Omega_{rw}(t)|}{2} \right) dt + \mathcal{C}_{loss} + \mathcal{F}_{loss}, \tag{3.3}$$

where $\mathcal{C}_{loss}$ and $\mathcal{F}_{loss}$ are given in Eqs. (2.27) and (2.28).

From Eq. (3.3), it is evident that a cost functional that minimizes the dissipative losses would also tend to reduce the integral involving the absolute value because the quadratic terms penalize large values of τ_{rw} and Ω_{rw}. Therefore, minimizing the cumulative dissipative losses serves as a useful proxy for energy consumption over a slew. Thus, an appropriate *smooth* cost functional for optimal control is to minimize is the total dissipative loss metric of Eq. (2.26) while still being a metric in line with the operation of a reaction wheel:

$$\mathcal{E}_{total}^{loss} = \sum_{i=1}^{N_{rw}} \mathcal{C}_{loss,i} + \sum_{i=1}^{N_{rw}} \mathcal{F}_{loss,i}. \tag{3.4}$$

We note three remarks by taking $\mathcal{E}_{total}^{loss}$ as the cost functional to a minimal electrical energy maneuver: (*i*) Trajectories which minimize $\mathcal{E}_{total}^{loss}$ minimize dissipative losses, and therefore the amount of heat the spacecraft has to reject is minimized. (*ii*) While Eq. (3.4) ultimately provides an estimate for energy consumption, it is always possible determine the true energy consumption $\mathcal{E}$ for an optimized slew *a posteriori* for comparison with conventional maneuvers. (*iii*) The metric $\mathcal{E}_{total}^{loss}$ serves to measure the electrical power under the assumption of a 100 percent

regenerative scheme,[57] which is derived in chapter 2.

3.2.2 Minimum Dissipative Losses Problem Formulation for Off-Eigenaxis and On-Eigenaxis Maneuvers

In this section, the energy cost functional developed in the previous section is used towards formulating an optimal control problem for minimizing the electrical energy required for slew. Rest-to-rest maneuvers (i.e. $\omega^0 = \omega^f = 0 \in \mathbb{R}^3$) from an initial orientation $q^0 \triangleq \left[e_0 \sin\left(\frac{\Phi_0}{2}\right), \cos\left(\frac{\Phi_0}{2}\right)\right]^\intercal \in \mathbb{R}^4$ to a final orientation given by $q^f \triangleq \left[e_f \sin\left(\frac{\Phi_f}{2}\right), \cos\left(\frac{\Phi_f}{2}\right)\right]^\intercal \in \mathbb{R}^4$ are considered. By a simple change of the boundary conditions, other operational slew scenarios could also be evaluated.

The optimal control problem formulation incorporates practical constraints on both the state and the control variables that are in-line with typical operations: (*i*) The reaction wheels start and end at the same bias speeds, Ω_{bias}. (*ii*) Per axis limits, ω_{max}, are imposed upon the spacecraft angular rate to avoid saturation of the rate-gyros. (*iii*) Hardware constraints are considered for the reaction wheels with respect to momentum storage, Ω_{max}, and maximum torque, τ_{max}, authority for each reaction wheel.

The optimal control problem formulation, presented as follows, is hereafter

referred to as the Minimum-Energy (ME) formulation:

$$
\text{(ME)}\begin{cases}
\text{State:} & x = [q, \omega, \Omega_{rw}]^{\mathsf{T}} \in \mathbb{R}^{7+N_{rw}}, \quad \text{Control:} \quad u = \tau_{rw} \in \mathbb{R}^{N_{rw}}, \\
\text{Minimize:} & J\left[x(\cdot), u(\cdot)\right] = \displaystyle\int_0^T \sum_{i=1}^{N_{rw}} \left(\frac{R}{K_T^2} (\tau_{rw,i}(t) + \beta \Omega_{rw,i}(t))^2 + \beta \Omega_{rw,i}^2(t) \right) dt \\
\text{Subject To:} & \\
& \begin{bmatrix} \dot{q} \\ \dot{\omega} \\ \dot{\Omega}_{rw} \end{bmatrix} = \begin{bmatrix} \frac{1}{2}\mathcal{Q}(\omega) q \\ J_{sc}^{-1}(-A\tau_{rw} - \omega \times (J_{sc}\omega + A J_{rw} \Omega_{rw})) \\ J_{rw}^{-1} \tau_{rw} \end{bmatrix} \\
& \\
& x(0) = [q^0,\ \omega^0,\ \Omega_{bias}]^{\mathsf{T}} \in \mathbb{R}^{7+N_{rw}}, \\
& x(T) = \left[q^f,\ \omega^f,\ \Omega_{bias}\right]^{\mathsf{T}} \in \mathbb{R}^{7+N_{rw}} \\
& \\
& |\omega_i| \leq \omega_{max},\ \forall\, i = 1, 2, 3 \\
& |\Omega_{rw,i}| \leq \Omega_{max},\ \forall\, i = 1, \ldots, N_{rw} \\
& |\tau_{rw,i}| \leq \tau_{max},\ \forall\, i = 1, \ldots, N_{rw}
\end{cases}
\tag{3.5}
$$

The state space of the system consists of the attitude of the spacecraft, angular velocity of the spacecraft body, and angular velocities of the reaction wheels (about their individual spin-axis). The control vector is taken as the vector of individual reaction wheel torques. The upper bound on the transfer time is given by T. For problem ME to be feasible, the value of T must be, at minimum, the transfer-time of the shortest-time maneuver (denoted t_{STM}) for the same boundary conditions. For a minimum energy problem, it is typical for the maneuver time horizon to be longer than shortest time, i.e. $T > t_{STM}$. From this point of view, a minimum energy shortest-time maneuver can be determined by setting $T = t_{STM}$. We note that t_{STM} can be determined by a simple modification to the cost functional by rewriting $J\left[x(\cdot), \tau_{rw}(\cdot), t_f\right] = t_f$ and allowing $0 \leq t \leq \infty$.

As problem ME does not impose a motion constraint to force an eigenaxis slew, off-eigenaxis motions are allowed if they are advantageous with respect to meeting a given constraint on the slew time. The analysis to follow is, however, also concerned with evaluating the energy requirements of eigenaxis slew profiles against the conventional eigenaxis control logic.[25] To achieve an eigenaxis maneuver under a slew-rate constraint, the ME formulation presented in Eq. (3.5) requires two modifications. To constrain the motion of the spacecraft, the angular velocity vector of the spacecraft must always be collinear with the eigenaxis.[23] Including the following path-constraint as part of problem ME achieves this goal:

$$\omega(t) \times e = 0 \in \mathbb{R}^3, \ \forall\, t \in [0, T]. \tag{3.6}$$

It is also necessary to enforce a spherical slew rate constraint. This can be done by including an additional path constraint of the form $\|w\| \leq \omega_{max}$. By inserting these two path constraints, both a shortest time eigenaxis-constrained maneuver, as well as a minimum energy eigenaxis maneuver (ME-EAM) may be determined. In the next section, we briefly describe some key necessary optimality conditions.

3.2.3 Derivation of the Necessary Conditions For Optimality

For the sake of brevity, only the necessary conditions pertaining to problem ME, given in Eq. (3.5), are considered in this section. The necessary conditions for the variants of problem ME (such as maneuvering along an eigenaxis) may be derived analogously.

At the heart of the Pontryagin's Minimum Principle is the Hamiltonian Minimization Condition (HMC). The HMC requires for an extremal control $u^* = \tau_{rw}$

to be optimal, that u^* must minimize the control Hamiltonian at each instant of time. Let $\lambda_q \in \mathbb{R}^4, \lambda_\omega \in \mathbb{R}^3, \lambda_\Omega \in \mathbb{R}^{N_{rw}}$ be the costate variables for the respective states. The HMC for problem ME can be summarized as:

$$\text{(HMC)} \begin{cases} \text{Min:} & H(\lambda, x, u) = \mathcal{P}_{total}^{loss}(x, u) + [\lambda_q{}^\intercal, \lambda_\omega{}^\intercal, \lambda_\Omega{}^\intercal] \begin{bmatrix} \frac{1}{2}\mathcal{Q}(\omega)q \\ J_{sc}^{-1}(-Au - \omega \times (J_{sc}\omega + AJ_{rw}\Omega_{rw})) \\ J_{rw}^{-1}u \end{bmatrix} \\ \text{Subject to:} & -\omega_{max} \le \omega_i \le \omega_{max}, \quad \forall\, i = 1, 2, 3 \\ & -\Omega_{max} \le \Omega_i \le \Omega_{max}, \quad \forall\, i = 1, \ldots, N_{rw} \\ & -\tau_{max} \le u_i \le \tau_{max}, \quad \forall\, i = 1, \ldots, N_{rw} \end{cases},$$

where $\mathcal{P}_{total}^{loss}(x, u) = \sum_{i=1}^{N_{rw}} \frac{R}{K_T^2}(\tau_{rw,i} + \beta\Omega_{rw,i})^2 + \beta\Omega_{rw,i}^2$. An application of the Karush-Kuhn-Tucker (KKT) conditions on HMC results in the following complementarity conditions that require each component of ω, Ω, u and the associated KKT multipliers $\mu \triangleq [\mu_\omega, \mu_\Omega, \mu_u]^\intercal \in \mathbb{R}^{3+2N_{rw}}$ to satisfy

$$\mu_{\omega_i} \begin{cases} \le 0 & \omega_i = -\omega_{max} \\ = 0 & -\omega_{max} < \omega_i < \omega_{max} \\ \ge 0 & \omega_i = \omega_{max} \end{cases}, \quad \mu_{\Omega_i} \begin{cases} \le 0 & \Omega_{rw,i} = -\Omega_{max} \\ = 0 & -\Omega_{max} < \Omega_{rw,i} < \Omega_{max} \\ \ge 0 & \Omega_{rw,i} = \Omega_{max} \end{cases}, \quad \mu_{u_i} \begin{cases} \le 0 & u_i = -\tau_{max} \\ = 0 & -\tau_{max} < u_i < \tau_{max} \\ \ge 0 & u_i = \tau_{max} \end{cases}. \tag{3.7}$$

Furthermore, the Hamiltonian Evolution Condition requires that the lower Hamiltonian $\mathcal{H}(\lambda(t), x(t), u^*(t))$, be constant for all time, i.e.

$$\frac{\partial \mathcal{H}}{\partial t} = 0 \ \ \forall t$$

To illustrate the application of the complementarity condition and Hamiltonian Evolution Condition as tests for optimality, problem ME was solved for a 180-degree z-axis slew. The associated spacecraft parameters are given in the Appendix. The maneuver time was taken to be $T = 279.9$ seconds (the minimum

transfer time for this particular maneuver), thereby considering a minimum energy shortest time maneuver. The solution gave a value for $\mathcal{E}$ as 143.9 J. The associated attitude, angular rate, and reaction wheel speed profiles are shown in Figure 3.1. The analysis of the minimum-energy shortest-time maneuvers compared to standard shortest-time maneuvers, in the subsequent section of this chapter.

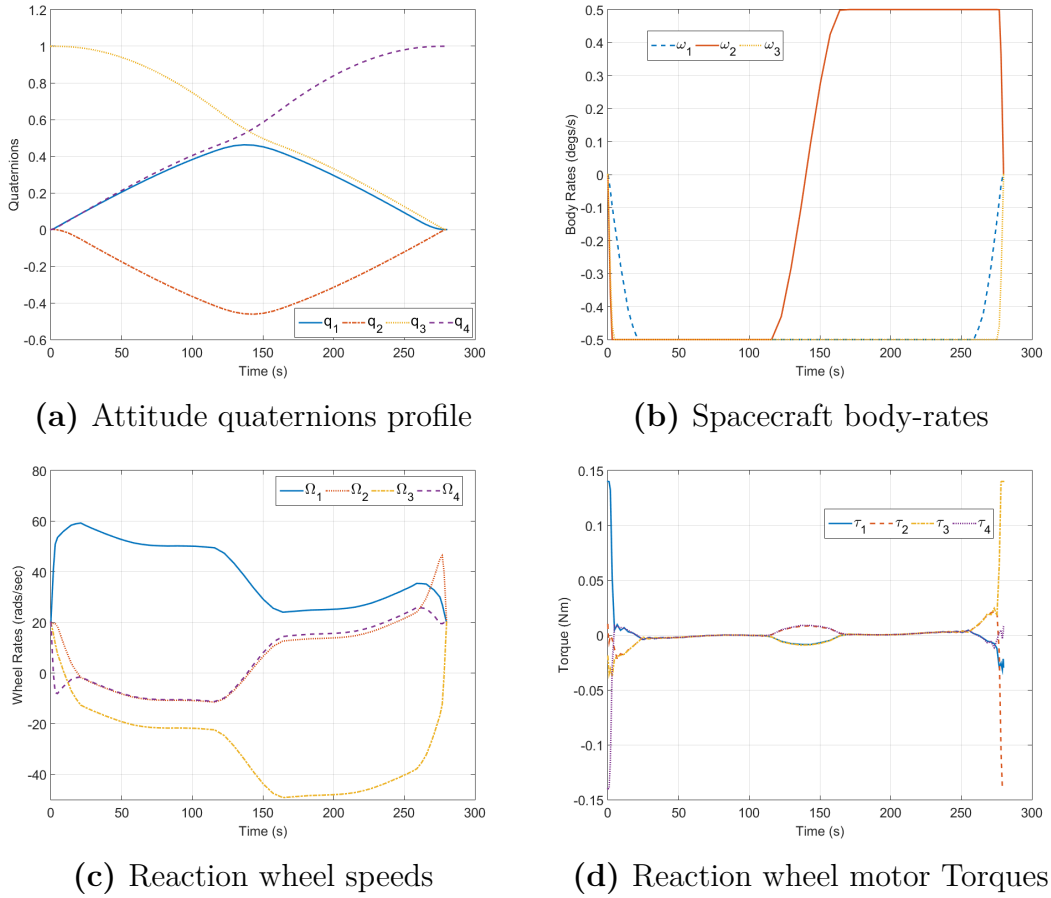

(a) Attitude quaternions profile

(b) Spacecraft body-rates

(c) Reaction wheel speeds

(d) Reaction wheel motor Torques

Figure 3.1: State and control profiles of a Minimal Energy Shortest Time Maneuver for a 180-deg rest-to-rest slew about the spacecraft z-axis: (a) attitude; (b) body rates; (c) reaction wheel rates; (d) body torques (control).

Figure 3.2 shows the satisfaction of the necessary conditions for the maneuver of Figure 3.1. The time history of the lower Hamiltonian is shown in Figure 3.2a. For a minimum time problem, Pontryagin's Minimum Principle states that the

value of the lower Hamiltonian should be -1 over the entire time horizon $[0, T]$. While the lower Hamiltonian in Figure 3.2a is observed to be nominally constant as required by the Hamiltonian Evolution Condition, the value is not -1 as predicted by the minimum principle. This discrepancy is a result of the fact that problem ME was solved as a fixed time problem instead of a minimum time problem. For the case of a fixed time problem,, the transversality conditions admit other constant values for the Hamiltonian. Hence, the value $\mathcal{H}(t) = -36.1\,\mathrm{J/s}$ in Figure 3.2a satisfied the necessary condition. Figure 3.2b shows the complementarity condition on the spacecraft angular rate, ω_2. As can be seen, the KKT multiplier varies in accordance with Eq. (3.7) which specifies that $\mu_{\omega_i} = 0$ unless the constraint on ω_i is active. Profiles for the other spacecraft body axes are similar, and so the results are omitted for brevity. The specifics on the other necessary conditions such as the details on transversality, the Hamiltonian value conditions, etc. while verified, have been omitted for brevity.

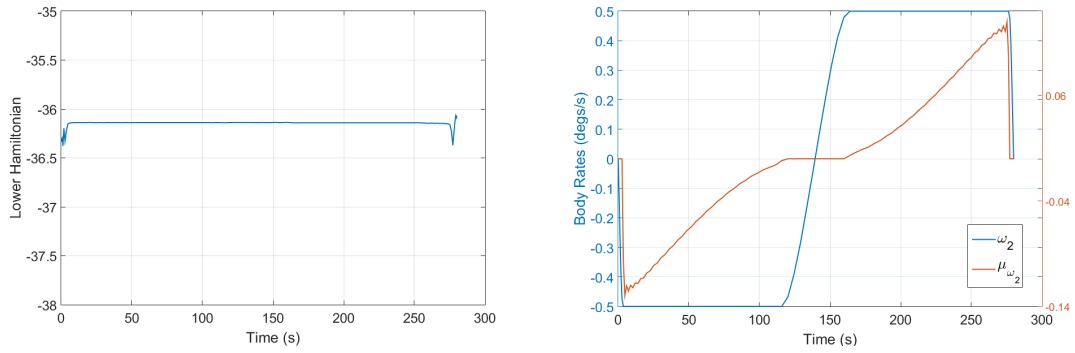

Figure 3.2: Verification of necessary conditions to the Minimum Energy Shortest Time Maneuver, 180-deg rest-to-rest slew about the spacecraft z-axis: (a) Consistency of the Lower Hamiltonian by Hamiltonian Evolution Equation; (b) Complementarity condition for ω_2. depicted in Figure 3.1.

In addition to verifying the satisfaction of the necessary conditions for each candidate optimal control solution it is also necessary to demonstrate the feasibil-

ity of candidate optimal control, u^*, in order to fully vet the numerical solutions (see the discussion on verification and validation in Ross[58]). Feasibility analysis is carried out by propagating u^* through the dynamics given in Eq. (3.5) using a standard Runge-Kutta (RK) integrator. The candidate optimal control is deemed feasible if and only if the solution returned by the RK integrator coincides with the solution returned by the numerical solver to within a predefined tolerance e.g. $\epsilon < 10^{-6}$ where ϵ is the relative error. All of the numerical solutions to problem ME presented in this chapter have been verified against the necessary conditions and have been deemed feasible per the propagation test.

3.3 Identifying the Mechanism for Energy Reduction

This section analyzes the minimum energy solutions to problem ME problem given in Eq. (3.5) for the case of minimum time (off-eigenaxis) slews. The results, however, are also applicable to conventional eigenaxis maneuvering schemes.

3.3.1 Comparison with the Shortest-Time Maneuver

The shortest-time maneuver (STM)[1,5,6] is a time-optimal attitude maneuver determined as the solution to an optimal control problem. The STM maximizes the agility of a spacecraft, building the angular velocity about all three body axes simultaneously, by taking full-advantage of the inertia ellipsoid,[20] nonlinear rotational dynamics, and all operational constraints imposed system. In order to solve the STM, a problem formulation analogous to problem ME is employed with $J\left[x(\cdot), u(\cdot)(\cdot), t_f\right] = t_f$. For the same 180-deg z-axis slew example as in the previous section, we obtain the solution given in Figure 3.3. Comparing the

STM of Figure 3.3 with the ME slew of Figure 3.1, we note the following: (*i*) the spacecraft attitude and angular rate profiles *have not* changed; (*ii*) the reaction wheel speed profiles *have* changed. The results illustrate what is obvious in retrospect. In order to effect the necessary momentum exchange with the spacecraft, the solution to the minimum-time maneuvering problem (Figure 3.3) must admit a feasible reaction wheel speed profile. However, due to the additional degree(s)-of-freedom inherent to the redundant reaction wheel array, feasible reaction wheel speed profiles may not be unique. In particular, if the null space of reaction wheel projection matrix A is nontrivial, there exists an infinite number of feasible reaction wheel speed profiles for a given slew. Hence, for a given maneuver time, it is possible to reduce the energy consumed by searching the reaction wheel null space in order to eliminate losses associated with the original minimum time solution by re-allocating the control. This suggests that, the relationship between the two different cost functionals that define the trade space of a redundant attitude control system is atypical. For example, conventional wisdom would suggest that reducing energy consumption would increase transfer time. However, in the case of a redundant attitude control system, it is in fact possible to reduce energy consumption without increasing the transfer time. Although an agile off-eigenaxis maneuver is considered here, it will be shown later that the same mechanism can be exploited for reducing the energy required to perform eigenaxis maneuvers.

The break-down of the energy requirements for the maneuvers of Figures 3.1 and 3.3 are summarized in Table 3.1. In Table 3.1, the cumulative electrical energy, $\mathcal{E}$ is given along with the energy dissipated as heat, $\mathcal{E}_{total}^{loss}$, and its two components of copper loss and friction loss. Although each maneuver has a transfer time of 279.9 seconds, the slews have significantly different energy requirements as seen by the difference in the values of $\mathcal{E}$. By solving problem ME, it is possible to

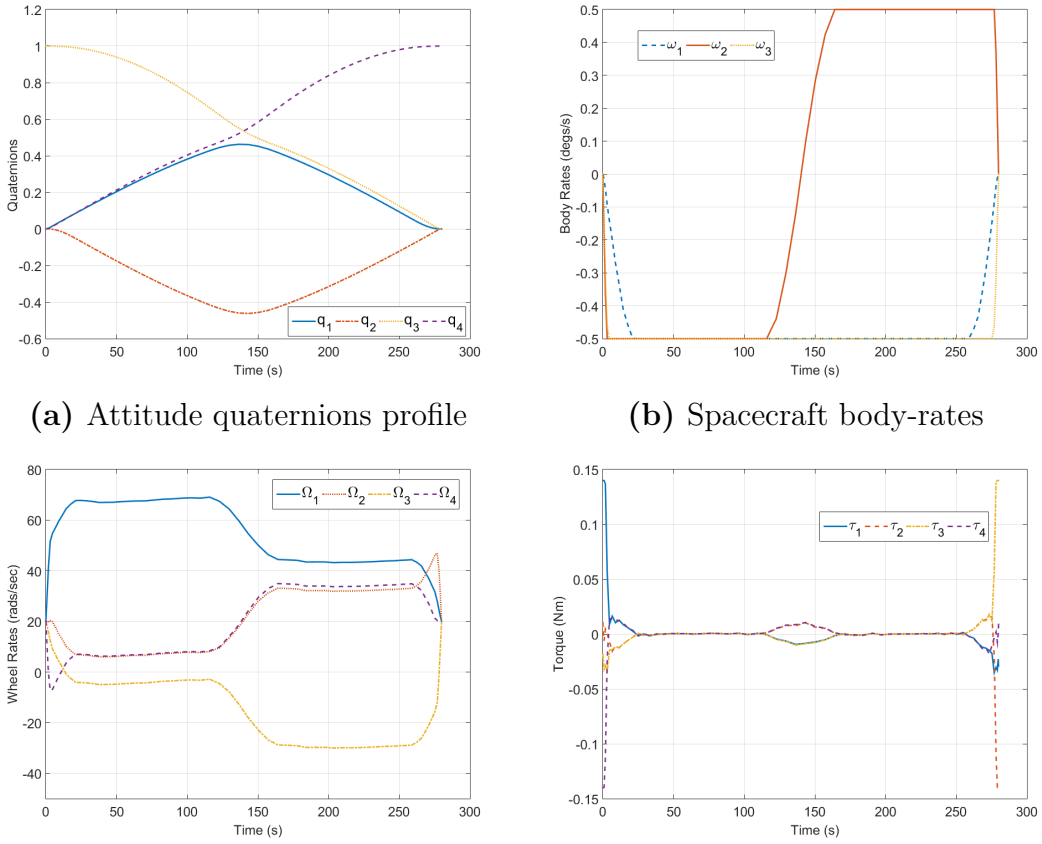

(a) Attitude quaternions profile

(b) Spacecraft body-rates

(c) Reaction wheel speeds

(d) Reaction wheel motor Torques

Figure 3.3: State and control profiles of a Minimal Energy Shortest Time Maneuver for a 180-deg rest-to-rest slew about the spacecraft z-axis: (a) attitude; (b) body rates; (c) reaction wheel rates; (d) body torques (control).

reduce the energy required by approximately 11%. The metrics in Table 3.1 show that solving the ME problem reduces the overall energy that is dissipated as heat, as seen by the copper loss and friction loss metrics, by approximately 11%. By marginally penalizing copper loss by 2%, the losses in overcoming wheel friction drag are substantially reduced, by 30%. Therefore, there exist less demanding shortest-time trajectories with respect to energy requirements as well as amount of generated dissipative losses. Therefore, shortest time maneuvering is not unique with respect to energy, and should a setting in which the most agile maneuvering is

required, there exists less demanding maneuvers. Due to the substantial decrease in friction loss, the minimal energy shortest time maneuver potentially will not be as demanding upon the reaction wheel motors as the traditional shortest time maneuver, and therefore potentially increase the longevity of the reaction wheels.

Table 3.1: Electrical energy metrics for a baseline shortest-time maneuver and a minimum-energy maneuver which is equivalent in transfer time (values in parenthesis represent percentage change from baseline).

Maneuver Type	$\mathcal{E}$ (J)	$\mathcal{E}_{total}^{loss}$ (J)	$\mathcal{C}_{loss}$ (J)	$\mathcal{F}_{loss}$ (J)
Shortest-time maneuver	162.0	136.3	79.7	56.6
ME shortest-time maneuver	143.9 (-11.2%)	121.0 (-11.2%)	81.3 (+1.9%)	39.7 (-29.8%)

3.3.2 Exploiting the Nullspace to Reduce Energy Requirements

In this section the utility of the reaction wheel nullspace (i.e.: the nullspace of the matrix A which projects from the reaction wheel actuator frame to the spacecraft body frame) is further explored, and a simplified problem that facilitates real-time implementation of (sub)-optimal null space solutions for reducing energy requirements is developed. As discussed in section 3.3.1 of this chapter, because the attitude profiles match in Figures 3.3 and 3.1the difference in electrical energy between the two time-optimal maneuvers given in Table 3.4 and Figures 3.3 and 3.1 is due to null motions. Null motions allow the energy profile to be altered while not effecting the attitude profile. Therefore, in a situation where an attitude profile must be tracked, null motions may be employed to ameliorate the energy requirements. To further develop and examine null motions, let

$$\{q_{ref}(t), \omega_{ref}(t), \Omega_{ref}(t), \tau_{ref}(t)\}, \quad t \in [0, t_f] \tag{3.8}$$

be an arbitrary feasible reference state-control profile that satisfies the dynamics, boundary conditions and constraints given in Eq. (3.5). By exploring null motion explicitly, we will show in the following that the energy consumption of any given feasible solution can be improved without changing the reference quaternion, $q_{ref}(t)$, or the body rate, $\omega_{ref}(t)$, profile.

For the tetrahedron wheel configuration with projection matrix A given in Table A.1, it is straightforward to show that

$$\text{null}(A) = \text{span}\left\{[1,1,1,1]^\intercal\right\} \subset \mathbb{R}^4.$$

Consider a modification on the reference control, τ_{ref}, in the null space of matrix A:

$$\tau(t) = \tau_{ref}(t) + \delta\tau(t) \cdot [1,1,1,1]^\intercal, \tag{3.9}$$

where $\delta\tau(t) : [0, t_f] \longrightarrow \mathbb{R}$ is an augmentation factor to the reference control through null motions. From the dynamics, it is easy to show that the modified control $\tau(t)$ produces the same quaternion, $q_{ref}(t)$, and the body rate, $\omega_{ref}(t)$, as the reference feasible trajectory. Similarly, the effect of the modified control on the wheel speed is given by

$$\Omega(t) - \Omega_{ref}(t) = \int_0^t \delta\tau(s)ds \cdot J_{rw}^{-1}\,[1,1,1,1]^\intercal\,. \tag{3.10}$$

For simplicity in exposition, we assume all reaction wheels are identical, therefore $J_{rw}^{-1} = cI \in \mathbb{R}^{N_{rw}\times N_{rw}}$, where $c \in \mathbb{R}_{>0}$ is the multiplicative inverse of the inertia of a reaction wheel. (If wheels are not identical, so that J_{rw} is not a multiple of identity matrix, the following analysis can be easily adapted.) It follows that

$\Omega(t) = \Omega_{ref}(t) + \delta\Omega(t) \cdot [1, 1, 1, 1]^\intercal$, where $\delta\Omega$ is one dimensional function satisfying

$$\dot{\delta\Omega} = c \cdot \delta\tau. \tag{3.11}$$

Because each wheel is assumed to begin and end with the same angular velocity, a practical operational constraint is given by the boundary conditions in Eq. (3.5), $\delta\Omega$ must have

$$\delta\Omega(0) = \delta\Omega(t_f) = 0. \tag{3.12}$$

Now it is clear that any function pair $(\delta\Omega(t), \delta\tau(t))$ that simultaneously satisfies the one dimensional linear dynamics in Eq. (3.11), boundary condition Eq. (3.12) and constraints

$$|\Omega_{ref,i} + \delta\Omega| \leq \quad \Omega_{max}, \qquad |\tau_{ref,i} + \delta\tau| \ \leq \ \tau_{max}, \quad i = 1, 2, \cdots, N_{rw} \tag{3.13}$$

produces a trajectory $\{q_{ref}(t), \omega_{ref}(t), \Omega(t), \tau(t)\}$ that satisfies all the constraints of the Minimum Energy optimal control problem given in Eq. (3.5). After some straightforward derivations, the energy consumption along such feasible solutions, generated through null motions, is given by

$$J = \frac{R}{K_T^2} \sum_{i=1}^{N_{rw}} \int_0^{t_f} \left[\delta\tau(t) + \tau_{ref,i}(t)\right]^2 + k \left[\delta\Omega(t) + \Omega_{ref,i}(t)\right]^2 dt. \tag{3.14}$$

where $k = \beta^2 + \beta K_T^2 / R$.

Based on this observation, it is possible to start from any given feasible solution of Eq. (3.5), e.g., shortest time maneuvers, and seek a function pair $(\delta\Omega(t), \delta\tau(t))$ to minimize the energy Eq. (3.14), without changing the spacecraft attitude and body rate trajectories. The function pair $(\delta\Omega(t), \delta\tau(t))$ can be determined by the following optimal control formulation, hereafter referred to as the Null Motion

(NM) problem.

$$
(\mathrm{NM})\begin{cases}
\text{State:} & \delta\Omega \in \mathbb{R}, \;\; \text{Control:} \;\; \delta\tau \in \mathbb{R} \\
\text{Minimize:} & J\left[\delta\Omega(\cdot), \delta\tau(\cdot)\right] = \frac{R}{K_T^2} \sum_{i=1}^{N_{rw}} \int_0^{t_f} \left[\delta\tau(t) + \tau_{ref,i}(t)\right]^2 + k\left[\delta\Omega(t) + \Omega_{ref,i}(t)\right]^2 dt. \\
\text{Subject To:} & \dot{\delta\Omega} = c\delta\tau, \;\; \delta\Omega(0) = \delta\Omega(t_f) = 0 \\
& |\Omega_{ref,i}(t) + \delta\Omega(t)| \leq \Omega_{max}, \\
& |\tau_{ref,i}(t) + \delta\tau(t)| \leq \tau_{max}, \quad i = 1, 2, \cdots, N_{rw}
\end{cases} \tag{3.15}
$$

The solution to problem NM generates a motion in the null space of the projection matrix A so that the feasibility of the system state trajectories are maintained, while the overall energy consumption is reduced.

It is important to point out that Problem NM can be solved with extreme efficiency due to the quadratic cost function and one dimensional linear dynamics. Indeed, when the wheel speed and torque constraints, (3.13), are not active, Problem NM admits an analytic solution given as

$$
\begin{aligned}
\delta\Omega(t) = &\left(\frac{\Omega_{\text{bias}}}{e^{c\sqrt{k}t_f}} - e^{-c\sqrt{k}t_f}\right)\left(e^{c\sqrt{k}t}(1 - e^{-c\sqrt{k}t_f}) + e^{-c\sqrt{k}t}(e^{c\sqrt{k}t_f} - 1)\right) \\
&- \frac{1}{N_{rw}} \sum_{i=1}^{N_{rw}} \Omega_{ref,i}(t),
\end{aligned} \tag{3.16}
$$

$$
\begin{aligned}
\delta\tau(t) = &-\left(\frac{\sqrt{k}\Omega_{\text{bias}}}{e^{c\sqrt{k}t_f}} - e^{-c\sqrt{k}t_f}\right)(e^{c\sqrt{k}t}(e^{-c\sqrt{k}t_f} - 1) + e^{-c\sqrt{k}t}(e^{c\sqrt{k}t_f} - 1)) \\
&- \frac{1}{N_{rw}} \sum_{i=1}^{N_{rw}} \tau_{ref,i}(t).
\end{aligned} \tag{3.17}
$$

where $\Omega_{\text{bias}} \in \mathbb{R}_{>0}$ is the bias for a single wheel speed (e.g. for the simulations in this dissertation, the speed bias for each wheel is set to 20.0 rads/sec).

We note that for a simulation study of the spacecraft parameters given in the appendix, in which several hundreds of simulations with various boundary

conditions and transfer times were performed, wheel speed saturations were not observed, and that motor torque saturation only occurred when the slew time was within 0.5% of t_{STM}. The former is very reasonable for many practical systems in which a portion of the reaction wheel momentum envelope is reserved to accommodate momentum accumulation. Hence, Eqs.(3.16)-(3.17) provide essentially a closed-form solution to Problem NM. In the rare instances where the wheel speed and/or torque constraints are active, an *analytic* solution to Problem NM can be complicated to derive, however a numerical solution to this one dimensional linear quadratic problem is easy to generate in real time onboard the spacecraft.

Solving Problem NM under

As noted in the last paragraph in the preceding section, the constraints in the Null Motion formulation of Eq. 3.15 are only active in a small window about the off-eigenaxis shortest time maneuver. This section derives the analytic solution to problem NM, given in Eqs. (3.16) and (3.17), when the constraints are not active.

To solve for the state-control pair solutions for problem NM in Eq.(3.15), Pontryagin's Minimum Principal is applied which generates a linear time-varying boundary value problem, NM^{λ} which is then analytically solved, resulting with optimal open-loop state and control profiles for problem NM. The open-loop state-control solution is then compared against solutions attained from the ME formulation, which serves to depict that the ME problem formulation minimizes $\mathcal{E}_{elec}^{rgn}$ by selecting Ω and τ through exploitation of the non trivial null space of the reaction wheel projection matrix.

The first step in determining the solution NM formulation, is building the control Hamiltonian for Eq. (3.5). To this end, the control Hamiltonian to problem

NM is given by

$$H(\lambda, \delta\Omega, \delta\tau, t) = \frac{1}{2}\sum_{i=1}^{N_{rw}}(\delta\tau + \tau_{ref,i}(t))^2 + k(\delta\Omega + \Omega_{ref,i}(t))^2 + \lambda c\delta\tau. \tag{3.18}$$

The HMC requires solving the finite dimensional optimization problem

$$\min_{\delta\tau\in\mathbb{R}} H(\lambda, \delta\Omega, \delta\tau, t),$$

which is unconstrained, at each instant of time t. Because the control is unconstrained, $\delta\tau$ which minimizes the control Hamiltonian must necessarily satisfy $\partial_{\delta\tau}H = 0$. Therefore the solution to the HMC is given by

$$\delta\tau(t) = -\frac{1}{N_{rw}}\left(\sum_{i=1}^{N_{rw}}\tau_{ref,i}(t) + c\lambda\right). \tag{3.19}$$

Since $\partial^2 H_{\delta\tau^2} = N_{rw} > 0$, Eq. (3.19) does indeed minimize H for all time-instants t. Substituting the solution of the HMC, Eq. (3.19), into the dynamics of problem NM, given in Eq. (3.11), and along with the adjoint equation $\dot{\lambda} = -\partial_{\delta\Omega}H \in \mathbb{R}$, generates a two dimensional linear time-varying boundary value problem:

$$(\mathrm{NM}^{\lambda})\begin{cases} \delta\dot{\Omega} & = -\dfrac{c^2}{N_{rw}}\lambda - \dfrac{c}{N_{rw}}\displaystyle\sum_{i=1}^{N_{rw}}\tau_{ref,i}(t) \\ \dot{\lambda} & = -N_{rw}k\delta\Omega - k\displaystyle\sum_{i=1}^{N_{rw}}\Omega_{ref,i}(t) \\ \delta\Omega(0) & = \delta\Omega(t_f) = 0 \end{cases} \tag{3.20}$$

Identifying that $\ddot{\lambda} = kc^2\lambda$, which is due to the reaction wheel torque $\tau_{\mathrm{rw}} = J_{\mathrm{rw}}\dot{\Omega}_{\mathrm{rw}}$, a closed-form for the costate λ may be identified:

$$\lambda = c_1 e^{\delta t} + c_2 e^{-\delta t}, \tag{3.21}$$

where $\delta = c\sqrt{k}$ and c_1 and c_2 are integration constants in $\mathbb{R}$.

Details:

$$\begin{aligned}
\ddot{\lambda} &= -N_{rw}k\delta\dot{\Omega} - k\sum_{i=1}^{N_{rw}}\dot{\Omega}_{ref,i} \\
&= -N_{rw}k\left(-\frac{c^2}{N_{rw}}\lambda - \frac{c}{N_{rw}}\sum_{i=1}^{N_{rw}}\tau_{ref,i}\right) - kc\sum_{i=1}^{N_{rw}}\tau_{ref,i} \\
&= kc^2\lambda
\end{aligned}$$

By solving $\ddot{\lambda} = kc^2\lambda$, which is just a second order linear ODE with constant coefficients (noting that $kc^2 > 0$), Eq. (3.21) is attained. □

With Eq. (3.21), along with the costate dynamics in Eq.(3.20), a closed form for $\delta\Omega$ is achieved from the costate dynamics in Eq. (3.20), given as

$$\delta\Omega = -c_1\gamma e^{\delta t} + c_2\gamma e^{-\delta t} - \frac{1}{N_{rw}}\sum_{i=1}^{N_{rw}}\Omega_{ref,i} \tag{3.22}$$

where $\gamma = \dfrac{c}{N_{rw}\sqrt{k}}$ and $\delta = c\sqrt{k}$.

Details:

$$\begin{aligned}
\delta\Omega &= -\frac{1}{N_{rw}k}\left(\dot{\lambda} + k\sum_{i=1}^{N_{rw}}\Omega_{ref,i}\right) \\
&= -\frac{1}{N_{rw}k}\left(c_1c\sqrt{k}e^{c\sqrt{k}t} - c_2c\sqrt{k}e^{-c\sqrt{k}t} + k\sum_{i=1}^{N_{rw}}\Omega_{ref,i}\right) \\
&= -c_1\frac{c}{N_{rw}\sqrt{k}}e^{c\sqrt{k}t} + c_2\frac{c}{N_{rw}\sqrt{k}}e^{-c\sqrt{k}t} - \frac{1}{N_{rw}}\sum_{i=1}^{N_{rw}}\Omega_{ref,i}
\end{aligned}$$

□

Note that, since each of the N_{rw} wheels begins and ends at the same wheel speed $\Omega_{\text{bias}} \in \mathbb{R}$ (so $\sum_{i=1}^{N_{rw}}\Omega_{ref,i}(0) = \sum_{i=1}^{N_{rw}}\Omega_{ref,i}(t_f) = N_{rw}\Omega_{\text{bias}}$), an analytical

solution to the open-loop time-varying state-control to problem NM may be attained: Since $\delta\Omega(0) = \delta\Omega(t_f) = 0$, c_1 and c_2 may be determined using the closed form expression for $\delta\Omega$.

$$\begin{bmatrix} -\gamma & \gamma \\ -\gamma e^{-\delta t_f} & \gamma e^{\delta t_f} \end{bmatrix} \begin{bmatrix} c_1 \\ c_2 \end{bmatrix} = \begin{bmatrix} \Omega_{\text{bias}} \\ \Omega_{\text{bias}} \end{bmatrix} \tag{3.23}$$

Solving the system in (3.23) results with

$$c_1 = \left(\frac{\Omega_{\text{bias}}}{\gamma(e^{\delta t_f} - e^{-\delta t_f})} \right) \left(e^{-\delta t_f} - 1 \right) \tag{3.24}$$

$$c_2 = \left(\frac{\Omega_{\text{bias}}}{\gamma(e^{\delta t_f} - e^{-\delta t_f})} \right) \left(e^{\delta t_f} - 1 \right) \tag{3.25}$$

Therefore an analytic solution of the open-loop time-varying state-control to problem NM is given as

Details of state $\delta\Omega$:

$$\begin{aligned}
\delta\Omega &= -c_1\gamma e^{\delta t} + c_2\gamma e^{-\delta t} - \frac{1}{N_{rw}} \sum_{i=1}^{N_{rw}} \Omega_{ref,i} \\
&= \left(\frac{-\Omega_{\text{bias}}}{\gamma(e^{\delta t_f} - e^{-\delta t_f})} \right) \left(e^{-\delta t_f} - 1 \right) \gamma e^{\delta t} + \left(\frac{\Omega_{\text{bias}}}{\gamma(e^{\delta t_f} - e^{-\delta t_f})} \right) \left(e^{\delta t_f} - 1 \right) \gamma e^{-\delta t} \\
&\quad - \frac{1}{N_{rw}} \sum_{i=1}^{N_{rw}} \Omega_{ref,i} \\
&= \left(\frac{\Omega_{\text{bias}}\gamma}{\gamma(e^{\delta t_f} - e^{-\delta t_f})} \right) \left(-e^{\delta t}(e^{-\delta t_f} - 1) + e^{-\delta t}(e^{\delta t_f} - 1) \right) - \frac{1}{N_{rw}} \sum_{i=1}^{N_{rw}} \Omega_{ref,i} \\
&= \left(\frac{\Omega_{\text{bias}}}{(e^{\delta t_f} - e^{-\delta t_f})} \right) \left(e^{\delta t}(1 - e^{-\delta t_f}) + e^{-\delta t}(e^{\delta t_f} - 1) \right) - \frac{1}{N_{rw}} \sum_{i=1}^{N_{rw}} \Omega_{ref,i} \\
&= \left(\frac{\Omega_{\text{bias}}}{(e^{c\sqrt{kt}t_f} - e^{-c\sqrt{kt}t_f})} \right) \left(e^{c\sqrt{kt}}(1 - e^{-c\sqrt{kt}t_f}) + e^{-c\sqrt{kt}}(e^{c\sqrt{kt}t_f} - 1) \right) \\
&\quad - \frac{1}{N_{rw}} \sum_{i=1}^{N_{rw}} \Omega_{ref,i}
\end{aligned}$$

□

Details of control $\delta\tau$.

$$
\begin{aligned}
\delta\tau &= -\frac{1}{N_{rw}}\left(\sum_{i=1}^{N_{rw}} \tau_{ref,i} + c\lambda\right) \\
&= -\frac{1}{N_{rw}}\left(\sum_{i=1}^{N_{rw}} \tau_{ref,i} + c(c_1 e^{\delta t} + c_2 e^{-\delta t})\right) \\
&= -\frac{1}{N_{rw}}\left(\sum_{i=1}^{N_{rw}} \tau_{ref,i} + \frac{c\Omega_{\text{bias}}}{\gamma(e^{\delta t_f} - e^{-\delta t_f})}(e^{\delta t}(e^{-\delta t_f} - 1) + e^{-\delta t}(e^{\delta t_f} - 1))\right) \\
&= \left(\frac{-\sqrt{k}\Omega_{\text{bias}}}{(e^{c\sqrt{k}t_f} - e^{-c\sqrt{k}t_f})}\right)(e^{c\sqrt{k}t}(e^{-c\sqrt{k}t_f} - 1) + e^{-c\sqrt{k}t}(e^{c\sqrt{k}t_f} - 1)) \\
&\quad - \frac{1}{N_{rw}}\sum_{i=1}^{N_{rw}} \tau_{ref,i}
\end{aligned}
$$

□

Applications of Problem NM

As a demonstrative example to the efficacy of the NM formulation of Eq. 3.15, consider the same 180-deg rotation about the spacecraft z-body axis with the transfer time is set to be $T = 281.8$ seconds – slightly longer than the minimum-time solution ($t_{STM} = 279.9$). Three feasible maneuvers are generated and compared: (*i*) A feasible fixed-time maneuver; (*ii*) A minimum energy maneuver obtained by solving problem ME per Eq. (3.5); (*iii*) A null-motion solution based on Eqs.(3.16)-(3.17) where the feasible reference trajectory $(\Omega_{ref}, \tau_{ref})$ is the same as given in (*i*).

Table 3.2 compares the energy metrics for these three maneuvers. It can be seen that both the ME (Minimum Energy) and NM (Null Motion) maneuvers perform nearly equivalently in term of energy consumption. While the ME formulation reduces energy requirements by coordinating the reaction wheel null

motions while shaping the angular velocity body profile of the spacecraft, the solution to problem NM also develops a highly efficient solution. This result is in spite of the fact that the minimization in problem NM is agnostic to the satellite attitude and rate profile and is performed only over the space of null motions.

Table 3.2: Equivalency between the Minimum Energy formulation and the Null Motion formulation for a 180-deg z-axis slew a transfer time of 281.8 seconds.

Maneuver Type	$\mathcal{E}$ (J)	$\mathcal{E}_{total}^{loss}$ (J)	$\mathcal{C}_{loss}$ (J)	$\mathcal{F}_{loss}$ (J)
Feasible Maneuver to problem ME	133.9	105.8	50.2	55.6
Problem ME solution	114.5	90.8	52.2	38.6
Problem NM solution	114.6	90.9	52.3	38.6

The null motion analysis presented in this section enables a few interesting applications, two of which are summarized as follows:

- The Null Motion formulation (3.15) and its analytic solution (3.16)-(3.17) provide a fast and computationally inexpensive way to refine any given feasible trajectory for energy reduction; thus generating sub-optimal minimum energy maneuvers. Sub-optimal, as the energy reductions are obtained by considering only a subset of the state space. Such substantial efficiency in solving Problem NM is a very attractive feature for real-time implementation.

- Problem NM provides a new means of Verification and Validation which is both computationally inexpensive and easily identifiable. Consider a candidate solution, $\{q^*, \omega^*, \Omega^*, \tau^*\}$, to the Minimum Energy Problem (ME). We can take this candidate solution as the reference in the Null Motion Problem (NM). If $\{q^*, \omega^*, \Omega^*, \tau^*\}$ is the true minimum energy maneuver, the solution to Problem (NM) should not admit additional energy reduction, i.e., the cost of Problem (NM) should be the same as the cost of the ME formulation. Independent to Pontryagin's Minimum Principle, the null motion

formulation (3.15) provides an alternative way for verifying the optimality of the minimum energy solution.

To illustrate the second point, consider a ME slew with $T = 307$ seconds, which will be seen in the next section to be the transfer time that balances both transfer time and energy. Figure 3.4.a shows that the solution to the NM problem gives $\delta\tau(t) \equiv 0$, which implies that there are no modifications to the nullspace can be made that would reduce the electrical energy further through null motions (i.e.: all possible energy savings through null motions have been exhausted). The NM solution therefore indicates that energy cannot be further reduced from the ME solution by performing null motions, a condition that a minimum energy maneuver must satisfy. Furthermore, the reaction wheel angular velocities are identical for both problem formulations (see Figure 3.4.b). Figure 3.5 shows the satisfaction of the necessary conditions to the lower Hamiltonian as well as the complementarity condition (for the spacecraft angular velocity vector ω_2). To generate the necessary conditions in Figure 3.5 requires access to the adjoints associated to the states of problem ME, and access to the adjoints requires an application of the Covector Mapping Principle[20,59] which is significantly more computationally expensive and extensive as compared to the requirements to generate the results shown in Figure 3.4. Therefore, the null motion formulation of Eq. (3.15) presents a computationally simple means to validate a candidate solution to whether the candidate solution has extracted all possible energy reducing null motions.

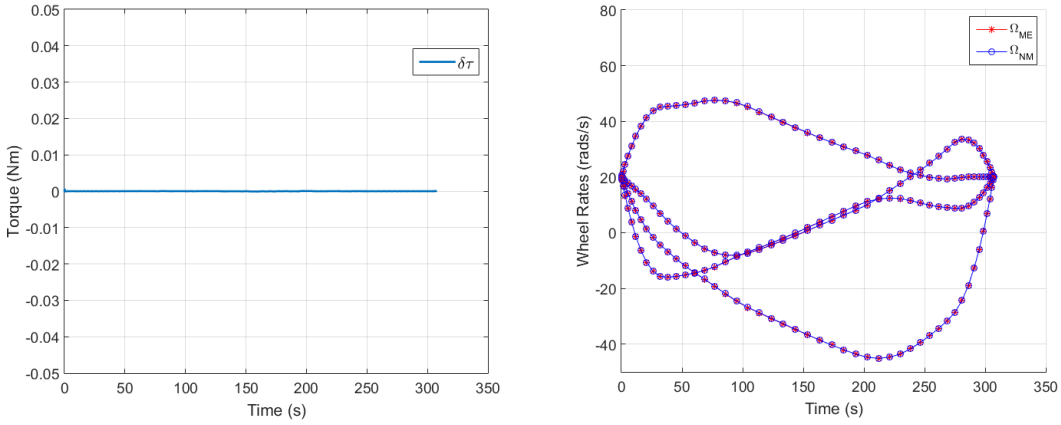

(a) (b)

Figure 3.4: Solution to Problem NM for a ME reference maneuver with a transfer time of 307 seconds, demonstrating that problem NM can serve as a computationally simple means to validate a minimal energy solution.

3.4 The Relationship Between Electric Energy and Transfer Time under Minimum Dissipative Losses

The purpose of this section is to study the relationship between transfer time and energy required to perform a slew for both eigenaxis and off-eigenaxis maneuvering. By identifying the energy/time relationships, the shortest-time maneuver satisfying a given energy budget may be identified, and a comparison may be made between on-and off-eigenaxis maneuvering concerning energy and transfer time. In determining the relationship, a 180 degree slew about the spacecraft's z-body axis is first considered, whose initial and final quaternions are $q^0 = [0, 0, 1, 0]^\intercal$ and $q^f = [0, 0, 0, 1]^\intercal$. Extensive simulations (over several hundreds) in which initial and final attitude were varied, confirmed that the relationship identified between energy and time presented for this 180 degree slew are indicative of the results for other slew sizes.The run time to generate simulation results, for each set of

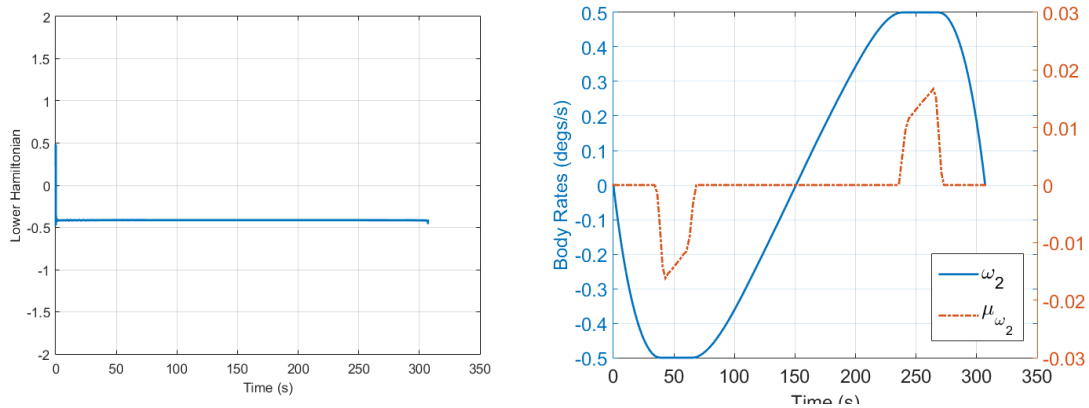

(a) (b)

Figure 3.5: Validation of necessary conditions for the minimal electrical energy slew with a transfer time of 307 seconds obtained by application of the covector mapping principle implemented in DIDO: (a) consistency of the lower Hamiltonian; (b) demonstration of complementary condition on ω_2 given in Eq. (3.7)

boundary conditions ranged from ten seconds up to about two minutes, with the average run time of approximately 55 seconds. We note that since maneuvers are often planed a priori, the solution times are amenable to practical generation.

Following the single-slew analysis, the energy and transfer-time relationship is analyzed in a typical setting for an imaging satellite: a multipoint maneuver consisting of a sequence of five slews. The multislew analysis demonstrates that the energy/time relationship identified for the 180 degree canonical maneuver holds under varying slew size, as well as path.

3.4.1 Off-Eigenaxis Slew Analysis

The shortest-time maneuver from section 3.2.2 provides the lower time-bound, t_{STM}, for which the rest-to-rest slew may be performed. By solving a series of ME formulation (off-eigenaxis) of fixed times $T \geq t_{STM}$, a Pareto front may be generated to show the minimum energy required to perform the slew for a given transfer time. This Pareto front for off-eigenaxis maneuvering is given in

Figure 3.6, with the minimized cost, $\mathcal{E}_{total}^{loss}$, shown as the lower curve with square markers that indicate the particular slew times solved. Recall the cost functional, $\mathcal{E}_{total}^{loss}$, in problem ME measures the cumulative dissipative losses incurred over a slew. From a solution to problem ME, the actual energy consumption, $\mathcal{E}$, may be calculated *a posteriori*, and is given by the top-most curve with asterix markers in Figure 3.6. We note that the optimal cost, $\mathcal{E}_{total}^{loss}$, is always slightly smaller than the actual consumed energy, $\mathcal{E}$, and forms a lower bounding curve. That the proxy $\mathcal{E}_{total}^{loss}$ forms a lower bounding curve is consistent to the fact that the control applied is optimal with respect to minimizing dissipative losses ($\mathcal{E}_{total}^{loss}$), but in general is non-optimal with respect to $\mathcal{E}$.

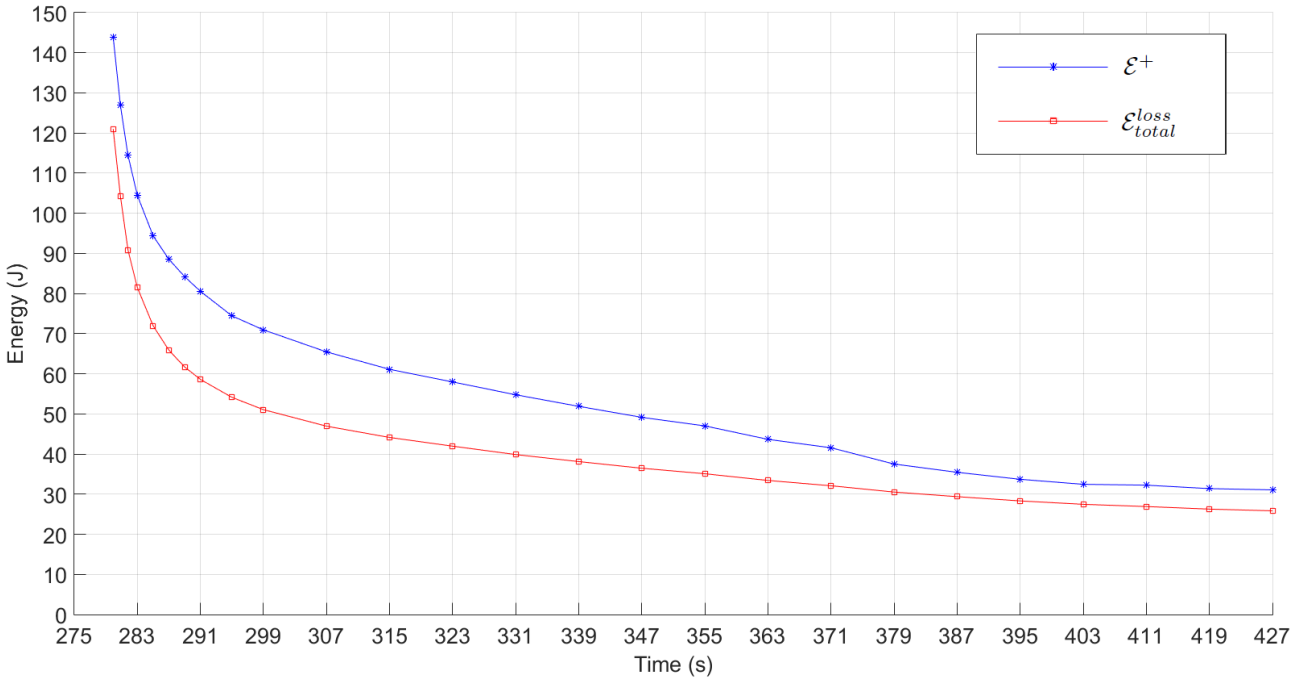

Figure 3.6: Pareto fronts to the 180-degree z-body-axis for minimum-energy off-eigenaxis maneuvering.

With the aid of the visualization provided by the Pareto front in Figure 3.6, the nonlinear relationship between the transfer time and the minimum energy required

to perform the slew is observed to consist of three phases when considering time as increasing from the shortest-time. Firstly, as transfer time is increased from the shortest-time, there exists a time window in which the energy required to perform the maneuver drastically decreases at a fast rate. Denoting this portion of the Pareto front as the head, this window of asymptotic decay beyond the shortest-time may be identified with the time interval $[t_{STM}, 307]$. Secondly, the relationship in Figure 3.6 showcases that there exists a point in time where further increasing transfer time results in insignificant reductions in energy. Defining this portion of the Pareto front as the tail, this time window may be defined as the interval $[395, \infty)$. Lastly, a third portion of the Pareto front may be identified simply as the region in between the head and tail of the Pareto front $[307, 395]$, and depicts that energy decays roughly proportionally to increasing transfer times.

The behavior of energy with respect to time within the head portion of the Pareto front validates the intuition that shortest-time maneuvers can indeed be costly maneuvers with respect to energy. More notably though, the head of the Pareto front signifies that small increases in transfer time from the shortest-time net significant savings in energy. In other words, there exists near time-optimal maneuvers which cost much less than their *minimum-energy* shortest-time maneuver counterpart. Thus, it is possible to balance energy and transfer time requirements when missions demand an agile setting, despite intuitive notions to the contrary.

The tail-portion of the Pareto front in Figure 3.6 is inversely analogous to the head region. Whereas small increases in transfer time near t_{STM} net substantial savings in energy in the head region, increases in transfer time within the tail portion of the Pareto front net only minor savings in energy. While the Pareto front of Figure 3.6 stops with a transfer time of 427 seconds, the energy and

time relationship in the tail section continues in like-manner for all time, slowly decaying over large intervals of time. Therefore, in a setting where transfer time is of no concern, the tail-portion of the energy-time relationship depicts that there is not much benefit from significantly increasing the transfer time of a maneuver with respect to energy consumption.

3.4.2 Minimum Energy Eigenaxis Slew Analysis

With the ME-EAM formulation along with the shortest-time EAM, a Pareto front describing the minimum energy transfer time relationship with respect to eigenaxis maneuvering may be built analogously to the Pareto front constructed in section 3.4.A. The result of this construction is given in Figure 3.7, and has been superimposed upon the off-eigenaxis Pareto front of Figure 3.6 to facilitate comparison. For each of the curves in Figure 3.7 the minimum-energy is reported as the $\mathcal{E}$ metric.

The Minimum Energy EAM Pareto front shown in Figure 3.7 (denoted with triangle markers that indicate the particular slew times solved) depicts an analogous relationship with respect to energy and transfer time compared to the off-eigenaxis Pareto front. Namely, near the shortest-time (for an eigenaxis maneuver), energy costs significantly increase, showing that there exist eigenaxis maneuvers with a near time optimal transfer time that require significantly less energy to execute. More interestingly, Figure 3.7 clearly shows that the minimum energy EAM curve lies completely encompassed within the region defined by the off-eigenaxis curve for all transfer times. Both maneuver types are analogous with respect to energy for slew times $T \geq 395$ seconds. This coincide point depicts that there exists a point in transfer time in which on-and off-eigenaxis maneuver types are equivalent with respect to energy consumption. In other words, *when the transfer time*

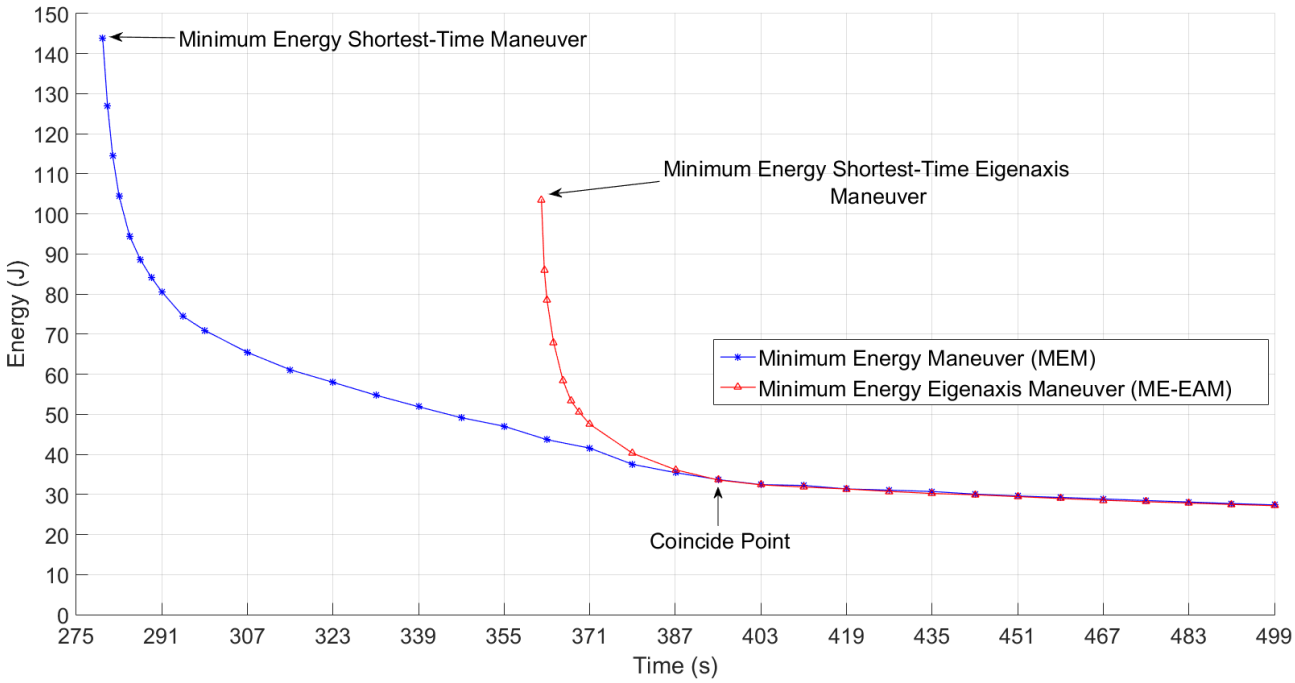

Figure 3.7: Pareto fronts for minimum electric energy off-eigenaxis and minimum electric energy eigenaxis maneuvering for a 180 degree z-body-axis slew; energy reported as $\mathcal{E}$.

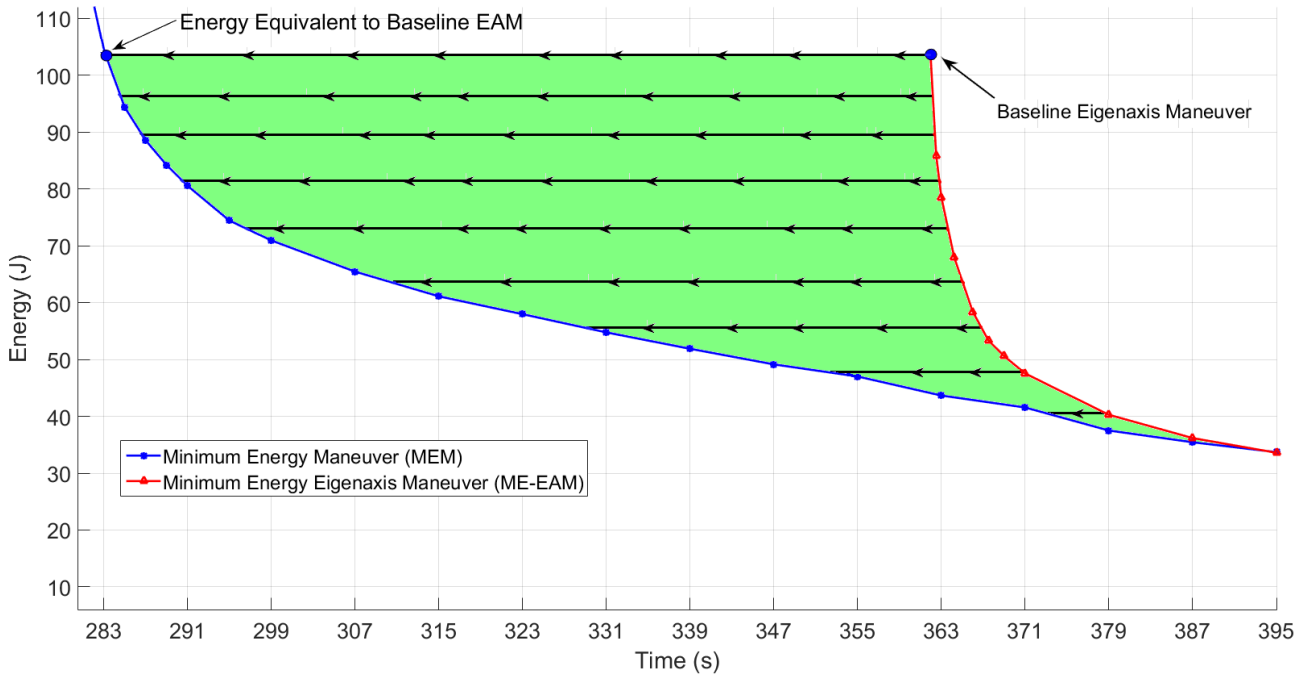

Figure 3.8: Trade space depicting the benefit of off-eigenaxis maneuvers, compared to eigenaxis, with respect to energy.

is sufficiently large, expanding the solution space from eigenaxis to non-eigenaxis slews provides no benefit in energy saving. For sufficiently-large transfer times, the minimum energy slew is an eigenaxis maneuver.

From the time optimal transfer time t_{STM}, of 279.9 seconds, to the coincide point of 395 seconds, the two Pareto fronts in Figure 3.7 imply the existence of a trade space between transfer time as well as energy between eigenaxis and off-eigenaxis maneuvering. A geometric argument may be made in discerning a trade off between the two maneuver types: A given energy budget may be visualized with a horizontal line in Figure 3.8, and in like manner, a time budget visualized as a vertical line as illustrated in Figure 3.9.

Figure 3.8 explores the trade space with respect to transfer time between eigenaxis and off-eigenaxis maneuvers. The horizontal lines in Figure 3.8 depict

that, *for every minimum energy eigenaxis slew, there exists an energy equivalent off-eigenaxis maneuver with a smaller transfer time.* Additionally, each of these off-eigenaxis maneuvers incur less dissipative losses. The extreme case with respect to transfer time is identified in Figure 3.8 by the maneuver which is energy equivalent to the minimum energy shortest-time eigenaxis maneuver, which is hereafter referred to as the "baseline EAM". Comparing to the baseline EAM, by allowing off-eigenaxis maneuvering, it is possible to decrease the transfer time by 21.7% (from 362.0 seconds to 283.1 seconds) without consuming any more energy than the baseline eigenaxis maneuver (103.5 J), while simultaneously incurring 12% less dissipative losses. Table 3.3 summarizes the energy metrics and time for the baseline eigenaxis maneuver and off-eigenaxis the energy-equivalent maneuver. Comparing this agile maneuver to time-optimal (shortest-time) maneuvering: For same energy budget of the baseline eigenaxis maneuver, the transfer time may be brought within 1% of t_{STM} by maneuvering off-eigenaxis while reducing the standard STM energy by (36.1%), and reducing dissipative losses by (40.6%). Table 3.4 summarizes the (percentage-change) difference in energy-metrics between the standard STM and the maneuver equivalent to the baseline EAM with respect to energy, depicting the reduction in energy and dissipative losses by opting for a *near* time-optimal maneuver.

Table 3.3: Metrics to the Minimum Energy Shortest-Time Eigenaxis Maneuver (baseline EAM), and energy equivalent off-eigenaxis maneuver (values in parenthesis represent percentage change from baseline EAM).

Maneuver Type	TT (s)	$\mathcal{E}_{elec}$ (J)	$\mathcal{E}_{total}^{loss}$ (J)	$\mathcal{C}_{loss}$ (J)	$\mathcal{F}_{loss}$ (J)
Baseline EAM	362.0	103.5	91.4	68.5	22.9
Energy Equivalent to baseline EAM	283.1 (-21.7%)	103.5 (0.0%)	80.8 (-11.6%)	42.7 (-37.7%)	38.2 (+66.8%)

Therefore, the transfer time may be substantially reduced through control re-allocation while simultaneously decreasing the amount of dissipative losses incurred to perform an agile maneuver, without exceeding the energy budget of

Table 3.4: Depiction of savings in energy and reduction of dissipative losses for a *near* time-optimal maneuver.

Maneuver Selection	%Δ TT	$\%\Delta\mathcal{E}_{elec}$	$\%\Delta\mathcal{E}^{loss}_{total}$	$\%\Delta\mathcal{C}_{loss}$	$\%\Delta\mathcal{F}_{loss}$
Shortest-time maneuver ⟶ Energy Equivalent to baseline EAM	+1.1%	-36.1%	-40.6%	-46.4%	-29.9.8%

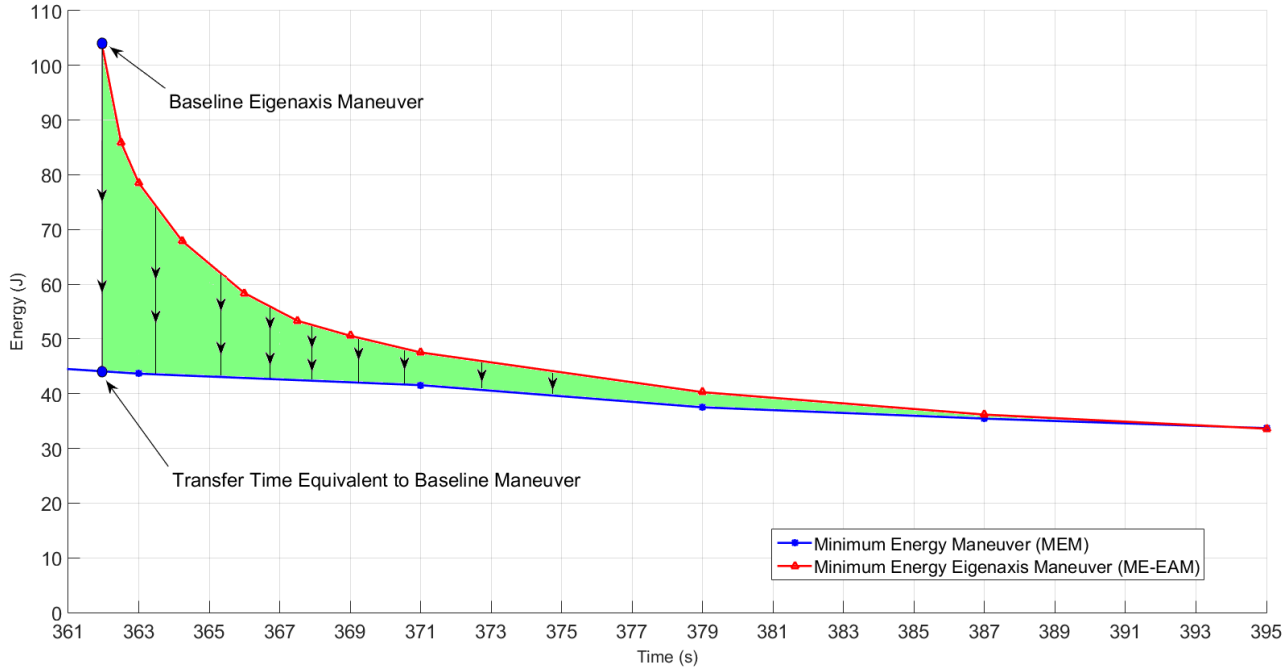

Figure 3.9: Trade Space depicting the benefit of off-eigenaxis maneuvers, compared to eigenaxis, regarding transfer time.

a canonical EAM. Additionally, with respect to shortest-time maneuvering, for a negligible increase in transfer time, the large effort associated to time-optimal maneuvering may be substantially decreased by opting for a near time-optimal maneuver, as depicted in Table 3.4. Synthesizing the analysis of these three maneuvers, along with the energy-time spectrum in Figure 3.7, it is apparent that there exists desirable agile maneuvering capabilities within (minimum) energy budgets of industry-standard eigenaxis maneuvering.

Next, we turn our attention to the trade space of energy with respect to transfer

times of minimum energy eigenaxis maneuvering: Figure 3.9 depicts that, in the case where EAM transfer times are acceptable to meet mission requirements, the energy can be substantially reduced from even minimum energy EAMs, by control re-allocation and maneuvering off-eigenaxis. The extreme case identified in the trade space of Figure 3.9 is the off-eigenaxis maneuver which completes in the same transfer time as the baseline eigenaxis maneuver. For the same transfer time as the baseline eigenaxis maneuver (which completes in 362.0 seconds), by maneuvering off-eigenaxis, the energy (given by $\mathcal{E}$) required to perform the baseline EAM is reduced by 57.5% (from 103.5 J to 44.0 J), and the cumulative dissipative losses incurred by performing the ME-EAM are reduced by 63.2% (from 91.4 J to 33.6 J). Comparing the individual dissipative losses between the two maneuvers, while the off-eigenaxis maneuver incurs 10% more friction loss (22.9 J to 25.1), it is able to reduce the copper loss by 87 % (from 68.5 J to 8.6 J). The considerable reduction in dissipative losses (from 68.5 J to 33.6 J), and therefore less heat to reject, is due to the substantial reduction in copper loss. Table 3.5 summarizes the metrics associated to the maneuver which is equivalent in transfer time to the baseline EAM.

Table 3.5: Metrics to the off-eigenaxis maneuver which is transfer time equivalent to the Minimum Energy Shortest-Time Eigenaxis Maneuver (values in parenthesis represent percentage change from the baseline EAM).

Maneuver Type	$\mathcal{E}_{elec}$ (J)	$\mathcal{E}_{total}^{loss}$ (J)	$\mathcal{C}_{loss}$ (J)	$\mathcal{F}_{loss}$ (J)
Transfer Time Equivalent to baseline EAM	44.0 (-57.5%)	33.6 (-63.2%)	8.6 (-87.4%)	25.1 (+9.6%)

The large amount of copper loss incurred by the baseline EAM is due to the torque demand required to maintain the motion along the eigenaxis. By being able to maneuver off-eigenaxis, the transfer-time equivalent maneuver is able to exploit the inertia properties of the spacecraft under both the nonlinear dynamics and constraints, requiring much less torque authority, and hence considerably

less copper loss. Therefore, *by maneuvering the spacecraft off-eigenaxis energy and dissipative losses may be substantially reduced when compared to conventional eigenaxis maneuvering.*

Shown in Figure 3.10 are the y-axis boresight traces for on-and off-eigenaxis maneuvers for the 180 degree z-body-axis slew. As expected, the eigenaxis maneuver traces out the shortest angular path, as represented by the straight-line path between the two orientations. Similarly, the boresight traces of the two maneuvers equivalent to the baseline eigenaxis maneuver each illustrate off-eigenaxis motion, as seen by deviating from the circular arc traced by the baseline EAM.

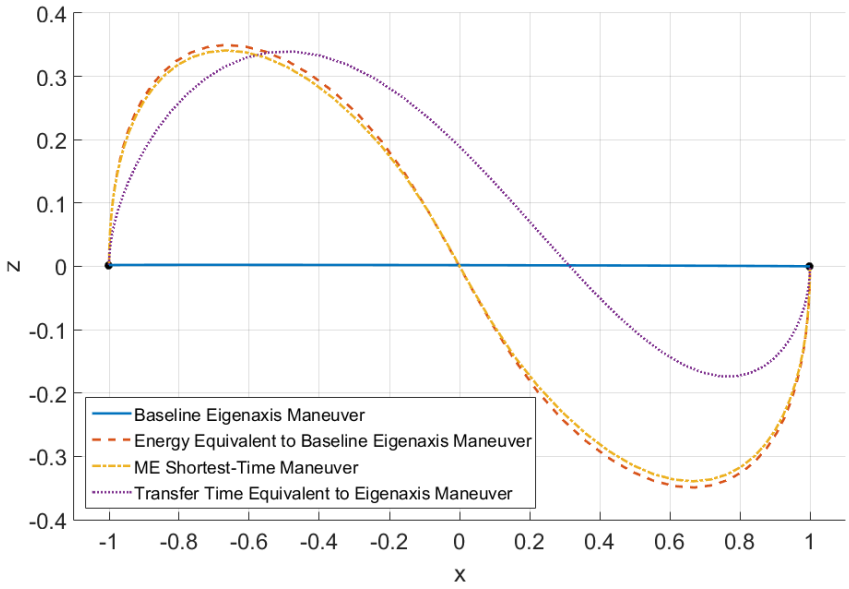

Figure 3.10: Boresight traces for various maneuver-types performing a 180 degree z-body-axis slew.

3.4.3 Operational Scenario: Multipoint Slew

This section expands upon the analysis of the previous sections, by considering a multipoint slew consisting of five sequential maneuvers. A multislew maneuver is considered here to demonstrate that *each* of the properties resultant from the

analysis of the single slew directly translate to a typical operational scenario for an imaging spacecraft involving multiple collection points. The five-point multislew is based off of the STAR pattern developed in Ref. [6], and consists of reorienting the imaging boresight (aligned with the spacecraft y-axis) over both medium angle ($\approx$30 degrees) and large angle ($\gg$ 30 degrees) slews. The relevant attitude parameters for both on-and off-eigenaxis maneuvering for the five-point multislew are given in Table 3.6.

Table 3.6: Sequence of quaternions for the five-point multislew maneuver.

Orientation	q_1	q_2	q_3	q_4
1	0.0602	0.1850	0.6165	0.7629
2	0.2860	0.0069	0.5607	0.7770
3	0.1864	0.0045	0.0854	0.9788
4	0.1195	0.1431	0.7921	0.5812
5	0.1314	0.1263	0.2458	0.9520
6	0.1693	0.0781	0.4666	0.8646

Four maneuver types are selected to explore the trade space between energy and transfer time between on-and off-eigenaxis maneuvering: (*i*) & (*ii*) The ME shortest-time maneuver and ME shortest-time eigenaxis maneuver which represent the minimum energy required to complete the multislew for time optimal off-and on-eigenaxis maneuvers; each respectfully referred to, as the "baseline off-eigenaxis maneuver" and "baseline eigenaxis maneuver"; (*iii*) The (off-eigenaxis) maneuvers which are energy equivalent (with respect to $\mathcal{E}$) to each baseline eigenaxis maneuver; (*iv*) The (off-eigenaxis) maneuvers which are equivalent with respect to transfer times of the baseline eigenaxis maneuver. Figure 3.11 depicts each of the four maneuver types as corner points on the energy-time trade-space for a conceptualized Pareto front.

For the multislew the ME shortest-time maneuvers, compared to their time optimal EAM counterparts (the baseline EAMs), are able to decrease transfer

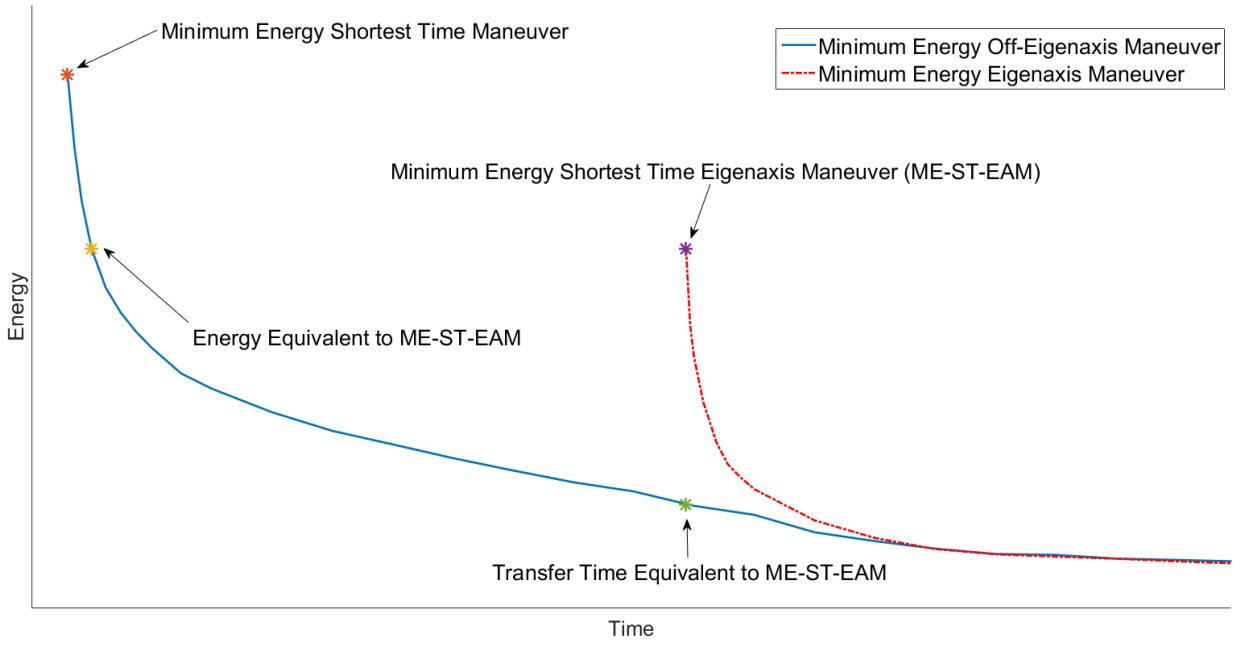

Figure 3.11: Visualization of the four maneuver types to explore the trade space between on-and off-eigenaxis maneuvering for the multislew scenario.

time by 19.6% (from 649.4 seconds to 522.0 seconds) but at the substantial cost of increased energy consumption, up by 124% (from 409.6 J to 918.5 J). It seems that experience and intuition is true, that min time solutions demand considerable effort, but because each individual slew has an energy and transfer time relationship analogs to Figure 3.7, there exist agile maneuvers (i.e. maneuvers with a smaller transfer time than eigenaxis maneuvering) with significantly less stringent energy requirements. By maneuvering off-eigenaxis, for the *same energy budget* as the baseline EAMs, the multislew may be completed within 5.7% of the time optimal transfer time (from 522.0 seconds to 551.9 seconds) while consuming 55.6% less energy than the baseline off-EAMs (from 918.5 J to 408.6 J). Comparing this agile maneuver, the transfer time of the baseline EAMs may be reduced by 15% (from 649.4 seconds to 551.9 seconds) for the same energy required to perform

canonical eigenaxis maneuvering. Considering the situation of minimizing energy, by allowing off-eigenaxis maneuvering, the maneuver-set transfer-time equivalent to the baseline EAMs is able to decrease the energy requirements by 53% (from 409.6 J to 191.4 J), the lowest of the four maneuver types. Table 3.8 summarizes the tradeoffs between energy and transfer time for various maneuver types. Viewing the four representative maneuver types together, the energy-equivalent and transfer-time equivalent off-eigenaxis maneuvers, compared to the baseline EAMs, depict that *there exists a significant penalty in slew time and energy when enforcing eigenaxis rotations*. Similarly demonstrated by this simulation example, is that the properties inherent to the single slew analysis translate to a multislew environment. By allowing the spacecraft to maneuver off-eigenaxis, the optimization may take full advantage of the attitude control-capability as represented by the spacecraft agilitoid ,[20] as seen by the energy and transfer time equivalent maneuvers to the baseline eigenaxis maneuver.

Maneuver Type	TT (s)	$\mathcal{E}$ (J)
ME Shortest-Time Maneuver	522.0	918.5
Energy Equivalent to Baseline Eigenaxis Maneuver	551.9	408.6
Baseline Eigenaxis Maneuver	649.4	409.6
Transfer Time Equivalent Baseline Eigenaxis Maneuver	649.4	191.4

Table 3.7: Transfer times and metric totals for the four maneuver-types to the five-point multislew.

Table 3.8: The difference in energy and transfer time by opting between various maneuver-types for the multipoint slew.

Change of Maneuver Type	%Δ TT	%Δ$\mathcal{E}$
Baseline Eigenaxis Maneuver $\longrightarrow$ ME Shortest-Time Maneuver	-19.6%	+124.2%
ME Shortest-Time Maneuver $\longrightarrow$ Energy Equivalent Eigenaxis Maneuver	+5.7%	-55.5%
Baseline Eigenaxis Maneuver$\longrightarrow$ Energy Equivalent Eigenaxis Maneuver	-15.0%	-0.2%
Baseline Eigenaxis Maneuver $\longrightarrow$ Transfer Time Equivalent Eigenaxis Maneuver	0%	-53.3%

The boresight traces over the course of the five-point multislew are given in

Figure 3.12 for the baseline off-and on-EAMs, along with the energy-equivalent and transfer-time equivalent maneuvers in Figure 3.13. The imaging boresight for the baseline EAMs, as expected, traces out shortest-circular arcs between the five capture-locations. Similarly expected, from Figure 3.12a, the motion of the boresight to the baseline off-EAMs deviates from the eigenaxis for each of the five orientations. For reference, the boresight trace to the standard STMs are identical to those given in Figure 3.12a. Similarly, the energy-equivalent and transfer-time equivalent maneuvers show that the entire multipoint slew is performed off-eigenaxis. That the traced-path between each of the five orientations for the three off-eigenaxis maneuver-types are each distinct, is due to the combination of the boundary conditions as well as the inertia properties of the spacecraft. Since the rotational-maneuvers are not restricted about an eigenaxis, the optimization may minimize energy by taking full advantage of the spacecraft's geometry per the boundary conditions when determining a feasible slew.

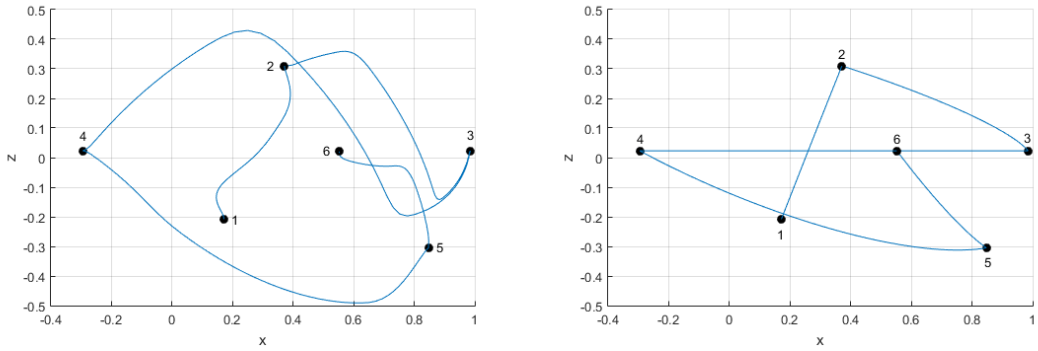

Figure 3.12: Boresight Traces to two of the four maneuver-types from Figure 3.11.

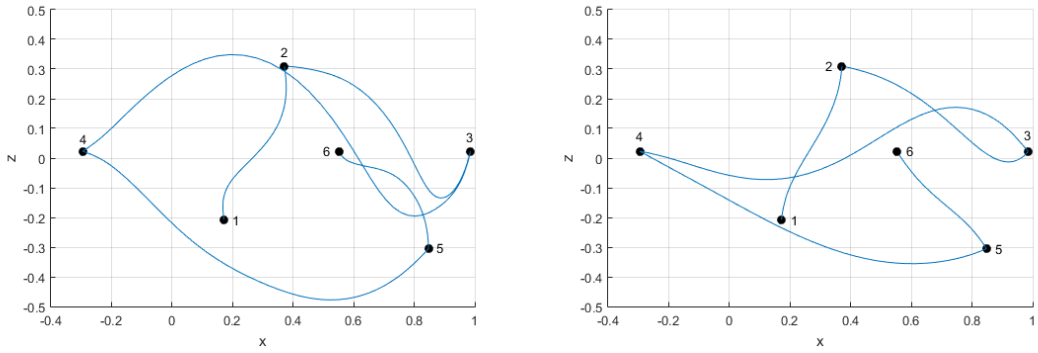

(a) **(b)**

Figure 3.13: Boresight traces to two of the four maneuver-types from Figure 3.11.

3.5 Conclusions

In this chapter, energy metrics that are in-line with the true operational cost of performing a slew are derived based on modeling the reaction wheels as DC motors in steady state. A family of nonlinear constrained optimal control problems were developed to reduce the electrical energy under minimal dissipative losses for both conventional eigenaxis maneuvering and off-eigenaxis maneuvering. A constraint was developed to enforce eigenaxis maneuvering, which allowed unconventional off-eigenaxis maneuvering to be compared to eigenaxis maneuvering, which allowed the study of how stringent upon energy and time eigenaxis maneuvering can be to a spacecraft.

This chapter has identified and studied the nonlinear relationship which arises between slew time and energy for reaction wheel attitude control under both conventional eigenaxis and agile off-eigenaxis maneuver schemes. This was done by formulating and solving a series of fixed-time optimal control problems where energy metrics, in-line with the true operational cost of performing a slew are derived based on modeling the reaction wheels as DC motors in steady state.. The nonlinear time-energy relationship showed two main results which hold both for eigenaxis and non-eigenaxis maneuvers: (i) There exist a continuum of near time-optimal maneuvers that require substantially less energy than their shortest-time counterpart. The saving in energy is realized via a re-allocation of the control effort by exploiting energy-reducing null motions within the control space while shaping the velocity of the spacecraft body. (ii) There exists a slew time beyond which savings in energy become negligible.

This chapter further demonstrates the existence of a trade-space between on- and off eigenaxis maneuvering. This trade-space shows that a significant penalty is incurred upon slew time and energy when enforcing eigenaxis maneuvering: (i)

By maneuvering off-eigenaxis, slew time may be significantly decreased for the same energy budget as an eigenaxis maneuver. (*ii*) By maneuvering off-eigenaxis, energy may be greatly decreased for the same slew time budget as a conventional eigenaxis maneuver.

The nonlinear relationship between slew time and energy, and the trade-space between on-and off eigenaxis maneuvering demonstrated in this chapter can be exploited for mission operations, planning and design. Lastly, a simplified optimal control formulation that operates over a subspace of the system state space was derived to approximate minimum-energy maneuvers via null motions. This development, directed at legacy control systems, was shown to generate, reduced energy solutions for any feasible attitude trajectory in real time.

Chapter 4

Minimizing the Nonsmooth Electrical Energy Metric though L1 Optimal Control

> "The best and most beautiful things in the world cannot be seen or even touched - they must be felt with the heart."
>
> *Helen Keller*

4.1 Introduction

In Chapter 2, the derivations of the electrical power-input equation for a reaction wheel showed that it is nonsmooth with respect to its arguments (which are angular velocity and torque of the reaction wheel relative to its spin axis). Indeed, the electrical power-input equation was shown (in Chapter 2) to be an L^1 norm of its arguments. Therefore, attempting to minimize the electrical energy of a reaction wheel spacecraft leads to a complicated nonsmooth optimal control problem.

From either a static (i.e. at each instant of time) or a dynamic (i.e. over the entire trajectory) perspective of optimization, majority of the existing work focused upon proxies to measure electrical energy and power which reduce mechanical power. Schaub & Lappas in Ref. [35] modeled total power of the reaction wheels as the L^1 norm of mechanical power and devised a feedback strategy to minimize the instantaneous ℓ^2 norm of mechanical power $\tau\Omega$ for each reaction wheel. Blenden and Schaub in Ref. [24] branched off of Ref. [35] by devising a feedback strategy minimizing mechanical power, under the assumption that 100% of the energy (modeled as *mechanical only*) may be recouped when braking a reaction wheel. Skaar and Kraige in Refs, [55] and [56] devised open-loop minimum effort reaction wheel slews for one and three wheels respectively where the cost functional was taken as the ℓ^2 norm of mechanical power of the reaction wheel(s). The NASA technical report by Williams of Ref. [54], is a very early work focused upon minimum effort reaction wheel slews. Techniques of dynamic optimization were invoked to minimize the copper loss of a single reaction wheel motor. Since no friction was assumed in the reaction wheel motor (i.e. the motor is ideal) the minimization was equivalent to minimizing the ℓ^2 norm of the reaction wheel motor torque, i.e.$\int_{t_0}^{t_f} \|\tau\|_2^2 \, dt$. Grassi in Ref. [60] approached minimizing the effort to reaction wheels by minimizing the copper-loss of each reaction wheel; because no friction was considered in the model, the minimization was analogous to minimizing the ℓ^2 norm of reaction wheel motor torque. Chapter 3, which studied and analyzed the relationship between electrical energy and transfer time,[61] acknowledged the difficulty posed of the electric power-input metric, by opting for a cost functional which minimized dissipative losses; a naturally occurring quadratic functional.

The prime directive of this chapter is to *directly* minimize the nonsmooth

reaction wheel electric power-input equation as the running cost, i.e.,

$$\begin{aligned}\text{Minimize: } J\left[x(\cdot),u(\cdot)\right] &= \int_0^T \mathcal{P}_{\text{array}}(t)\,dt \\ &= \frac{1}{2}\int_0^T \left\{\sum_{i=1}^{N_{\text{rw}}} \mathcal{P}_i(t) + \sum_{i=1}^{N_{\text{rw}}} \left|\mathcal{P}_i(t)\right|\right\} dt \\ &= \frac{1}{2}\int_0^T \left\{\sum_{i=1}^{N_{\text{rw}}} \mathcal{P}_i(\Omega_{\text{rw}},\tau_{\text{rw}}) + \sum_{i=1}^{N_{\text{rw}}} \left|\mathcal{P}_i(\Omega_{\text{rw}},\tau_{\text{rw}})\right|\right\} dt \end{aligned} \tag{4.1}$$

thereby circumventing the use or need of proxies.

In this chapter we adopt an augmentation method which transforms the nonsmooth L^1 minimum energy slews problems into an equivalent smooth optimal control problem. This is achieved through a judicious addition of ancillary decision variables and path constraints. Once the problem is transformed into a smooth version, standard techniques of optimal control may be invoked to obtain a solution. It will be shown in this chapter, that the transformation from nonsmooth to an equivalent smooth formulation substantially increases the dimensionality of the optimal control problem, adding additional control variables, as well as additional path constraints, thereby generating a complicated system of differential algebraic equations.

4.2 An Illustrative Example of Solving L1 Optimal Control Problems

To illustrate the process of solving a nonsmooth L^1 optimal control problem by developing an equivalent smooth formulation, a simple rigid body motion planning problem is considered. This problem is based on a formulation by Gong et al. from Ref [62]. The problem seeks to minimize the amount of work required move a block (of unit mass) along a flat surface, from a fixed starting position and velocity, to

a fixed end position and velocity, in a fixed amount of time, through application of a limited amount of force (see Figure 4.1).

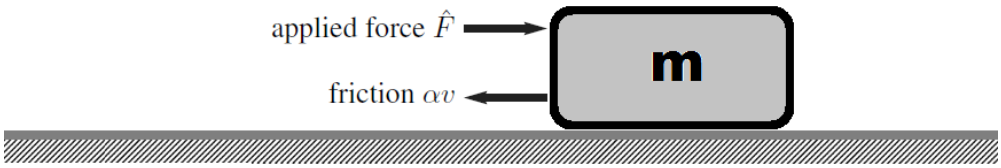

Figure 4.1: Schematic of the Gong motion-planning problem: Minimize the work to move a rigid body from one fixed position and velocity to another in a fixed amount of time under the influence of a viscous friction term.

The example L^1 motion-planing problem, which serves to be the problem for this section, is given as follows and is hereafter referenced as problem "G_{ns}":

$$
(G_{\text{ns}}) \left\{ \begin{array}{ll}
\text{State:} & \boldsymbol{x} = [x, v]^{\mathsf{T}} \in \mathbb{R}^2, \quad \text{Control:} \quad \hat{F} \in \mathbb{R} \\
\text{Minimize:} & J\left[\boldsymbol{x}(\cdot), \hat{F}(\cdot)\right] = \displaystyle\int_{t_0}^{t_f} \left| v(t)\hat{F}(t) \right| \, dt \\
\text{Subject To:} & \\
& \begin{bmatrix} \dot{x} \\ \dot{v} \end{bmatrix} = \begin{bmatrix} v \\ -\alpha v + \hat{F} \end{bmatrix} \\
& t_0 = 0, t_f = 1 \\
& \boldsymbol{x}(t_0) = \begin{bmatrix} 0 & v^0 \end{bmatrix}^{\mathsf{T}} \in \mathbb{R}^2 \\
& \boldsymbol{x}(t_f) = \begin{bmatrix} x^f & v^f \end{bmatrix}^{\mathsf{T}} \in \mathbb{R}^2 \\
& \left| \hat{F} \right| \leq \hat{F}_{max}
\end{array} \right.
$$

The state vector consists of the position and velocity of the mass. The control is taken as the force acting perpendicular to the mass, and is bounded by a fixed-amount $\hat{F}_{max}$, $\alpha \in \mathbb{R}_{>0}$ is a parameter representing viscous friction term. The cost functional is a metric which describes the amount of work-effort performed,

and the absolute value (about the running cost) emphasizes that effort is taken to *either* speed up or slow down the mass-block (i.e. effort to accelerate or decelerate the mass). The presence of the L^1 cost functional makes problem G_{ns} non-differentiable with respect to state as well as control. Through the addition of auxiliary decision variables and constraints linear in the running cost, the nonsmooth G_{ns} may be transformed into an equivalent *smooth* optimal control problem. The set of auxiliary decision variables and associated path constraints, which transform the nonsmooth problem G_{ns} into an equivalent smooth formulation is based on the approaches outlined in Refs. [58, 63]. Considered first, is the quantity which the L^1 norm acts upon:

$$z(t) \triangleq v(t)\hat{F}(t). \tag{4.2}$$

Next, the positive and negative portions of z are defined as

$$z_a(t) \triangleq \left\{v(t)\hat{F}(t)\right\}^+ \qquad \text{and} \qquad z_b(t) \triangleq \left\{-v(t)\hat{F}(t)\right\}^+, \tag{4.3}$$

where $\{\cdot\}^+$ is the operator which takes only the positive part, and is defined as

$$\{f(t)\}^+ = \begin{cases} f(t) & \text{if } f(t) > 0 \\ 0 & \text{if } f(t) \leq 0 \end{cases}.$$

By the manner in which z, z_a, and z_b are defined, the following relationships hold for all $t \in [t_0, t_f]$:

$$z(t) = z_a(t) - z_b(t) \tag{4.4}$$

$$|z(t)| = z_a(t) + z_b(t) \tag{4.5}$$

$$z_a(t), z_b(t) \geq 0 \tag{4.6}$$

Next, the minimization of

$$\int_{t_0}^{t_f} \left| v(t)\hat{F}(t) \right| \, dt$$

may be achieved by minimizing

$$\int_{t_0}^{t_f} z_a(t) + z_b(t) \, dt \tag{4.7}$$

when the following four path constraints are satisfied for all time $t \in [t_0, t_f]$:

$$z_a(t) \geq 0 \qquad z_b(t) \geq 0 \qquad z_a(t) - z(t) \geq 0 \qquad z_b(t) + z(t) \geq 0 \tag{4.8}$$

The motivation to why minimizing the cost functional in Eq. (4.7) under the constraints in Eq. (4.7) leads to the minimization of Eq. (4.7), is from the fact the sum of two nonnegative numbers, $z_a(t) + z_b(t)$, is being minimized; if one is nonzero, then the other must take on the value of zero for minimum to be obtained. Note that z_a and z_b are *both* control variables, and hence need not be continuous, and are free to be chosen. Fix $t \in [t_0, t_f]$ and suppose that $z(t) \triangleq v(t)\hat{F}(t)$ is piecewise continuous on $[t_0, t_f]$. If $z(t) \geq 0$, then $z_a(t) \geq z(t) \geq 0$ and $z_b(t) \geq 0 \geq -z(t) \leq 0$, so $z_a(t) + z_b(t) \geq z(t)$. Therefore $\min\{z_a(t) + z_b(t)\} = z(t)$. If $z(t) < 0$, then $z_a(t) \geq 0$ and $z_b(t) \geq -z(t) > 0$, so $z_a(t) + z_b(t) \geq -z(t)$. Therefore $\min\{z_a(t) + z_b(t)\} = -z(t)$. Consider an interval $[t_i, t_j]$ in which $z(t) \geq 0$, then

$$\int_{t_i}^{t_j} z_a(t) + z_b(t) \, dt \geq \int_{t_i}^{t_j} z(t) \, dt \geq 0 \tag{4.9}$$

Consider an interval $[t_i, t_j]$ in which $z(t) < 0$, then

$$\int_{t_i}^{t_j} z_a(t) + z_b(t) \, dt \geq \int_{t_i}^{t_j} -z(t) \, dt > 0 \tag{4.10}$$

Therefore, when for all $t \in [t_0, t_f]$, $z_a(t) \geq 0, z_b(t) \geq 0, z_a(t) - z(t) \geq 0, z_b(t) + z(t) \geq 0$, minimizing $\int_{t_0}^{t_f} z_a(t) + z_b(t)\, dt$ is equivalent to minimizing $\int_{t_0}^{t_f} |z|\, dt$. Note that, from the preceding arguments, the following nonlinear relation is obtained: $z_a(t) z_b(t) = 0$ for all $t \in [t_0, t_f]$. Therefore, the nonsmooth problem formulation G_{ns} may be transformed into an equivalent smooth formulation, by the addition of the defined axillary decision variables and approach outlined in Eqs. (4.2)-(4.8). This formulation is denoted G_{s} and is given as follows:

$$
\text{(Gs)} \left\{ \begin{array}{ll}
\text{State:} & \boldsymbol{x} = [x, v]^{\mathsf{T}} \in \mathbb{R}^2, \quad \text{Control:} \quad \boldsymbol{u} = \left[\hat{F}, z_a, z_b\right] \in \mathbb{R}^3 \\
\text{Minimize:} & J\left[\boldsymbol{x}(\cdot), \hat{F}(\cdot)\right] = \displaystyle\int_{t_0}^{t_f} z_a(t) + z_b(t)\, dt \\
\text{Subject To:} & \\
& \begin{bmatrix} \dot{x} \\ \dot{v} \end{bmatrix} = \begin{bmatrix} v \\ -\alpha v + \hat{F} \end{bmatrix} \\
& \\
& t_0 = 0, t_f = 1 \\
& \\
& \boldsymbol{x}(0) = \begin{bmatrix} x^0 & v^0 \end{bmatrix}^{\mathsf{T}} \in \mathbb{R}^2 \\
& \boldsymbol{x}(t_f) = \begin{bmatrix} x^f & v^f \end{bmatrix}^{\mathsf{T}} \in \mathbb{R}^2 \\
& \\
& \left|\hat{F}\right| \leq \hat{F}_{max} \\
& \\
& z_a(t) \geq 0 \\
& z_b(t) \geq 0 \\
& z_a(t) - v(t)\hat{F}(t) \geq 0 \\
& z_b(t) + v(t)\hat{F}(t) \geq 0
\end{array} \right.
$$

The only difference between G_{ns} and G_{s} is the addition of the ancillary controls z_a, z_b along with the four path constraints $z_a(t), z_b(t) \geq 0$ and $z_a(t) - v(t)\hat{F}(t) \geq 0$, and $z_b(t) + v(t)\hat{F}(t) \geq 0$, which allow the minimization of the desired cost functional of problem G_{ns}. The "cost" for generating the equivalent smooth formulation of problem G_{ns} is an increase of two controls and four path constraints. While numerically solving optimal control problems with path constraints is a difficult problem,[20,64] standard numerical techniques in (smooth) optimal control[33] may be applied to obtain candidate solutions to problem G_{ns}.

Since problem G_{s} is smooth, the necessary conditions of optimality via Pontryagin's Minimum Principle may be obtained. Access to the necessary conditions allows the validation of numerical candidate solutions for optimality. What follows is a derivation of the necessary conditions of optimality to problem G_{s}, which will be used to validate the candidate numerical solutions. Define the costate as $\lambda = \Big[\lambda_x, \lambda_v\Big] \in \mathbb{R}^2$, and the control Hamiltonian as

$$H(\lambda, x, u) = z_a + z_b + \lambda_x v + \lambda_v\Big(-\alpha v + \hat{F}\Big). \tag{4.11}$$

The Hamiltonian Minimization Condition (HMC) is given as given as

$$\text{(HMC)} \begin{cases} \text{Min:} & H(\lambda, x, u) = z_a + z_b + \lambda_x v + \lambda_v\Big(-\alpha v + \hat{F}\Big) \\ \text{Subject to:} & \\ & -\hat{F}_{max} \leq \hat{F} \leq \hat{F}_{max} \\ & z_a(t) \geq 0 \\ & z_b(t) \geq 0 \\ & z_a(t) - v(t)\hat{F}(t) \geq 0 \\ & z_b(t) + v(t)\hat{F}(t) \geq 0 \end{cases} \tag{4.12}$$

Because of the addition of the path and box constraints upon the control vari-

ables, the Karush-Kuhn-Tucker (KKT) conditions must be applied to determine the necessary conditions of the HMC. The KKT conditions are applied through building the Lagrangian of the Hamiltonian. Since there are five path constraints in the HMC in Eq. (4.12), the path covector of KKT multipliers μ is of dimension five, and is defined as $\mu = \left[\mu_{\hat{F}}, \mu_a, \mu_b, \mu_{pos}, \mu_{neg}\right]^\intercal \in \mathbb{R}^5$ where subscripts describes the variable associated to each covector. The Lagrangian of the Hamiltonian is given as

$$\begin{aligned}\overline{H}(\mu, \lambda, x, u) &= H(\lambda, x, u) + \mu^\intercal h(x, u) \\ &= z_a + z_b + \lambda_x v + \lambda_v\Big(-\alpha v + \hat{F}\Big) \\ &\qquad + \mu_{\hat{F}}\hat{F} + \mu_a z_a + \mu_b z_b + \mu_{pos}\Big(z_a - v\hat{F}\Big) + \mu_{neg}\Big(z_b + v\hat{F}\Big).\end{aligned}$$

From the KKT conditions, at each time instant, the Lagrangian of the Hamiltonian must be stationary to the control u, that is $\partial_u \overline{H} = 0 \in \mathbb{R}^3$. Therefore the stationary condition gives three equations which all optimal solutions must necessarily satisfy:

$$0 = \begin{bmatrix} \lambda_v + \mu_{\hat{F}} - v(\mu_{pos} - \mu_{neg}) \\ 1 + \mu_a + \mu_{pos} \\ 1 + \mu_b + \mu_{neg} \end{bmatrix} \tag{4.13}$$

The KKT conditions additionally require the control u and path covector μ to satisfy the complementarity conditions. For brevity only the condition on $\hat{F}$ and

$\mu_{\hat{F}}$ is presented, as all other complementarity conditions are analogously defined:

$$\mu_{\hat{F}} \begin{cases} \leq 0 & \hat{F} = -\hat{F}_{max} \\ = 0 & -\hat{F}_{max} < \hat{F} < \hat{F}_{max} \\ \geq 0 & \hat{F} = \hat{F}_{max} \end{cases} \tag{4.14}$$

Along with the necessary conditions given by the stationary and complementarity conditions, another invaluable necessary condition is arrived upon by considering the lower Hamiltonian. The lower Hamiltonian, $\mathcal{H}$, is acquired by evaluating the control Hamiltonian along an extremal solution, u^*, of the HMC. That is

$$\mathcal{H}(\lambda, x) \triangleq H(\lambda, x, u^*).$$

Since the control Hamiltonian is time invariant, the Hamiltonian Evolution Condition states that candidate optimal solutions are such that the lower Hamiltonian is constant for all time; that is

$$\frac{d}{dt}\mathcal{H}(\lambda, x) = 0 \qquad \text{for all } t \in [t_0, t_f].$$

The adjoint equations are

$$\begin{aligned} \dot{\lambda}_x &= 0 \\ \dot{\lambda}_v &= -\lambda_x + \alpha\lambda_v + \hat{F}(\mu_{pos} - \mu_{neg}) \end{aligned} \tag{4.15}$$

Problem G_{s} was solved by DIDO with the data given in Table 4.1. The numerical results obtained is shown in Figure 4.2. The states x and v are shown in Figure 4.2a and are seen to satisfy the boundary conditions of problem G_{s}. Due to L^1 optimization, and the intuition of the controls obtained in Refs. [65–67],

Table 4.1: Simulation parameters for Problem G_{s}

parameter	value
x^0	0
v^0	1
x^f	1
v^f	0.5
F_{max}	3
α	1

the optimal control is expected to have a bang-off-bang structure for problem G_{s}, which is the case as Figure 4.2b. Figure 4.4a demonstrates the validity of the Hamiltonian Evolution Condition with the lower Hamiltonian being $\mathcal{H}(t) \approx -2.5$ for all $t \in [t_0, t_f]$. Figure 4.4b depicts that the control, $\hat{F}$ and associated KKT multiplier $\mu_{\hat{F}}$, satisfy the complimentary condition given in Eq. (4.14). The numerical solution obtained by DIDO satisfies the three stationary conditions, given in Eq. (4.13): Figure 4.3a shows the consistency of one of the three stationary conditions (the other two, while satisfied, are omitted for brevity). Lastly, when deriving the adjoint equations the costate associated with the state variable x must necessarily be constant for all time (see Eq. (4.15)), which is the case as seen in Figure 4.3b. Other necessary conditions such as the Hamiltonian value condition or transversality conditions, have each been verified but are omitted due to brevity. Therefore, the candidate solution to problem G_{s} passes the necessary conditions of optimality.

The feasibility of u^*, the extremal control, is verified by propagating u^* through the dynamics using a standard Runge-Kutta (RK) integrator. As seen in Figure 4.5, the solution returned by the RK integrator coincides with the solution obtained by the numerical optimal control solver.

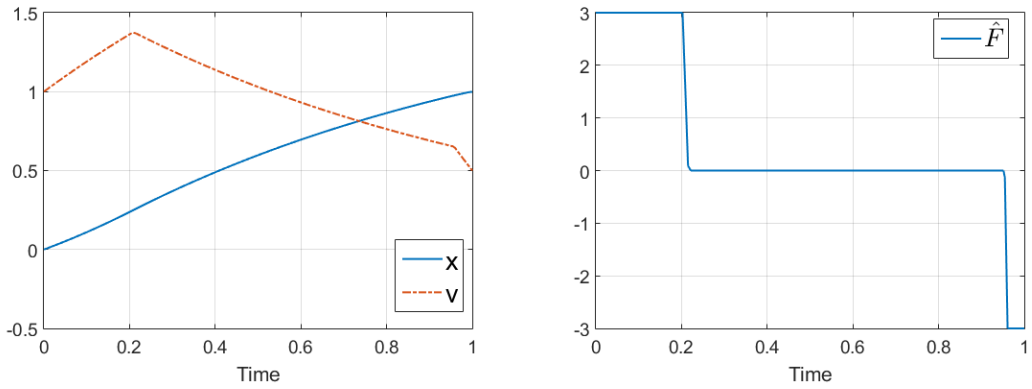

Figure 4.2: State and control profiles to problem G_s: (a) position (x) and velocity (v) of the rigid body; (b) force applied to the mass.

4.3 Development of the Minimum Electrical Energy Slew Problem Formulation

The goal of this section is to revisit the energy-time relationship studied in Chapter 3 for minimum dissipative losses (and hence reduced electrical energy), but now study the relationship under the *true cost* of the electric power-input equation of Eq. (2.19), hence truly study the minimum electrical energy and transfer time relationship for reaction wheel spacecraft. The cost functional to minimize the electrical energy of a reaction wheel array generates a L^1 optimal control problem of mixed control and state. In this section, the method to solve L^1 of mixed control and state illurstrated in Section 4.2, is applied to solve for minimum electrical energy spacecraft slews. Practical constraints pertinent to an operational environment are considered, just as those considered in Chapter 3 which studied the energy-time relationship minimizing dissipative losses. Namely, these constraints consist of (i) constraints upon the maximum generatable torque by the reaction wheels; (ii) constraints upon the rate gyros upon the spacecraft

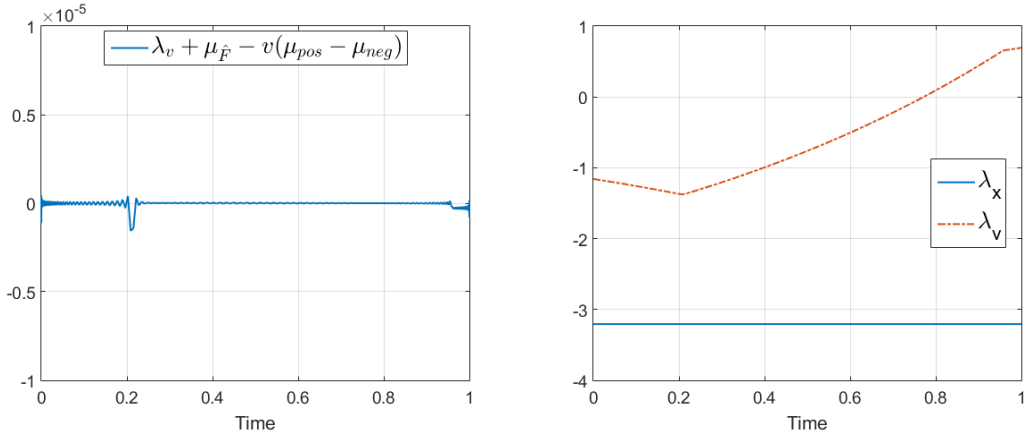

(a) (b)

Figure 4.3: (a) Verification of a stationary condition, in Eq. (4.13), to problem G_s; (b) Costates to problem G_s, λ_x is constant which is consistent with the necessary conditions of optimality.

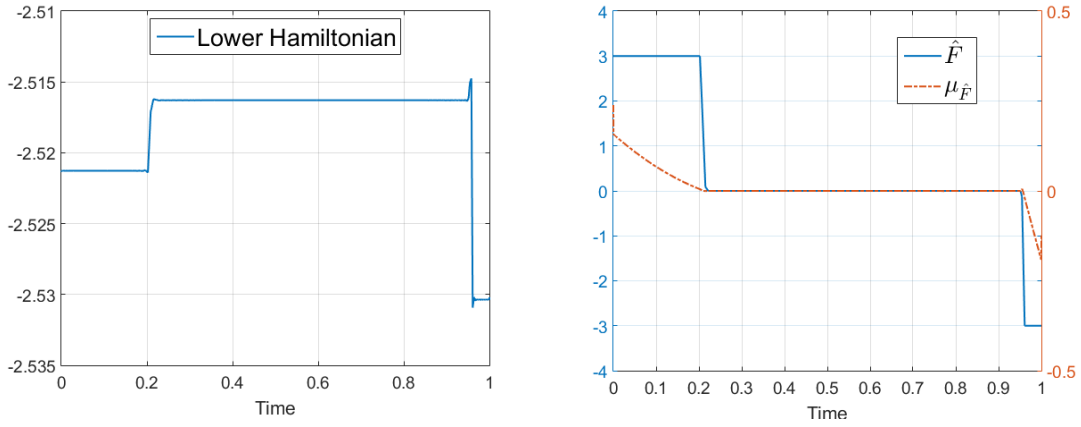

(a) (b)

Figure 4.4: (a) Consistency of the Lower Hamiltonian in Eq. (4.15); (b) Consistency of the complementarity condition in Eq. (4.14).

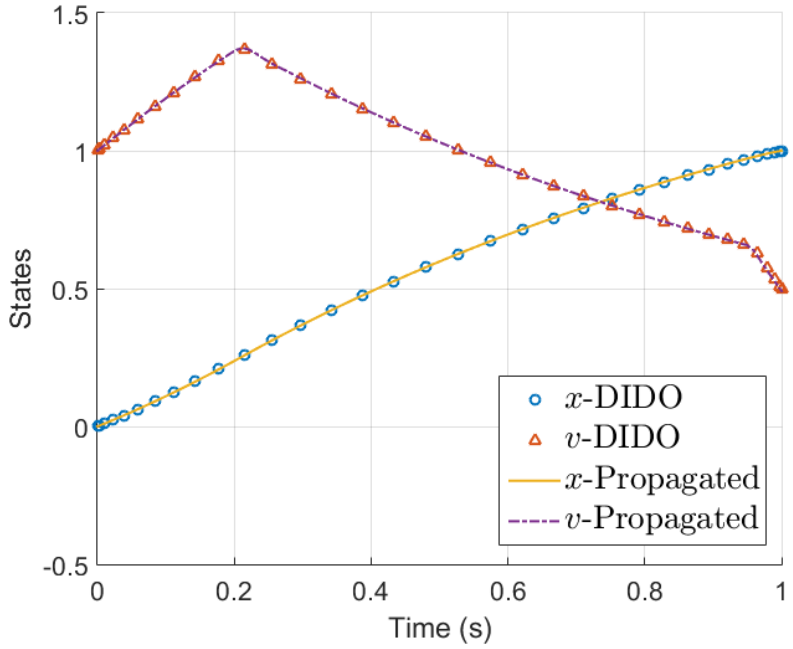

Figure 4.5: Successful feasibility of the solution to problem G_{s}.

body; (*iii*) constraints upon maximum reaction wheel speed; (*iv*) constraining the attitude so that the slew is an eigenaxis maneuver; (*v*) enforcing specific starting and ending speeds of the reaction wheels.[15] An optimal control problem which minimizes the electric power-input equation may be formulated as follows, and is

denoted as problem P_{ns}:

$$
(P_{\text{ns}})\begin{cases}
\text{State:} & x = [q, \omega, \Omega_{\text{rw}}]^{\mathsf{T}} \in \mathbb{R}^{7+N_{\text{rw}}} \\
\text{Control:} & u = \tau_{\text{rw}} \in \mathbb{R}^{N_{\text{rw}}}, \\
\text{Minimize:} & J\left[x(\cdot), u(\cdot)\right] = \dfrac{1}{2}\displaystyle\int_0^T \left\{ \sum_{i=1}^{N_{\text{rw}}} \mathcal{P}_i(\Omega_{\text{rw}}, \tau_{\text{rw}}) + \sum_{i=1}^{N_{\text{rw}}} \left|\mathcal{P}_i(\Omega_{\text{rw}}, \tau_{\text{rw}})\right| \right\} dt \\
\text{Subject To:} & \\
& \begin{bmatrix} \dot{q} \\ \dot{\omega} \\ \dot{\Omega}_{\text{rw}} \end{bmatrix} = \begin{bmatrix} \frac{1}{2}\mathcal{Q}(\omega) q \\ J_{\text{sc}}^{-1}(-A\tau_{\text{rw}} - \omega \times (J_{\text{sc}}\omega + AJ_{\text{rw}}\Omega_{\text{rw}})) \\ J_{\text{rw}}^{-1}\tau_{\text{rw}} \end{bmatrix} \\
& \\
& x(0) = [q^0,\ \omega^0,\ \Omega_{\text{bias}}]^{\mathsf{T}} \in \mathbb{R}^{7+N_{\text{rw}}} \\
& x(T) = \left[q^f,\ \omega^f,\ \Omega_{\text{bias}}\right]^{\mathsf{T}} \in \mathbb{R}^{7+N_{\text{rw}}} \\
& \\
& |\omega_i| \leq \omega_{\max},\ \forall\, i = 1, 2, 3 \\
& |\Omega_{\text{rw},i}| \leq \Omega_{\max},\ \forall\, i = 1, \ldots, N_{\text{rw}} \\
& |\tau_{\text{rw}}| \leq \tau_{\max},\ \forall\, i = 1, \ldots, N_{\text{rw}}
\end{cases}
\tag{4.16}
$$

where $\mathcal{P}_i(\Omega_{\text{rw}}, \tau_{\text{rw}})$ is the electrical power equation and is given by Eq. (2.19). The state consists of the quaternion attitude parameterization, angular velocity of the spacecraft body (relative to the spacecraft body), and angular speed of the reaction wheels (relative to their spin axes). The control for problem P_{ns} is taken as the reaction wheel motor toques. The boundary conditions and the nonlinear dynamics of problem P_{ns} describe a slew with specified starting and ending orientation and velocity of the spacecraft body and the wheels. The amount $\Omega_{\text{bias}} \in \mathbb{R}^{N_{\text{rw}}}$ in the boundary conditions is given to satisfy the operational constraint that the wheels must begin and end with the same velocity, which is enforced to avoid

stickage issues that occur when operating the reaction wheels near zero speeds.[15] A total of $2N_{\mathrm{rw}} + 3$ path constraints enforce the limits upon rate-gyro, reaction wheel angular velocity, and reaction wheel generatable motor torque. The cost functional of P_{ns} minimizes the electrical power-input equation for each reaction wheel, which was derived in Chapter 2. Therefore P_{ns} is a formulation for minimum electrical energy slews. Considering Eq. (4.16), it is clear that due to the cost functional, formulation P_{ns} is a complex and challenging high-dimensional problem.

From the techniques developed in Section 4.2, the nonsmooth problem P_{ns} may be solved without resorting to proxies, mollification or homotopic approaches. Therefore, minimum electrical energy slews may be obtained. This is attained by generating an equivalent smooth formulation of problem P_{ns}. The smooth formulation is obtained through a process, analogous to the one developed for the L^1 motion planning problem of Section 4.2. Each nonsmooth term $|\mathcal{P}_i(\Omega_{\mathrm{rw}}, \tau_{\mathrm{rw}})|$ of the electric power-input equation must be cast into an equivalent smooth representation. Therefore each $|\mathcal{P}_i(\Omega_{\mathrm{rw}}, \tau_{\mathrm{rw}})|$ requires two auxiliary decision variables $z_{a,i}$ and $z_{b,i}$, along with four path constraints $z_{a,i} \geq 0$, $z_{b,i} \geq 0$, $z_{a,i} - \mathcal{P}_i(\Omega_{\mathrm{rw}}, \tau_{\mathrm{rw}}) \geq 0$, and $z_{b,i} + \mathcal{P}_i(\Omega_{\mathrm{rw}}, \tau_{\mathrm{rw}}) \geq 0$; by doing so, $z_{a,i}$ and $z_{b,i}$ represent the positive and negative portions of the electric power $\mathcal{P}$ respectively. From this judicious choice of ancillary controls and path constraints, P_{ns} may be transformed into an equivalent *smooth* formulation. This formulation is presented as follows, and is denoted as P_{s} (for electric power-input smooth version):

$$
(P_{\rm s})\left\{\begin{array}{ll}
\text{State:} & x = [q, \omega, \Omega_{\rm rw}]^{\mathsf{T}} \in \mathbb{R}^{7+N_{\rm rw}} \\
\text{Control:} & u = \left[\tau_{\rm rw},\ \ z_{a,1},\ \ z_{b,1},\ \ \ldots,\ \ z_{a,N_{\rm rw}},\ \ z_{b,N_{\rm rw}}\right]^{\mathsf{T}} \in \mathbb{R}^{3N_{\rm rw}} \\
\text{Minimize:} & J\left[x(\cdot), u(\cdot)\right] = \dfrac{1}{2}\displaystyle\int_0^T \left\{\sum_{i=1}^{N_{\rm rw}} \mathcal{P}_i(\Omega_{\rm rw}, \tau_{\rm rw}) + \sum_{i=1}^{N_{\rm rw}} (z_{a,i} + z_{b,i})\right\} dt \\
\text{Subject To:} & \\
 & \begin{bmatrix} \dot{q} \\ \dot{\omega} \\ \dot{\Omega}_{\rm rw} \end{bmatrix} = \begin{bmatrix} \frac{1}{2}\mathcal{Q}(\omega) q \\ J_{\rm sc}^{-1}(-A\tau_{\rm rw} - \omega \times (J_{\rm sc}\omega + AJ_{\rm rw}\Omega_{\rm rw})) \\ J_{\rm rw}^{-1}\tau_{\rm rw} \end{bmatrix} \\
 & \\
 & x(0) = [q^0,\ \omega^0,\ \Omega_{\rm bias}]^{\mathsf{T}} \in \mathbb{R}^{7+N_{\rm rw}} \\
 & x(T) = \left[q^f,\ \omega^f,\ \Omega_{\rm bias}\right]^{\mathsf{T}} \in \mathbb{R}^{7+N_{\rm rw}} \\
 & \\
 & z_{a,i} \geq 0,\ \forall\, i = 1, \ldots, N_{\rm rw} \\
 & z_{b,i} \geq 0,\ \forall\, i = 1, \ldots, N_{\rm rw} \\
 & z_{a,i} - \mathcal{P}_i(\Omega_{\rm rw}, \tau_{\rm rw}) \geq 0,\ \forall\, i = 1, \ldots, N_{\rm rw} \\
 & z_{b,i} + \mathcal{P}_i(\Omega_{\rm rw}, \tau_{\rm rw}) \geq 0,\ \forall\, i = 1, \ldots, N_{\rm rw} \\
 & |\omega_i| \leq \omega_{\max},\ \forall\, i = 1, 2, 3 \\
 & |\Omega_{{\rm rw},i}| \leq \Omega_{\max},\ \forall\, i = 1, \ldots, N_{\rm rw} \\
 & |\tau_{{\rm rw},i}| \leq \tau_{\max},\ \forall\, i = 1, \ldots, N_{\rm rw}
\end{array}\right. \tag{4.17}
$$

The "cost" to generate the equivalent smooth $P_{\rm s}$ from $P_{\rm ns}$ is an increase of $2N_{\rm rw}$ controls, and $4N_{\rm rw}$ path constraints. For a spacecraft which utilizes a redundant set of four reaction wheels, problem $P_{\rm s}$ consists of 11 state variables, 12 controls, and 27 path constraints. Therefore, while there is a substantial increase in dimensionality incurred to generate $P_{\rm s}$, this formulation is smooth, whereas

P_{ns} is nonsmooth. Because P_{s} is smooth, it is straightforward obtain the necessary conditions for optimality by application of Pontryagin's Minimum Principle. Added to this, since P_{s} is smooth, well established methods in numerical optimal control may be utilized to solve the formulation.

4.4 The Minimum Energy Shortest Time Maneuver

To demonstrate the benefit of directly minimizing the electric power-input equation, problem P_{s} is solved for a time-optimal 180-degree slew about the spacecrafts z-axis with spacecraft parameters from Table A.1 of Appendix A. This simulation (with parameters) is the same considered in Chapter 3 which studied the energy-time relationship under the minimization of cumulative dissipative losses of coper and fiction (represented by $\mathcal{E}_{total}^{loss}$ in Eq. (2.26)). Therefore, from Section 3.3.1 of Chapter 3, the time optimal transfer time to this simulation is 279.9 seconds. The numerical approach used to obtain a candidate state-control pair for problem P_{s}, including associated dual variables for optimality analysis, is the same used to solve the time optimal formulation which minimized the electrical dissipative losses given by problem ME in Eq. (3.5) in Section 3.2.3. By choosing the same simulation parameters and numerical approach, the sate and control trajectories from all three problem formulations may be compared: (*i*) Minimizing transfer time, (*ii*) Minimizing Dissipative losses, whose formulation is given in Eq. (3.5). (*iii*) Minimizing the electrical power-input equation, whose formulation is given in Eq. (4.17).

Problem P_{s}, as given in Eq. (4.17) was solved for the optimal transfer time, which is known to be 279.9 seconds from the results in Chapter 3, using the pseu-

dospectral methods implemented in the software package DIDO. The numerical results (i.e. candidate state-control pair) obtained by DIDO is shown in Figure 4.6. A comparison of the electrical energy metrics among the three formulations (minimum time, minimum dissipative losses, minimum electrical power-input) is shown in Table 4.2. By being able to directly minimize the electrical power-input equation, the agile (indeed, most agile–in fact, time optimal) maneuver is able to be completed with the least amount of electrical energy of 136.5 J, compared to 162 J when just minimizing transfer time, and 143.9 J when dissipative losses are minimized (resulting with a *reduced* energy maneuver). The fact that the energy spent due to dissipative losses $\mathcal{E}_{total}^{loss}$ when minimizing the power-input equation is greater than the maneuver which specifically minimizes $\mathcal{E}_{total}^{loss}$ (128.5 J verses 121.0 J) makes intuitive sense, since minimizing the electrical power-input equation does not necessarily mean that dissipative losses are minimized; it is expected that a maneuver which minimizes $\mathcal{E}$ would produce a suboptimal value for the metric $\mathcal{E}_{total}^{loss}$ (simply from the fact of which functional is being minimized); the same vice-versa: That the least electrical energy is obtained by minimizing $\mathcal{E}$ (which is the integral of the electrical power input equation over the maneuver time). This fact emphasizes that care should be taken when choosing a cost functional. Each of these metrics are important, it just depends upon the desired result: One minimizes electrical energy via minimizing the power-input equation, and the other minimizes dissipative losses (and hence reduces thermal stresses induced by the reaction wheel array) via $\mathcal{E}_{total}^{loss}$. The derivation of the necessary conditions to problem P_{s} are omitted due to brevity, since the derivations are very similar to those presented in the subsequent chapter on attitude steering (Chapter 5), as well as to the derivations to problem G_{s}. For the sake of validating the candidate state-control solution shown in Figure 4.6, a few necessary conditions to problem P_{s} are

stated, and the candidate solution is shown to satisfy these necessary conditions. Since P_{s} is time invariant, optimal solutions to problem P_{s} must necessarily have a lower Hamiltonian which is constant over the entire horizon $[t_0, t_f]$. Figure 4.7a demonstrates the consistency of the lower Hamiltonian, with $\mathcal{H}(t) \approx -38.8$ for all $t \in [t_0, t_f]$. Because limits upon the angular velocity of the spacecraft body axes are imposed in problem P_{s}, in concern for saturation of the rate gyros which are used to determine the spacecraft attitude, in the form $-\omega_{\max} \leq \omega_i \leq \omega_{\max}$ for each axis $i = 1, 2, 3$, each ω_i and associated KKT multiplier $\mu_{\omega,i}$ must satisfy the complementarity condition. That is $\mu_{\omega,i} \geq 0$ if $\omega_i = \omega_{\max}$, $\mu_{\omega,i} = 0$ if $-\omega_{\max} \leq \omega_i \leq \omega_{\max}$, or $\mu_{\omega,i} \leq 0$ if $\omega_i = -\omega_{\max}$. Satisfaction of the complimentary condition for ω_2 is shown in Figure 4.7b. While not depicted, the solution to problem P_{s} shown in Figure 4.6 passed feasibility to a specified tolerance within 10^{-4}. While this section omits other necessary conditions (e.g. stationary conditions, terminal transversality condition, other complementarity conditions), the candidate solution in Figure 4.6 has been successfully verified against each of them.

Table 4.2: Electrical Energy Metrics of for a 180 degree rotation about the spacecraft z-axis: Minimizing transfer time; minimizing dissipative losses $\mathcal{E}_{total}$; minimizing electrical energy Eq. (4.17). Each maneuver has a transfer time of 279.9 seconds.

Cost Functional	$\mathcal{E}$ (J)	$\mathcal{E}_{total}^{loss}$ (J)	$\mathcal{C}_{loss}$ (J)	$\mathcal{F}_{loss}$ (J)
Min transfer time (t_f)	162.0	136.3	79.7	56.6
Min Dissipative Losses ($\mathcal{E}_{total}^{loss}$)	143.9 (-11.2%)	121.0 (-11.2%)	81.3 (+1.9%)	39.7 (-29.9%)
Min Electrical Power-Input ($\mathcal{E}$)	136.5 (-15.7%)	128.5 (-5.7%)	87.3 (+9.5%)	41.2 (-27.2%)

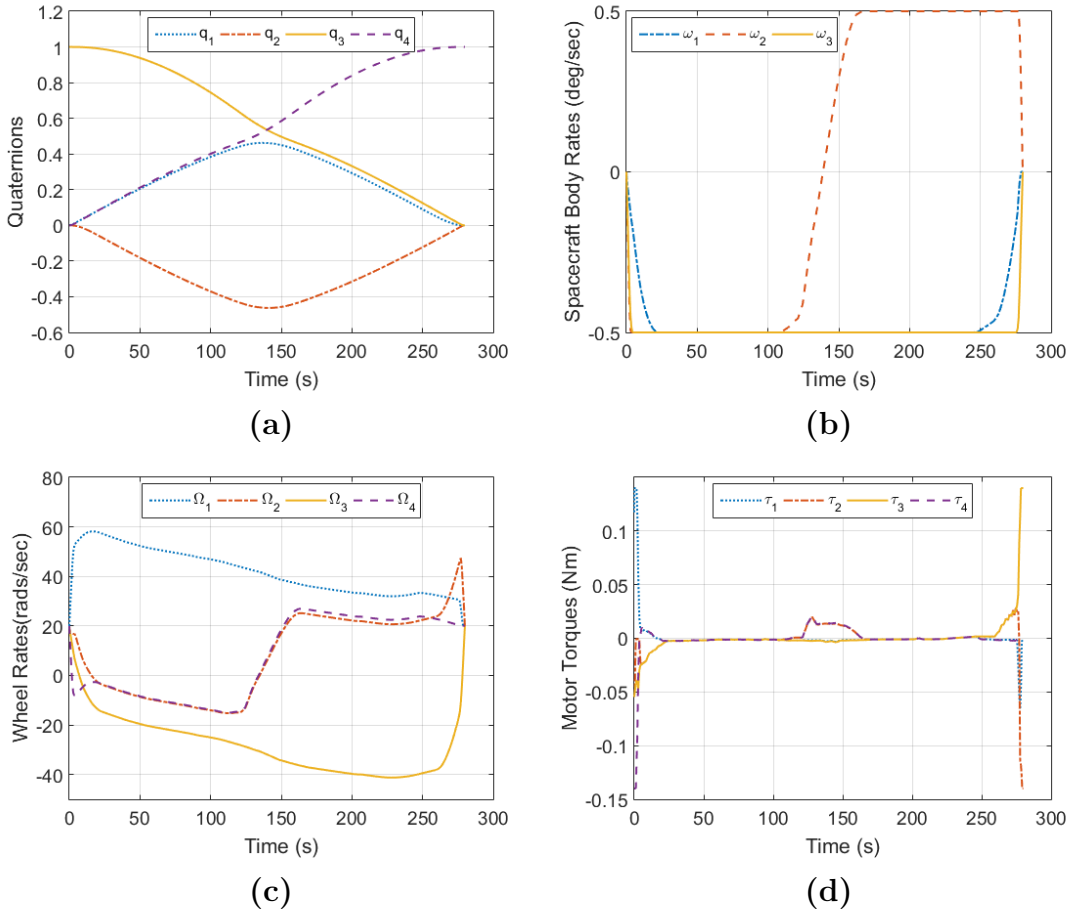

Figure 4.6: State and control profiles of a minimum electrical energy 180-deg rest-to-rest slew about the spacecraft z-axis, minimizing the electrical power-input equation: (a) attitude; (b) body rates; (c) reaction wheel rates; (d) reaction wheel motor torques.

4.5 Revisiting the Transfer Time and Minimum Energy Relationship

In this section, the relationship between energy and transfer time for both eigenaxis maneuvering and off-eigenaxis maneuvering, which was studied in Chapter 3 of this dissertation and in Refs. [57, 61], is revisited under the electrical power-input equation of Eq. (2.25) using P_s. Before exploring this new avenue, a synopsis of the original transfer time and energy relationship, performed in Refs. [57, 61],

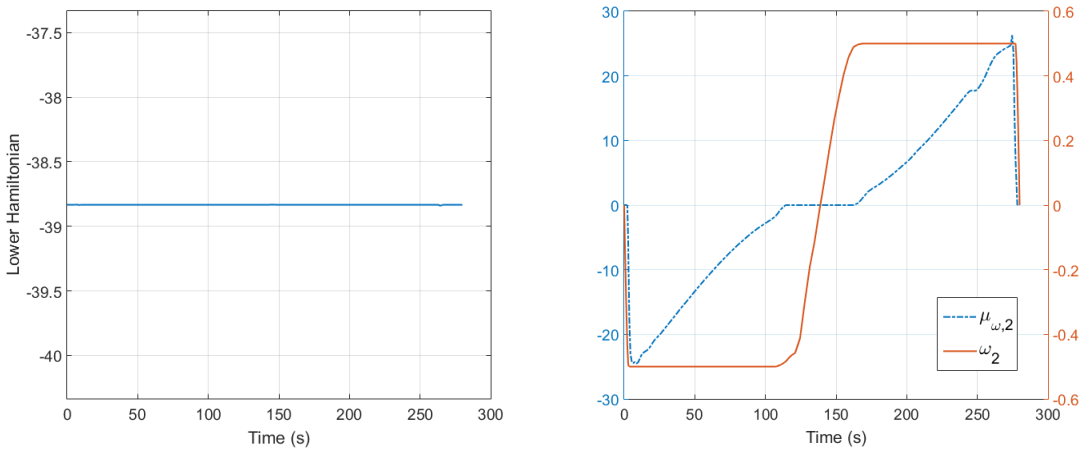

Figure 4.7: Verification of necessary conditions to the minimum electrical energy 180-deg rest-to-rest slew about the spacecraft z-axis: (a) Consistency of the Lower Hamiltonian; (b) Complementarity condition for ω_2.

is first presented. In both Refs. [57, 61], and in Chapter 3 of this dissertation, the relationships between electrical energy and transfer time for these two maneuver types (off-eigenaxis and on-eigenaxis) were studied under minimum dissipative losses of Eq. (2.26) for a 180 degree slew about the spacecraft's z-axis. At the time of that study, minimizing the electrical power-input equation posed too great a challenge. Instead, Refs. [57,61] reduced the electrical energy by instead minimizing dissipative losses. These relationships between electrical energy and transfer time were identified by generating a set of a Pareto fronts (one for off-eigenaxis maneuvering, and another for conventional eigenaxis maneuvering) that described the amount of electrical energy required per transfer time for each type of maneuver (be it off, or on eigenaxis maneuvering) when minimizing the cumulative copper loss and friction loss, given by the metric $\mathcal{E}_{total}^{loss}$ given in Eq. (2.26). The manner by which these two Pareto fronts were generated, was through solving a sequence of fixed-time optimal control problems with final-time being varied, beginning with the time-optimal transfer time to each maneuver type (e.g. time

optimal off-eigenaxis, and time optimal eigenaxis). The optimal control formulations used for off-eigenaxis (and with a slight modification, for eigenaxis–details are provided in Section 3.2.2) maneuvering, was problem ME given in Eq. (3.5). Through these simulations and subsequent analysis, a host of results were obtained, and that all of these results from the relationship between energy and transfer time for the chosen slew (180 degree maneuver about the z-axis of the spacecraft) are indicative for other slews. A key reason to revisit this study, is that the cost functional to problem ME minimized the electrical dissipative losses. That is,

$$\text{Minimize: } J\left[x(\cdot), u(\cdot)\right] = \int_0^T \sum_{i=1}^{N_{rw}} \left(\frac{R}{K_T^2} (\tau_{rw,i}(t) + \beta \Omega_{rw,i}(t))^2 + \beta \Omega_{rw,i}^2(t) \right) dt$$

This thought is now laid to rest, for in this chapter a method has been developed to minimize the power-input equation. The success of the method was demonstrated for a time optimal minimum electrical energy slew in the preceding Section 4.4, where it was shown that even-further electrical energy savings upon the minimum dissipative losses maneuvers may be obtained by directly minimizing the electrical power-input equation; see Table 4.2. Therefore, equipped with the new method developed in this chapter, the relationship between electrical energy and transfer time is revisited once again, although now under the electric power-input equation. The same slew (180 degrees about the spacecraft's z-axis whose initial and final quaternions are $q^0 = [0, 0, 1, 0]^\intercal$ and $q^f = [0, 0, 0, 1]^\intercal$) and spacecraft parameters (those from Table A.1 of Appendix A) which were exactly those used in Refs. [57, 61] and in Chapter 3 to study energy and transfer time relationship, are used for this "revisited"-study of the time/energy relationship between the two maneuver types (off-and on-eigenaxis). By this choice of simulation parameters (spacecraft and slew), a comparison may be made, upon the efficacy of directly

minimizing electrical energy against minimizing dissipative losses in regards to the least amount of energy usage per transfer time. Along with using the same simulation parameters as in Refs. [57,61] and Chapter 3, the same approach is taken to generate the two Pareto fronts (one for off-eigenaxis, and another for eigenaxis). For off-eigenaxis maneuvering, problem P_{s} is solved for a sequence of transfer times, beginning at the time optimal transfer time for the simulation parameters, which was identified as 279.9 seconds. The approach for eigenaxis maneuvering is identical, that is a sequence of fixed time maneuvers are solved which begin at the time-optimal transfer time for an eigenaxis maneuver (determined to be 362.0 seconds), except that problem P_{s} must be modified to constrain all motion to be along an eigenaxis. This modified formulation is presented as follows, and

is hereafter referred to as problem P-EAM$_\mathrm{s}$:

$$
(\text{P-EAM}_\mathrm{s})\begin{cases}
\text{State:} & x = [q, \omega, \Omega_{\mathrm{rw}}]^{\mathsf{T}} \in \mathbb{R}^{7+N_{\mathrm{rw}}} \\
\text{Control:} & u = \left[\tau_{\mathrm{rw}},\ \ z_{a,1},\ \ z_{b,1},\ \ \ldots,\ \ z_{a,N_{\mathrm{rw}}},\ \ z_{b,N_{\mathrm{rw}}}\right]^{\mathsf{T}} \in \mathbb{R}^{3N_{\mathrm{rw}}} \\
\text{Minimize:} & J\left[x(\cdot), u(\cdot)\right] = \dfrac{1}{2}\displaystyle\int_0^T \left\{ \sum_{i=1}^{N_{\mathrm{rw}}} \mathcal{P}_i(\Omega_{\mathrm{rw}}, \tau_{\mathrm{rw}}) + \sum_{i=1}^{N_{\mathrm{rw}}} (z_{a,i} + z_{b,i}) \right\} dt \\
\text{Subject To:} & \\
& \begin{bmatrix} \dot{q} \\ \dot{\omega} \\ \dot{\Omega}_{\mathrm{rw}} \end{bmatrix} = \begin{bmatrix} \frac{1}{2}\mathcal{Q}(\omega) q \\ J_{\mathrm{sc}}^{-1}(-A\tau_{\mathrm{rw}} - \omega \times (J_{\mathrm{sc}}\omega + A J_{\mathrm{rw}} \Omega_{\mathrm{rw}})) \\ J_{\mathrm{rw}}^{-1} \tau_{\mathrm{rw}} \end{bmatrix} \\
& x(0) = [q^0,\ \omega^0,\ \Omega_{\mathrm{bias}}]^{\mathsf{T}} \in \mathbb{R}^{7+N_{\mathrm{rw}}} \\
& x(T) = \left[q^f,\ \omega^f,\ \Omega_{\mathrm{bias}}\right]^{\mathsf{T}} \in \mathbb{R}^{7+N_{\mathrm{rw}}} \\
& z_{a,i} \geq 0,\ \forall\, i = 1, \ldots, N_{\mathrm{rw}} \\
& z_{b,i} \geq 0,\ \forall\, i = 1, \ldots, N_{\mathrm{rw}} \\
& z_{a,i} - \mathcal{P}_i(\Omega_{\mathrm{rw}}, \tau_{\mathrm{rw}}) \geq 0,\ \forall\, i = 1, \ldots, N_{\mathrm{rw}} \\
& z_{b,i} + \mathcal{P}_i(\Omega_{\mathrm{rw}}, \tau_{\mathrm{rw}}) \geq 0,\ \forall\, i = 1, \ldots, N_{\mathrm{rw}} \\
& \omega \times e(q^0, q^f) = 0 \in \mathbb{R}^3 \\
& \|\omega\|_2^2 \leq \omega_{max} \\
& |\Omega_{\mathrm{rw},i}| \leq \Omega_{\max},\ \forall\, i = 1, \ldots, N_{\mathrm{rw}} \\
& |\tau_{\mathrm{rw},i}| \leq \tau_{\max},\ \forall\, i = 1, \ldots, N_{\mathrm{rw}}
\end{cases}
\tag{4.18}
$$

The path constraint $\omega \times e(q^0, q^f) = 0 \in \mathbb{R}^3$ constrains all (rotational) motion to be along an eigenaxis, and the individual limits upon each axis of the spacecraft in problem P_s has been replaced with a spherical slew-rate constraint in the form $\|\omega\|_2^2 \leq \omega_{max}$. The Pareto fronts to both eigenaxis and off-eigenaxis maneuvering

generated when minimizing the electrical power-input equation is shown in Figure 4.8, and were generated by the process mentioned in the section preceding problem formulation P-EAM$_s$. By minimizing the electric power-input equation, Figure 4.8 shows the relationship between minimum *electrical* energy and transfer time. Figure 4.8, *every one* of the relationships identified between electrical energy and transfer time for both off-eigenaxis and eigenaxis maneuvering, under minimum dissipative losses, made in Refs. [57,61] (and Chapter 3), hold true when minimizing electrical energy directly through the power-input equation. Namely, each Pareto front may be separated into distinct phases, each providing telling information on the relationship between electrical energy and transfer time, which is especially useful for planing purposes.

(*i*) Head: This region is near the shortest time maneuver and depicts that there exits a host of near time-optimal maneuvers with a substantially less energy budget than the shortest time counterpart; for off-eigenaxis maneuvering, this phase may be considered as the time-interval $[t_{\text{stm}}, 299]$ in Figure 4.8. From this observation the STM may no longer be considered a desirable maneuver, for by decreasing transfer time by a negligible amount reduces energy by substantial amounts. This result could be useful for being able to attain very agile maneuvers within a restrictive energy budget.

(*ii*) Body: In this portion of the energy/time relationship, electrical energy requirements decay linearly with respect to increasing transfer time. Additionally, the body-phase is much more pronounced for off-eigenaxis maneuvering, which is due to the extra degrees of freedom provided by off-eigenaxis maneuvering. For the Pareto front associated to off-eigenaxis maneuvering, the body portion of the Pareto front may be considered in the time interval [299, 387] in Figure 4.8.

(*ii*) Coincide Point: There exists a point in transfer time where eigenaxis maneuvering and off-eigenaxis maneuvering perform equivalently with respect to energy; this point in transfer time is at $T = 387$seconds in Figure 4.8. This point demonstrates that there exists a point in transfer time that no reduction energy is attained by maneuvering off eigenaxis.

(*iii*) Tail: This portion of the energy/time relationship depicts that there exists a point where there are *extremely* diminishing returns upon energy when increasing transfer time. Additionally, the tail portion begins at the Coincide point for off-and on-eigenaxis maneuvering and lasts for all time past the Coincide point, $[387, \infty)$ in Figure 4.8. Therefore, the concept of reducing energy requirements by increasing the slew time only works up to a certain point in transfer time.

Additionally, and perhaps most importantly, the trade space between off-and on-eigenaxis maneuvering identified when studying the energy/time relationship when minimizing the dissipative loss metric, exists when directly minimizing electrical energy via the electric power input equation. From this tradespace shown in Figure 4.8, is demonstrated that there exists a host of agile maneuvers which exist within the energy budget of conventional eigenaxis maneuvering.

The Pareto fronts obtained from the two minimization approaches (reducing energy through minimizing dissipative from Chapter 3 and directly minimizing electrical energy in this chapter) are superimposed upon one another in Figure 4.9, so a comparison may be made between the effect of minimizing electrical energy directly (through the power-input equation) and the effect of reducing energy by minimizing dissipative losses. The dashed Pareto set in Figure 4.9 was obtained when minimizing dissipative losses only, and the solid line is the Pareto set obtained when directly minimizing electrical energy. Clearly, Figure 4.9 shows that

Pareto front obtained by *directly* minimizing electrical energy (obtained by minimizing the electrical power-input equation) dominates the Pareto front obtained by only minimizing dissipative losses. From figure 4.9, it can be seen that while the geometric structure of the energy/time relationships hold between each minimization scheme, both the off-eigenaxis and eigenaxis are more pronounced when minimizing the true cost given by the power-input equation; most notably the coincide point, which was identified to be at 395 second transfer time when minimizing dissipative losses, is now at 387 seconds when directly minimizing electrical energy.

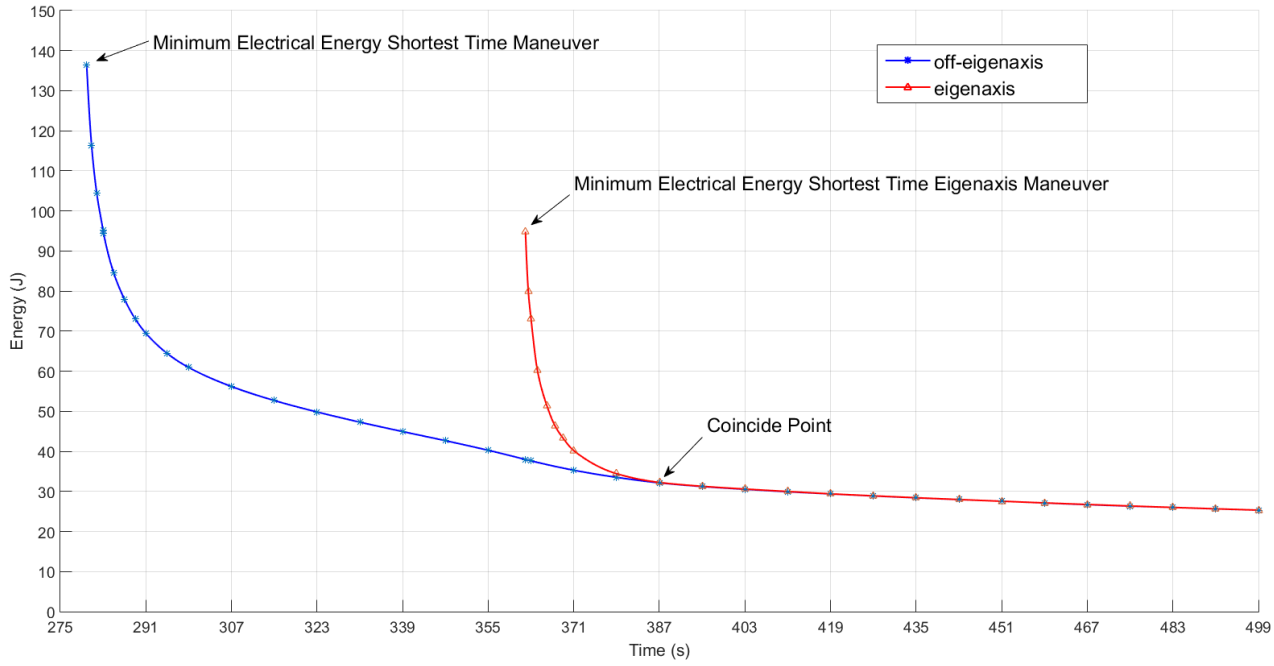

Figure 4.8: Relationship between minimum electrical energy and transfer time to the 180-degree z-body-axis minimizing the electrical power-input equation whose problem formulation is given by P_{s} of Eq. (4.17). The vertical axis is electrical energy as measured by $\mathcal{E}$.

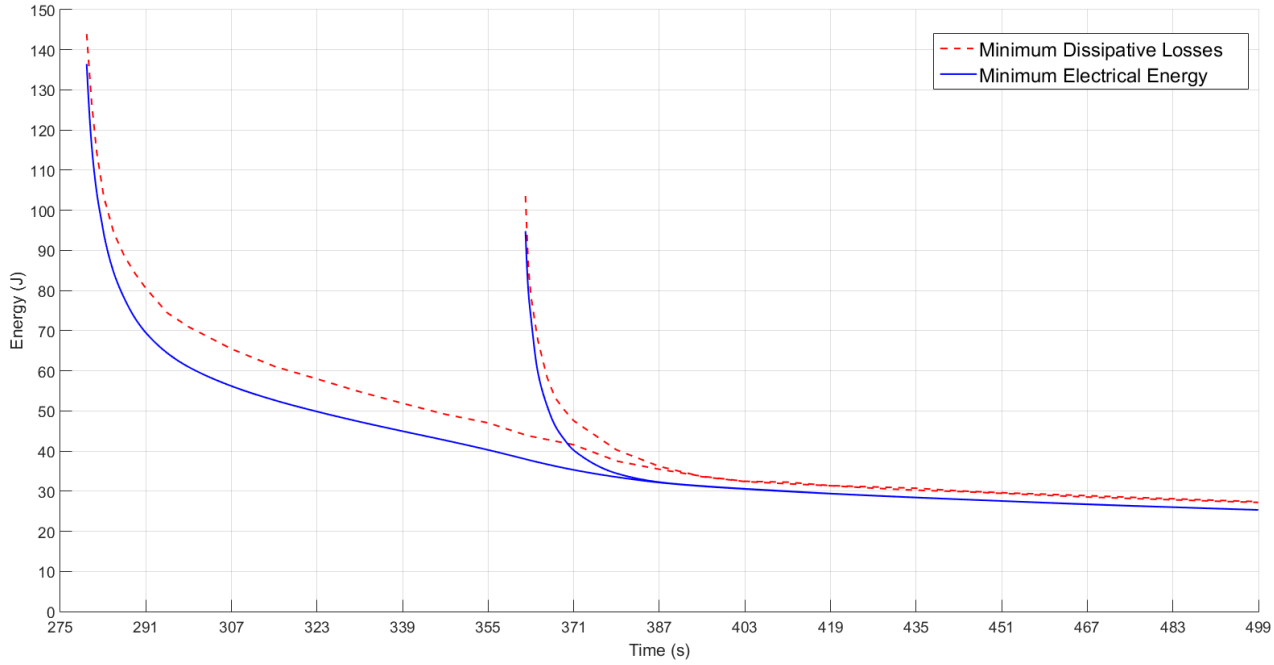

Figure 4.9: Comparison between the relationship between energy and transfer time under minimum dissipative losses against under minimum electrical energy.

4.6 Conclusion

The minimization of electrical energy to perform a slew using reaction wheels was shown to be a problem in L^1 optimal control. To overcome the challenge of nonsmoothness with respect to both control and state variables, an augmentation method was adopted which generated an equivalent smooth formulation. This method lifted the formulation through the addition of ancillary controls and path constraints upon the controls. Standard techniques in computational optimal control were applied to solve for minimum electrical energy slews under a host of operational constraints in line with a flight scenario. As an application, the identification of the relationship between electrical energy and transfer time under minimum electrical energy was identified for both on-and off-eigenaxis

maneuvering. The tradespace between on-and off-eigenaxis maneuvering under minimum dissipative losses was shown to hold under minimum electrical energy, thereby demonstrating that agile off-eigenaxis maneuvering exists within the energy budgets of typical eigenaxis maneuvering. The minimum electrical energy slews demonstrated that transfer time, energy, and dissipative losses may be substantially reduced by maneuvering off-eigenaxis.

Chapter 5

Attitude Steered Maneuvering

> "Discovery consists in seeing what everyone else has seen and thinking what no one else has thought"
>
> *Albert Szent-Gyorgi*

This chapter examines the effectiveness of reducing the energy consumption of a reaction-wheel array over the course of a slewing maneuver by steering the attitude of the spacecraft, in situations where it is not possible to command the reaction wheel torque directly. To explore this avenue, a set of constrained nonlinear nonsmooth L_1 optimal-control problems are formulated and solved. It is demonstrated that energy consumption, dissipative losses, and peak-power load of the reaction-wheel array can each be reduced substantially, by controlling the input to the attitude control system through attitude steering, thereby avoiding software modifications to flight software.

5.1 Introduction

Power is *the* driving resource upon a spacecraft and impacts every facet and phase of its existence, whether from the initial design phase, where resources are

allocated for energy storage that effect the payload of the spacecraft, or whether till late mission life when power systems begin to degrade. Power directly effects the efficacy of scientific data collection, from running the instruments, to operating the attitude control system (ACS) which slews the spacecraft to orientations of interest. Minimizing power and energy demands has the potential of prolonging the operational lifespan of the spacecraft, thereby enhancing the scientific utility of the spacecraft, and lowering the overall monetary-cost of a mission. Prolonging life expectancy is especially pertinent given the recent failures of the reaction wheel actuators on the NASA's Kepler, Mars Odyssey, and Dawn spacecrafts [68], and the anomalies detected on NASA's Cassini spacecraft [69] during it's more than nineteen year exploration. Power not only has an effect on the efficacy of science, but has a fundamentally direct and meaningful impact from an econometric standpoint, as well as from a social-media standpoint when considering the public's response to scientific failures.

Synthesizing the above exposition, it is apparent that minimizing the power or energy required to perform a slew is a highly desirable goal. Situations in which the power management becomes highly beneficial, is late in mission life when power systems begin to degrade. Due to the high cost and invested effort involved with a spacecraft, it behooves the science community to attempt to keep scientific data collections active as long as possible, extending the operation of the spacecraft well-past the original mission requirements. An example exemplifying longevity past original mission requirements, was NASA's Far Ultraviolet Spectroscopic Explorer (FUSE) spacecraft, whose three year mission was extended to over eight years of scientific observations and collections [70]. Deep-space operations are another facet exemplifying the necessity to preserve power: Solar cells are a renewable source of energy, but are only effective up to the orbit of Mars;

beyond that distance the solar radiant flux is not adequate to power spacecraft, and therefore alternate methods to generate power, such as thermoelectric heat engines are required to generate energy for deep-space missions [71]. Because the power output of radioisotope thermoelectric generators which drive deep-space spacecraft fade over time, NASA has a vested interest in both extracting more power, along with increasing the amount of time before the power-output profiles degrade [72]. Regardless of the power and energy source, as a spacecraft ages onboard power generation and energy storage systems capabilities begin to degrade. Consider Voyager 1, which has had to have its scientific instruments shut off one by one, as a result *not* of malfunction, but rather as a result of dwindling power-output profiles [8]. One approach to possibly ameliorate the requirement for more power, especially when power systems begin to degrade, is to reduce the power requirements of the attitude control system. Reaction wheels can be a considerable load upon a spacecraft [73]. The execution of slew maneuvers, notably large-angle slews, may cause short-in-duration though large-in-magnitude power demands, which in turn may cause electrical transients [44]. These transients can degrade power quality across the entire electrical bus, which often services sensitive scientific instruments as well as the attitude control system. They can also potentially create a violation of power constraints placed upon the spacecraft. Similarly, in a system with degraded power margins, peak power loads (which can occur during the execution of a large angle slew) can generate electrical surges [44]. Reducing power demands can potentially bring greater utility out of a spacecraft, especially late in operational life well past its original mission.

While minimizing the electrical energy consumed by the reaction wheel array is highly favorable, attempting to solve this problem poses significant challenges from both a computational as well theoretical standpoint. These challenges arise

due to the fact that the electric power-input equation is nonsmooth [57], and it is this challenge which has lead many researchers to instead minimize *proxies* to the reaction wheel power equation, such as mechanical power. It was shown in Ref. [44], that minimizing the electric power-input equation may be formulated as a L^1 optimal control problem. An approach to minimize the power-input equation was devised in [44] by generating an equivalent *smooth* formulation, by virtue of lifting the dimensionality of the original nonsmooth problem via the addition of ancillary decision variables, and appropriate constraints upon these variables. In a setting where the reaction wheel motor torques may not be directly controlled and that modifications to the flight software to allow-so are unfeasible, e.g. due to cost, minimum energy solutions must be able to work with a heritage attitude control system, methods based upon controlling reaction wheel motor torque are not applicable. One approach to reduce the energy requirements of such systems, is by steering the attitude of the spacecraft based on the knowledge of the underlying control allocation scheme (e.g. least-squares), spacecraft parameters (e.g. inertia tensor), and relevant constraints (e.g. saturation limits). This allows the behavior of the attitude control system to be modified without the need to otherwise alter the flight control logic.

A family of electrical power and energy metrics were derived in [57], to study the relationship between electrical energy and transfer time between on-and off-eigenaxis maneuvering. This study was from the perspective of a global approach within the framework of optimal control, with a performance index which minimized dissipative losses of the reaction wheels, and under the assumption that the reaction wheels can be directly controlled. An early work in optimal energy slews was seen in [54], where the copper loss of a single reaction wheel motor was minimized. References of [54–56] also approached energy minimization of

reaction wheel spacecraft through an optimal control framework. Although each approach to minimize energy varied in either performance index or number of reaction wheels, they matched in control input, with each assuming that the reaction wheel motor torques may be *directly controlled*. A feedback solution to the minimization of the instantaneous L^2 norm of mechanical power to a redundant actuator array was devised in [35]. This was accomplished by augmenting the instantaneous reaction wheel torque profiles from a least-squares control allocation through the addition of null motions. The efficacy of null motions to reduce the energy associated to a least-squares control allocation scheme was further investigated in [24], although under a performance index that assumed power may be regenerated when a reaction wheel decelerates. A feedback control law for simultaneous attitude and power tracking was developed in [74], where null motions were utilized to track a power profile. The problem of distributing the control torque unto the reaction wheels, to minimize the instantaneous L^1 norm of mechanical power, was posed as a constrained convex optimization problem in Refs. [53, 75], and solved through an application of lexicographic optimization.

A point of commonality among the literature which seek slewing strategies for the reduction of energy, is the assumption that reaction wheel inputs may be *directly* accessed and modified. Schemes which seek to reduce energy consumption either take control to be the motor torques generated by the reaction wheels, or *directly* augment the torque allocation scheme e.g. through the application of null motions. This assumption is tantamount to assuming that the attitude control system is equipped with an accessible feed-forward component, which may not be the case. Indeed, in a conventional ACS it is typical that attitude is taken as input.[25] Therefore in the quest for energy-reducing schemes, there exist situations in which the control allocation performed by the spacecraft needs to be

incorporated when designing a minimum (electrical) energy solution. That there exists a situation in which the reaction wheel motor torques can not be *directly* modified nor accessed raises, then the question of how minimum energy slews can be implemented when the *spacecraft* is in control of the torque allocation. The objective of this chapter is to seek minimum energy slews for the case when the reaction wheels can not be directly controlled. The approach taken by this chapter is to steer the attitude of the spacecraft, which may be thought of as determining a path for the boresight, with the goal of obtaining a minimum electric energy maneuver. Therefore, the goal of this work is to develop minimum energy maneuvers, by steering the attitude of the spacecraft, under the knowledge of the control allocation scheme implemented by the spacecraft, which is assumed to be L^2 allocation, i.e: least-squares allocation. In order to obtain minimum energy attitude steering, a fixed-endpoint, fixed-time optimal control problem is formulated in this chapter. This formulation directly considers the nonlinear rotational dynamics, which are required for the analysis of large angle slews. Also considered in the formulation are practical constraints upon both the state and the control variables, which arise in an operational setting. For example hardware constraints involving the saturation limits of the rate gyros, and the maximum speed and torque authority of the reaction wheels. Lastly, the formulation *directly* considers the nonsmooth reaction wheel power-input equation in order to minimize electrical energy.

The remainder of this chapter is organized as follows: First the rotational dynamics of a spacecraft employing a L^2 allocation scheme is derived. Following the dynamics, the reaction wheel power model and energy metrics are presented. The next section presents a set of high dimensional nonlinear optimal control problem formulations for the minimization of electrical energy by steering the attitude

of the spacecraft, along with the necessary conditions derived from Pontryagin's Minimum Principle. The last section demonstrates the efficacy of steering the attitude of the spacecraft by comparing the feedback implementation of the designed minimum electric energy attitude steering maneuver against a conventional eigenaxis maneuver.

5.2 Modeling Least Squares Control Allocation

The present chapter assumes that the spacecraft attitude control system implements a least squares control allocation scheme. This assumption requires that the spacecraft model in Chapter 2, must be modified in order to reflect that equations of motion are now driven by torques allocated under this specific control allocation scheme. The only modification to the spacecraft equations of motion, in order to account for a least squares control allocation scheme, is to the reaction wheels dynamics. The angular momentum of each reaction wheel about its spin axis is modeled by the following equation:

$$h(t) = J_{\text{rw}}\Omega_{\text{rw}}(t) - J_{\text{rw}}A^{\intercal}\omega(t), \tag{5.1}$$

where J_{rw} is a diagonal matrix with N_{rw} entries along the main-diagonal, whose i-th entry is the inertia of the i-th reaction wheel, which is assumed to be time invariant with respect to the spacecraft body frame. The vector $\Omega_{\text{rw}}(t) \in \mathbb{R}^{N_{\text{rw}}}$ is comprised of the angular rates of the reaction wheels about their respective spin axes. The angular momentum increment resulting from the spacecraft relative to the wheels is described by $J_{\text{rw}}A^{\intercal}\omega(t)$. Because reaction wheels are normally operated at a bias rate, $\Omega_{\text{rw},i}(t) \gg a_i^{\intercal}\omega(t)$ so Eq. (5.1) may be reasonably approximated

as

$$h(t) = J_{\text{rw}}\Omega_{\text{rw}}(t). \tag{5.2}$$

Noting that in Eq. (5.2) the reaction wheel control torque is given as $\tau_{\text{rw}}(t) = \dot{h}(t)$, the torque upon the spacecraft in the body frame is expressed by

$$\tau_{\text{sc}}^{\mathcal{B}}(t) = \dot{H}_{\text{rw}}^{\mathcal{B}}(t) = A(-\dot{h}(t)) = -A\tau_{\text{rw}}(t).$$

Therefore, under a least-squares control allocation scheme, the standard selection of reaction wheel motor torques to produce a commanded body torque, is taken as

$$\tau_{\text{rw}}(t) = -A^{+}\tau_{\text{sc}}^{\mathcal{B}}(t),$$

where A^{+} is the standard Moore-Penrose inverse of the matrix A, that gives the least-squares solution in terms of commanded torques [25]. Synthesizing the above derivations, the equations of rotational motion of a spacecraft which implements a standard Moore Penrose control allocation scheme with N_{rw} reaction wheels is given as

$$\begin{bmatrix} \dot{\omega}(t) \\ \dot{\Omega}_{\text{rw}}(t) \end{bmatrix} = \begin{bmatrix} J_{\text{sc}}^{-1}(AA^{+}\tau_{\text{sc}}^{\mathcal{B}}(t) - \omega(t) \times (J_{\text{sc}}\omega(t) + AJ_{\text{rw}}\Omega_{\text{rw}}(t))) \\ -J_{\text{rw}}^{-1}A^{+}\tau_{\text{sc}}^{\mathcal{B}}(t) \end{bmatrix}$$

5.3 Minimum Energy Attitude Steering

In this section, the dynamical model for a spacecraft implementing a least-squares control allocation scheme and the electrical energy model for reaction wheel actuators, are incorporated into an optimal control formulation for the minimizing the electrical energy required to perform a slew. The slewing maneuvers of interest to this work, are rest-to-rest maneuvers from an initial orien-

tation given by $q^0 \triangleq \left[e_0 \sin\left(\frac{\Phi_0}{2}\right), \cos\left(\frac{\Phi_0}{2}\right)\right]^\mathsf{T} \in \mathbb{R}^4$ to a final orientation given by $q^f \triangleq \left[e_f \sin\left(\frac{\Phi_f}{2}\right), \cos\left(\frac{\Phi_f}{2}\right)\right]^\mathsf{T} \in \mathbb{R}^4$, with $\omega^0 = \omega^f = 0 \in \mathbb{R}^3$. Other scenarios can be evaluated by appropriately altering the boundary conditions.

The optimal control formulation presented in this section incorporates practical constraints upon both state and control, each in-line with a typical operational scenario: (*i*) Reaction wheel speed-bias, $\Omega_{\text{bias}} \in \mathbb{R}$, is enforced per wheel to avoid operating the wheels near zero-speed. (*ii*) Per axis limits, $\omega_{\max} \in \mathbb{R}$, are imposed upon the spacecraft angular rate to avoid rate gyro saturation. (*iii*) Per wheel momentum storage, $\Omega_{\max} \in \mathbb{R}$, and torque authority, $\tau_{\max} \in \mathbb{R}$, constraints are also considered. The optimal control problem formulation is presented as follows, and is denoted hereafter as problem "A_{ns}":

$$
(A_{\text{ns}}) \begin{cases}
\text{State:} & x = [q, \omega, \Omega_{\text{rw}}]^\mathsf{T} \in \mathbb{R}^{7+N_{\text{rw}}}, \quad \text{Control:} \quad u = \tau_{\text{sc}}^{\mathcal{B}} \in \mathbb{R}^3, \\
\text{Minimize:} & J\left[x(\cdot), u(\cdot)\right] = \displaystyle\int_0^T \sum_{i=1}^{N_{\text{rw}}} \left\{\mathcal{P}_i\right\}^+ dt \\
\text{Subject To:} & \\
& \begin{bmatrix} \dot{q} \\ \dot{\omega} \\ \dot{\Omega}_{rw} \end{bmatrix} = \begin{bmatrix} \frac{1}{2}\mathcal{Q}(\omega) q \\ J_{\text{sc}}^{-1}(AA^+\tau_{\text{sc}}^{\mathcal{B}} - \omega \times (J_{\text{sc}}\omega + AJ_{\text{rw}}\Omega_{\text{rw}})) \\ -J_{\text{rw}}^{-1} A^+ \tau_{\text{sc}}^{\mathcal{B}} \end{bmatrix} \\
& x(0) = [q^0,\ \omega^0,\ \Omega_{\text{bias}}]^\mathsf{T} \in \mathbb{R}^{7+N_{\text{rw}}} \\
& x(t_f) = \left[q^f,\ \omega^f,\ \Omega_{\text{bias}}\right]^\mathsf{T} \in \mathbb{R}^{7+N_{\text{rw}}} \\
& |\omega_i| \leq \omega_{\max},\ \forall\, i = 1, 2, 3 \\
& |\Omega_{\text{rw},i}| \leq \Omega_{\max},\ \forall\, i = 1, \ldots, N_{\text{rw}} \\
& \left|(A^+\tau_{\text{sc}}^{\mathcal{B}}(t))_i\right| \leq \tau_{\max},\ \forall\, i = 1, \ldots, N_{\text{rw}}
\end{cases}
\tag{5.3}
$$

The state of the system consists of the attitude of the spacecraft in quaternion parameterization, the angular velocity of the spacecraft body (with respect to the

body frame), and the reaction wheel angular velocities (about their individual spin axes). Because the spacecraft is assumed to be allocating control authority to the reaction wheels (through a least-squares allocation scheme) the control vector is taken as the three-vector of torques acting on the spacecraft body. The cost functional is taken with the reaction wheel power-input of the reaction wheel array as the running cost; therefore problem A_{ns} minimizes the energy required to perform a slew. The upper bound on the transfer time for the slew is given by T. For a minimum-energy problem, it is typical for the final time to extend to the right of the allowed horizon, i.e. $t_f > T$. Therefore, for the problem to be feasible, the value of T must be, at minimum, the transfer-time of the shortest-time maneuver, t_{STM}, for the same parameters and boundary conditions. From this point of view, a minimum energy shortest-time maneuver can be determined by setting $T = t_{\text{STM}}$. The transfer time of the a shortest time maneuver, t_{STM}, can be determined by a simple modification to the cost functional by rewriting $J\left[x(\cdot), \tau_{\text{rw}}(\cdot), t_f\right] = t_f$ and allowing $0 \leq t \leq \infty$. The boundary conditions and the dynamics comprise the rest-to-rest attitude maneuvers and dictate the evolution of the system. Last in the formulation are the constraints associated to rate-gyro saturation, maximum reaction wheel speed, and torque generatable by the reaction wheels. Given that the control is taken as the spacecraft body torques and not the reaction wheel motor torques themselves, which have a hard-limit on maximum generatable torque, $\tau_{\max}$, an additional path constraint is required. To accommodate the hardware limits of maximum torque generatable by the reaction wheels, $\tau_{\max}$, requires the incorporation of N_{rw} paths constraints into the formulation, given by $\left|(A^{+}\tau_{\text{sc}}^{\mathcal{B}}(t))_i\right| \leq \tau_{\max},\ \forall\, i = 1, \ldots, N_{\text{rw}}$.

Problem A_{ns} does not enforce any constraints to constrain the attitude maneuver to be an eigenaxis slew. Therefore, off-eigenaxis slewing maneuvers are

feasible to problem A_{ns}, and hence are potential solutions to problem A_{ns} should they be more advantageous with respect to the energy metric when meeting a given constraint on the slew time. Given the extra degrees of freedom that off-eigenaxis maneuvering permits, coupled with the non-symmetric inertia tensors of real-world spacecraft, it seems plausible that off-eigenaxis maneuvers would be more advantageous with respect to energy when compared to their eigenaxis counterparts. Indeed this is the case as seen in [57]. The analysis to follow in this chapter is concerned with evaluating the energy requirements under attitude steering, for off-eigenaxis slew profiles against the conventional eigenaxis control logic [25]. To achieve an eigenaxis maneuver under a slew-rate constraint, the A_{ns} formulation presented in Eq. (5.3) requires two alterations: (i) To constrain the motion of the spacecraft, the angular velocity vector of the spacecraft must always be collinear with the eigenaxis [23]. Including the following path-constraint as part of problem A_{s} achieves this goal:

$$\omega(t) \times e(q^0, q^f) = 0 \in \mathbb{R}^3, \ \forall t, \tag{5.4}$$

It is noted in Eq. (5.4), that the eigenaxis e is a function of the initial and final attitude quaternion. For an eigenaxis slew it is also necessary to enforce a spherical slew rate constraint in concerns of saturating the rate gyros. This can be done by including an additional path constraint of the form $\|w\|_2 \leq \omega_{\max}$, which replaces the three path constraints $|\omega_i| \leq \omega_{\max}, \ \forall\, i = 1, 2, 3$.

5.3.1 Managing the Nonsmooth Energy Formulation

Using the method from Chapter 4, minimization of electrical energy may be cast as an L^1 problem:

$$\text{Minimize:} \quad J\left[x(\cdot), u(\cdot)\right] = \frac{1}{2}\int_0^T \left\{\sum_{i=1}^{N_{\text{rw}}} \mathcal{P}_i(t) + \sum_{i=1}^{N_{\text{rw}}} \left|\mathcal{P}_i(t)\right|\right\} dt$$

Based on this reformulation of the cost functional in problem A_{ns}, its is clear that the only terms involving the absolute value operator must transformed to obtain an equivalent smooth formulation. An appropriate choice of ancillary decision variables is based off of [58, 63], for each $i = 1, \ldots, N_{\text{rw}}$: $z_i(t) \triangleq \mathcal{P}_i(t)$. Next, the positive and negative portions of z are defined as

$$z_{a,i}(t) \triangleq \left\{\mathcal{P}_i(t)\right\}^+ \qquad \text{and} \qquad z_{b,i}(t) \triangleq \left\{-\mathcal{P}_i(t)\right\}^+, \tag{5.5}$$

where $\{\cdot\}^+$ is defined in Eq. (2.22). By the manner in which z, z_a, and z_b are defined, the following relationships hold for all $t \in [t_0, t_f]$ [44]:

$$z_i(t) = z_{a,i}(t) - z_{b,i}(t), \qquad |z(t)| = z_a(t) + z_b(t), \qquad z_a(t), z_b(t) \geq 0. \tag{5.6}$$

Because the cost functional is minimizing the absolute value of z, each ancillary control variable as defined in Eq. (5.5) are obtained through the path constraints of Eq. (5.6) along with the path constraints:

$$z_{a,i} - \mathcal{P}_i \geq 0, \ \forall\, i = 1, \ldots, N_{\text{rw}} \quad \text{and} \quad z_{b,i} + \mathcal{P}_i \geq 0, \ \forall\, i = 1, \ldots, N_{\text{rw}}, \tag{5.7}$$

Amalgamating Eqs. (5.6) and (5.7), an equivalent smooth formulation to problem A_{ns} may be arrived upon, and is given in the following formulation(which, hereafter

is referred to as problem $A_{\rm s}$):

$$
(A_{\rm s}) \left\{
\begin{array}{ll}
\text{State:} & x = [q, \omega, \Omega_{rw}]^{\mathsf{T}} \in \mathbb{R}^{7+N_{\rm rw}} \\
\text{Control:} & u = \left[\tau_{\rm sc}^{\mathcal{B}}, \quad z_{a,1}, \quad z_{b,1}, \quad \ldots, \quad z_{a,N_{\rm rw}}, \quad z_{b,N_{\rm rw}}\right]^{\mathsf{T}} \in \mathbb{R}^{3+2N_{\rm rw}} \\
\text{Minimize:} & J\left[x(\cdot), u(\cdot)\right] = \dfrac{1}{2}\displaystyle\int_0^T \left\{\sum_{i=1}^{N_{\rm rw}} \mathcal{P}_i + \sum_{i=1}^{N_{\rm rw}} (z_{a,i} + z_{b,i})\right\} dt \\
\text{Subject To:} & \\
& \begin{bmatrix} \dot{q} \\ \dot{\omega} \\ \dot{\Omega}_{rw} \end{bmatrix} = \begin{bmatrix} \frac{1}{2}\mathcal{Q}(\omega) q \\ J_{\rm sc}^{-1}(AA^{+}\tau_{\rm sc}^{\mathcal{B}} - \omega \times (J_{\rm sc}\omega + AJ_{\rm rw}\Omega_{\rm rw})) \\ \\ -J_{\rm rw}^{-1}A^{+}\tau_{\rm sc}^{\mathcal{B}} \end{bmatrix} \\
& x(0) = [q^0,\ \omega^0,\ \Omega_{\rm bias}]^{\mathsf{T}} \in \mathbb{R}^{7+N_{\rm rw}} \\
& x(t_f) = \left[q^f,\ \omega^f,\ \Omega_{\rm bias}\right]^{\mathsf{T}} \in \mathbb{R}^{7+N_{\rm rw}} \\
& \\
& z_{a,i} \geq 0,\ \forall\, i = 1, \ldots, N_{\rm rw} \\
& z_{b,i} \geq 0,\ \forall\, i = 1, \ldots, N_{\rm rw} \\
& z_{a,i} - \mathcal{P}_i \geq 0,\ \forall\, i = 1, \ldots, N_{\rm rw} \\
& z_{b,i} + \mathcal{P}_i \geq 0,\ \forall\, i = 1, \ldots, N_{\rm rw} \\
& |\omega_i| \leq \omega_{\max},\ \forall\, i = 1, 2, 3 \\
& |\Omega_{rw,i}| \leq \Omega_{\max},\ \forall\, i = 1, \ldots, N_{\rm rw} \\
& \left|(A^{+}\tau_{\rm sc}^{\mathcal{B}})_i\right| \leq \tau_{\max},\ \forall\, i = 1, \ldots, N_{\rm rw}
\end{array}
\right.
$$

The increase in dimensionality needed to obtain the equivalent *smooth* formulation to problem $A_{\rm ns}$ is to add $2N_{\rm rw}$ (ancillary) control variables, along with $4N_{\rm rw}$ constraints (thereby bringing the total path constraints in problem $A_{\rm ns}$ to $6N_{\rm rw}+3$). While there is a computational-cost for increasing the dimensionality to the optimal control problem $A_{\rm ns}$, it allows the *original* problem to directly be solved without having to resort to information loss, either through resorting to proxies

to the cost functional, linearizing the dynamics, or through homotopic approaches in which a sequence of problems are solved which converge to a solution to the original problem. Problem A_s may be readily solved numerically using any of the standard computational optimal control algorithms. Additionally, Pontryagin's Minimum Principle may be directly applied to problem A_s to obtain necessary conditions for optimality. For a spacecraft simultaneously utilizing four reaction wheels to perform attitude control, problem A_s has a 22-dimensional state-control pair (11 for state and 11 for control). Additionally to the high dimension of the state model, are nonlinear and coupled dynamics, as well a considerable number linear and nonlinear constraints, totaling to 27 path constraints. Therefore, determining an optimal solution to problem A_s is particularly challenging, both numerically and most-certainly analytically.

5.3.2 Necessary Conditions for Optimality

In this section, the necessary conditions for optimality for problem A_s are obtained through the application of Pontryagin's Minimum Principle. Necessary conditions serve an important role in the validation of a numerical solution, serving as a fail-test for potential solutions to problem A_s. At the heart of Pontryagin's Minimum Principle is the Hamiltonian Minimization Condition (HMC). The HMC states that, for an extremal control u^* to be optimal, it necessarily must minimize the control Hamiltonian at each instant of time. Due to the presence of state and control path constraints in problem A_s the necessary conditions from the HMC are obtained by applying the Karush-Kuhn-Tucker (KKT) conditions through the consideration of the Lagrangian of the control Hamiltonian:

$$\overline{H}(\mu, \lambda, x, u) = H(\lambda, x, u) + \mu^\intercal h(x, u) \tag{5.8}$$

where $H(\lambda, x, u) \in \mathbb{R}$ is the control Hamiltonian, $\mu \in \mathbb{R}^{3+6N_{\text{rw}}}$ the path covector consisting of the KKT multipliers associated to the HMC, and $h \in \mathbb{R}^{3+6N_{\text{rw}}}$ the vector of path constraints. By the KKT conditions, at each instant of time, the Lagrangian of the Hamiltonian must necessarily be stationary with respect to the control u:

$$\frac{\partial \overline{H}}{\partial u} = \frac{\partial \overline{H}}{\partial u} + \left(\frac{\partial h}{\partial u}\right)^{\mathsf{T}} \mu = 0 \in \mathbb{R}^{3+2N_{\text{rw}}} \tag{5.9}$$

Along with the stationary condition, the KKT conditions require the path covectors and path constraints satisfy the complementarity conditions: For each $i = 1, \ldots, 3 + 6N_{\text{rw}}$

$$\mu_i \begin{cases} \geq 0 \ \text{ if } h_i(x,u) = h_i^U \\ = 0 \ \text{ if } h_i^L < h_i(x,u) < h_i^U \\ \leq 0 \ \text{ if } h_i(x,u) = h_i^L \end{cases} \tag{5.10}$$

To simplify the presentation of the necessary conditions of problem A_{s}, the minimization of $\mathcal{E}$ is rewritten as it is equivalent to the minimization of the following cost functional:

$$J_{\text{equiv}}\left[x(\cdot), u(\cdot)\right] = \int_0^T \sum_{i=1}^{N_{\text{rw}}} \left(\frac{R}{K_\tau^2}\right) \tau_{\text{rw},i}^2 + \left(\frac{R\beta_{\text{v}}}{K_\tau^2} + 1\right) \beta_{\text{v}} \Omega_{\text{rw},i}^2 + (z_{a,i} + z_{b,i})\, dt. \tag{5.11}$$

The equivalency of the cost functional in Eq. (5.11) to that in Problem A_{s} is by the invariance of minimization under scalar multiplication and under vertical translations, along with the following relationship[57]

$$\int_0^T \sum_{i=1}^{N_{\text{rw}}} \tau_{\text{rw},i}(t) \Omega_{\text{rw},i}(t)\, dt = \sum_{i=1}^{N_{rw}} \frac{J_{\text{rw},i}}{2} \left(\Omega_{\text{rw},i}^2(T) - \Omega_{\text{rw},i}^2(0)\right), \tag{5.12}$$

which is arrived through Eq. (2.8). The control Hamiltonian for problem A_{s} is therefore given by

$$H(\lambda,x,u)=\sum_{i=1}^{N_{\mathrm{rw}}}\left(\left(\frac{R}{K_\tau^2}\right)\tau_{\mathrm{rw},i}^2+\left(\frac{R\beta_{\mathrm{v}}}{K_\tau^2}+1\right)\beta_{\mathrm{v}}\Omega_{\mathrm{rw},i}^2+(z_{a,i}+z_{b,i})\right)+\lambda_q^{\intercal}\left(\frac{1}{2}\mathcal{Q}(\omega)q\right)$$
$$+\lambda_\omega^{\intercal}\Big(J_{\mathrm{sc}}^{-1}(AA^{+}\tau_{\mathrm{sc}}^{\mathcal{B}}-\omega\times(J_{\mathrm{sc}}\omega+AJ_{\mathrm{rw}}\Omega_{\mathrm{rw}}))\Big)+\lambda_\Omega^{\intercal}\Big(-J_{\mathrm{rw}}^{-1}A^{+}\tau_{\mathrm{sc}}^{\mathcal{B}}\Big), \quad (5.13)$$

where each $\lambda_q\in\mathbb{R}^4,\lambda_\omega\in\mathbb{R}^3,\lambda_\Omega\in\mathbb{R}^{N_{\mathrm{rw}}}$, is a vector of costates with subscript corresponding to the associated state variable vector. The Lagrangian of the (control) Hamiltonian, is given by

$$\overline{H}(\mu,\lambda,x,u)=H(\lambda,x,u)+\mu_a^{\intercal}z_a+\mu_b^{\intercal}z_b+\sum_{i=1}^{N_{\mathrm{rw}}}\mu_{pos,i}(z_{a,i}-\mathcal{P}_i)+\sum_{i=1}^{N_{\mathrm{rw}}}\mu_{neg,i}(z_{b,i}+\mathcal{P}_i)$$
$$+\mu_\omega^{\intercal}\omega+\mu_\Omega^{\intercal}\Omega+\mu_\tau^{\intercal}\Big(A^{+}\tau_{\mathrm{sc}}^{\mathcal{B}}\Big) \quad (5.14)$$

where each $\mu_a,\mu_b,\mu_{pos},\mu_{neg},\mu_\Omega,\mu_\tau\in\mathbb{R}^{N_{\mathrm{rw}}},\mu_\omega\in\mathbb{R}^3$, is a vector of KKT covectors with subscript corresponding to the associated vector of path constraints. While Eq. (5.14) is somewhat lengthy, expressions for the stationary conditions in Eq. (5.9) may be attained through a straightforward application of matrix calculus:

$$0=\frac{\partial\overline{H}}{\partial\tau_{\mathrm{sc}}^{\mathcal{B}}}=\Big(\lambda_\omega^{\intercal}J_{\mathrm{sc}}^{-1}AA^{+}\Big)^{\intercal}-\Big(\lambda_\Omega^{\intercal}J_{\mathrm{rw}}^{-1}A^{+}\Big)^{\intercal}+(\mu_\tau A^{+})^{\intercal} \quad (5.15)$$

$$0=\frac{\partial\overline{H}}{\partial z_{a,i}}=1+\mu_{a,i}+\mu_{pos,i}\qquad\forall i=1,\ldots,N_{\mathrm{rw}} \quad (5.16)$$

$$0=\frac{\partial\overline{H}}{\partial z_{b,i}}=1+\mu_{b,i}+\mu_{neg,i}\qquad\forall i=1,\ldots,N_{\mathrm{rw}} \quad (5.17)$$

While the KKT conditions require that each of the seven collections of KKT covectors making up μ have associated to them complementarity conditions, for

the sake of brevity, only μ_a and μ_ω are presented as the the rest follow in like manner:

$$\mu_{\omega,i}\begin{cases}\geq 0 \ \text{ if } \omega_i = \omega_{\max} \\ = 0 \ \text{ if } -\omega_{\max} < \omega_i < \omega_{\max} \\ \leq 0 \ \text{ if } \omega_i = -\omega_{\max}\end{cases}, \qquad \mu_{a,j}\begin{cases}= 0 \ \text{ if } 0 < z_{a,j} < \infty \\ \leq 0 \ \text{ if } z_{a,j} = 0\end{cases} \tag{5.18}$$

Along with the complementarity conditions and stationary conditions, another extremely important necessary condition for the validation of numerically computed solution is arrived upon by considering the lower Hamiltonian and how it evolves over time. The lower Hamiltonian, $\mathcal{H}$, is acquired by evaluating the (control) Hamiltonian along an extremal solution, u^*, of the HMC, i.e. $\mathcal{H}(\lambda, x) \triangleq H(\lambda, x, u^*)$, and evolves over time according to $\dot{\mathcal{H}}(\lambda, x) = \partial_t \overline{H}$ (known as the Hamiltonian Evolution Equation [58]). Therefore, because problem A_s is time invariant, the Hamiltonian Evolution Equation states that optimal solutions to problem A_s must necessarily have lower Hamiltonian which is constant for all time, i.e.

$$\frac{d}{dt}\mathcal{H}(\lambda, x) = 0 \qquad \forall\, t \in [0, T]. \tag{5.19}$$

The use of the adjoint equations to problem A_s, which evolve according to $-\dot{\lambda} = \partial_x \overline{H}$, for the purpose of validating numerical solutions of problem A_s is not helpful because the equations are complicated. For example, the adjoint associated to the

quaternions evolve according to

$$\begin{aligned}
\dot{\lambda}_{q_1} &= \tfrac{1}{2}\left(\lambda_{q_2}\omega_3 - \lambda_{q_2}\omega_2 + \lambda_{q_4}\omega_1\right) \\
\dot{\lambda}_{q_2} &= \tfrac{1}{2}\left(-\lambda_{q_1}\omega_3 + \lambda_{q_3}\omega_1 + \lambda_{q_4}\omega_2\right) \\
\dot{\lambda}_{q_3} &= \tfrac{1}{2}\left(\lambda_{q_1}\omega_2 - \lambda_{q_2}\omega_1 + \lambda_{q_4}\omega_3\right) \\
\dot{\lambda}_{q_4} &= \tfrac{1}{2}\left(-\lambda_{q_1}\omega_1 - \lambda_{q_2}\omega_2 - \lambda_{q_3}\omega_3\right)
\end{aligned}$$

Therefore, the necessary conditions used in this chapter to demonstrate the validity of a numerical solution for optimality include the stationary conditions, complimentary conditions, and the consistency of the lower Hamiltonian.

Along with verifying the satisfaction of the necessary conditions for the candidate optimal control solution it is also necessary to demonstrate the feasibility of the candidate optimal control, u^*. This feasibility analysis is carried out by propagating u^* through the dynamics using a standard Runge-Kutta (RK) integrator. The candidate optimal control is deemed feasible if and only if the solution returned by the RK integrator coincides with the solution obtained by the numerical solver, to within a predefined tolerance, i.e. $\epsilon < 10^{-6}$ where ϵ is the error. For an in depth discussion on the verification and validation of optimal control solutions, see Ross [58]. All results present in this chapter successfully passed feasibility within the predefined tolerance specified in this section.

5.4 Minimum Energy Attitude Steering

This section demonstrates the existence and efficacy of minimum energy rest-to-rest slews by steering the attitude of a spacecraft which implements its own control allocation scheme (thereby precluding the direct control of the motor toques generated by the reaction wheels). The spacecraft is assumed to distribute

the control torque through a least-squares allocation scheme (i.e. Moore-Penrose). To demonstrate the minimum energy attitude steering maneuver, a 180-degree rest-to-rest slew about the spacecraft's z-axis is considered, whose initial and final quaternions are $q^0 = [0, 0, 1, 0]^\intercal$ and $q^f = [0, 0, 0, 1]^\intercal$ and parameters are given in the Appendix.

The maneuver type which serves as the baseline is a conventional shortest time eigenaxis maneuver (ST-EAM) under least-squares control allocation. In order to obtain the ST-EAM under L^2 allocation, a problem formulation is constructed and solved which is analogous to A_{ns}: (*i*) Replace the cost functional with transfer time, i.e. $J\left[x(\cdot), u(\cdot), t_f\right] = t_f$, (*ii*) Add the path constraint in Eq. (5.4) which enforces eigenaxis maneuvering, and (*iii*) Incorporate the spherical slew rate constraint $\|w\|_2 \leq \omega_{\max}$ and remove the path constraint $|\omega_i| < \omega_{\max}$ for each $i = 1, 2, 3$.

The shortest-time eigenaxis maneuver to the 180-degree slew completes in 362.0 seconds, and requires 108 J of energy. The state and control profiles associated to the ST-EAM are shown in Figure 5.1. Pontryagin's Minimum Principle states that the lower Hamiltonian should be -1 over the entire time horizon for minimum-time problems, and Figure 5.4a depicts the consistency of the lower Hamiltonian associated to the solution. The monotonicity of the quaternions in Figure 5.1a depict that the obtained solution is in fact an eigenaxis maneuver. Figure 5.1b shows the build up of the angular velocity of the spacecraft is about the z-axis (the eigenaxis for this particular maneuver). The control profile seen in Figure 5.1c is bang-bang, which is consistent for shortest time maneuvers. The reaction wheel speeds seen in Figure 5.1d are observed to begin and end the maneuver at their specified biases of 20 rad/sec.

By solving problem A_{s}, with the upper bound on transfer time to be the slew

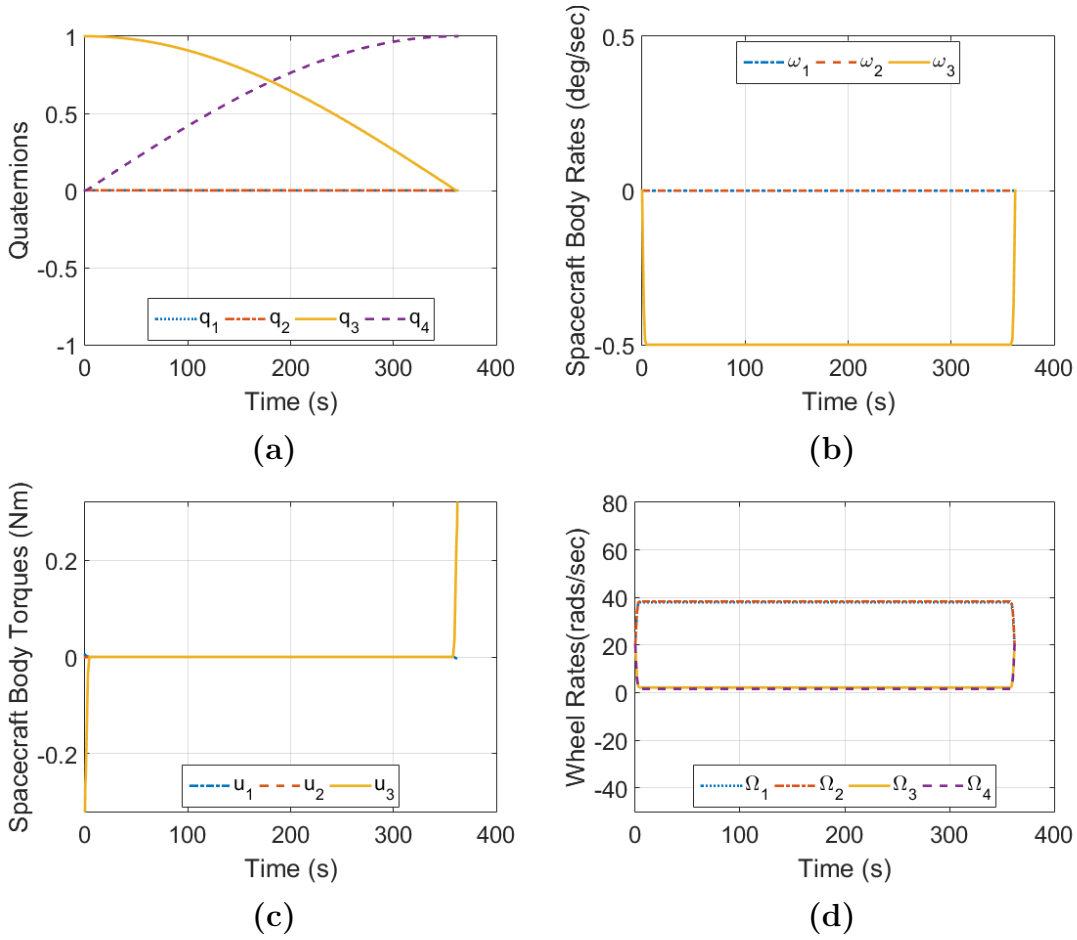

Figure 5.1: State and control profiles of a Shortest Time Eigenaxis Maneuver for a 180-deg rest-to-rest slew about the spacecraft z-axis: (a) attitude; (b) body rates; (c) body torques (control); (d) reaction wheel rates.

time for the baseline eigenaxis maneuver, i.e. $T = 362.0$ seconds, a minimum energy maneuver is obtained by steering the attitude of the spacecraft and hence working about the ACS which allocates the control toque through a least-squares scheme. The solution obtained solving A_s completes the slew with the same transfer time as the baseline eigenaxis maneuver, yet requires 36.4% less energy (69.1 J as compared to 108.1 J). The state and control profiles to this minimum energy solution is given in Figure 5.2, and differ dramatically from the state and control profiles obtained by solving for the baseline eigenaxis maneuver. Problem A_s does

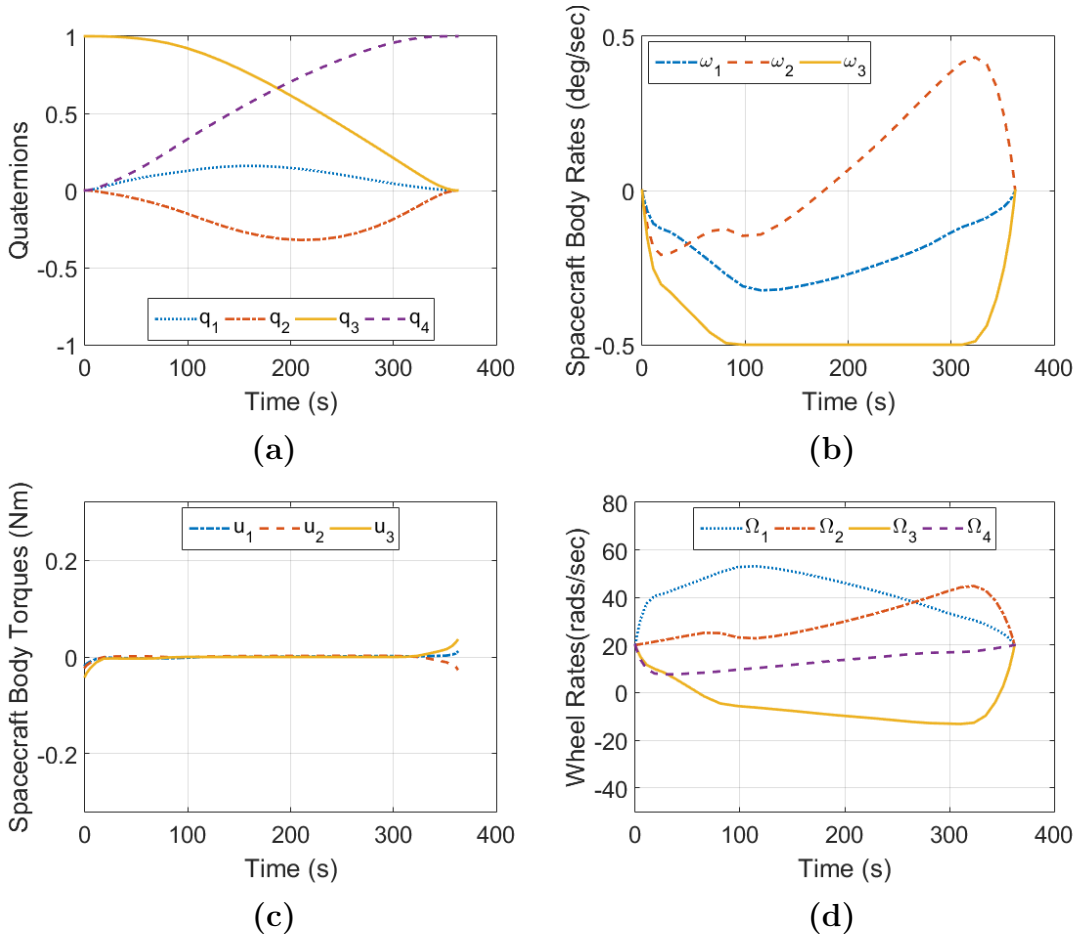

Figure 5.2: State and control profiles of a Minimum Energy Attitude Steered Maneuver, for a 180-deg rest-to-rest slew about the spacecraft z-axis: (a) attitude; (b) body rates; (c) body torques; (d) reaction wheel rates.

not restrict motion to be along the eigenaxis, and so off-eigenaxis maneuvering is feasible to problem A_s. The non-monotonicity of the quaternion attitude profiles in Figure 5.2a demonstrates that the minimum energy attitude steering maneuver utilizes off-eigenaxis maneuvering to complete the slew. Off-eigenaxis maneuvering allows the spacecraft to build the body-velocities simultaneously about each its axes, with saturation about the spacecraft z-axis from 85 seconds to 310 seconds, as seen in Figure 5.2b Figures 5.2c and 5.2d depict the control (spacecraft body torque) and the reaction wheel speeds. Comparing the torques of the minimum

Table 5.1: Metrics to the baseline eigenaxis maneuver in Figure 5.1, and the minimum energy attitude steering maneuver in Figure 5.2 (values in parenthesis represent percentage change from the baseline).

Maneuver Type	TT (s)	$\mathcal{E}$ (J)	$\mathcal{E}_{total}^{loss}$ (J)	$\mathcal{C}_{loss}$ (J)	$\mathcal{F}_{loss}$ (J)
Shortest Time Eigenaxis Maneuver	362.0	108.7	106.3	61.1	45.2
Minimum Energy Attitude Steering	362.0 (0.0%)	69.1 (-36.4%)	56.4 (-46.9%)	8.2 (-86.6%)	48.3 (+6.9%)

energy maneuver to those from the conventional baseline eigenaxis maneuver, the bang-bang profiles are now replaced with markedly less-demanding control profiles. This difference in torque authority translates into an 87% reduction in copper loss from the baseline eigenaxis maneuver (from 61.1 J to 8.2 J). The speed profile to each reaction wheel for the minimum energy maneuver is given in Figure 5.2d. On account of the effort towards maneuvering off-eigenaxis, the friction loss incurred by the minimum energy attitude steered maneuver increases by 7% from the conventional EAM (45.2 J to 48.3 J). Even with the small increase in frictional losses, the minimum energy steered solution reduces the dissipative losses by 47% (56.4 J as compared to 106.3), and therefore has less heat to reject than the canonical EAM. Table 5.1 summarizes the slew-time and energy metrics between the conventional EAM and the minimum energy solution.

To demonstrate the efficacy by which minimum energy attitude steered solutions reduce power requirements, the time histories of power and cumulative energy consumed by the reaction wheel array for the solution to problem A_{s} is compared against the baseline eigenaxis maneuver, and are given in Figure 5.3. In the comparison of RWA power usage, Figure 5.3a shows that the minimum-energy solution reduces the peak power demand by nearly 96% (from 28.3 W to 1.2 W), average power by 85% (from 2.0 W to 0.3 W), thereby reducing the peak-to-average power ratio by 76% (from 14.5 to 3.5). Table 5.2 summarizes the comparison of peak and average power between the two maneuver schemes. In Figure 5.3b, the total energy consumption of the RWA for the two maneuver

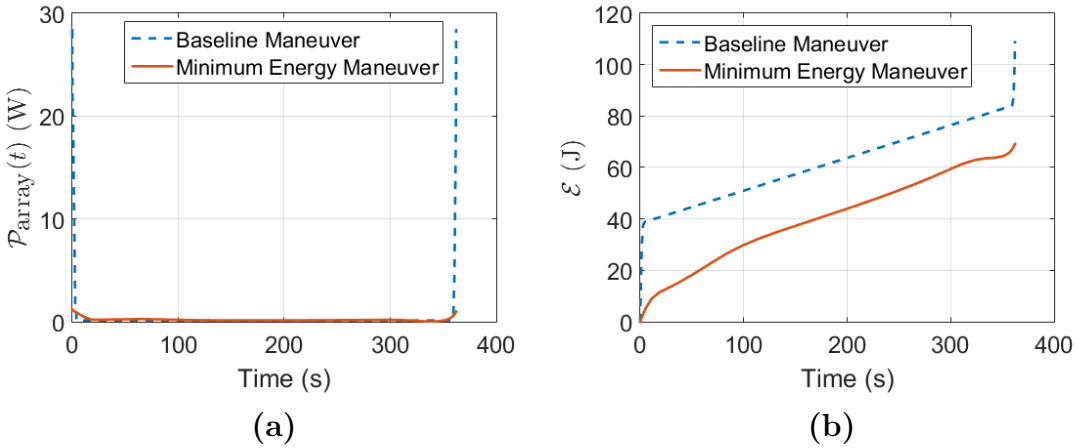

Figure 5.3: Comparison between the baseline eigenaxis maneuver and minimum energy attitude steering: (a) Electrical power consumed by the RWA; (b) Cumulative electrical energy consumed by the RWA.

schemes is shown. It is clear that by steering the attitude of the spacecraft, the energy required to perform the slew is substantially reduced and that *enforcing eigenaxis maneuvering limits the spacecraft with respect to energy.*

Table 5.2: Reaction wheel array power usage of the baseline eigenaxis maneuver compared to the minimum energy attitude steered maneuver (values in parenthesis represent percentage change from the baseline).

Maneuver Type	Peak Power (W)	Average Power (W)	Peak-to-Average Power Ratio
Shortest Time Eigenaxis Maneuver	28.3	2.0	14.5
Minimum Energy Attitude Steering	1.2 (-95.8%)	0.3 (-85.0%)	3.9 (-73.1%)

Lastly, the minimum-energy solution obtained from solving problem A_{s} is to be vetted against the necessary conditions of optimality. Figures 5.4b and 5.5 show the the numerical solution obtained from solving problem A_{s} satisfies the necessary conditions given by Pontryagin's Minimum principle. The (lower) Hamiltonian associated to the numerical solution obtained by solving the minimum energy maneuver is shown in Figure 5.4b, and is consistent with the Hamiltonian Evolution Equation of Pontryagin's Minimum Principle, which requires that the Hamiltonian be a fixed constant for all time over the finite horizon $[0, T]$. While

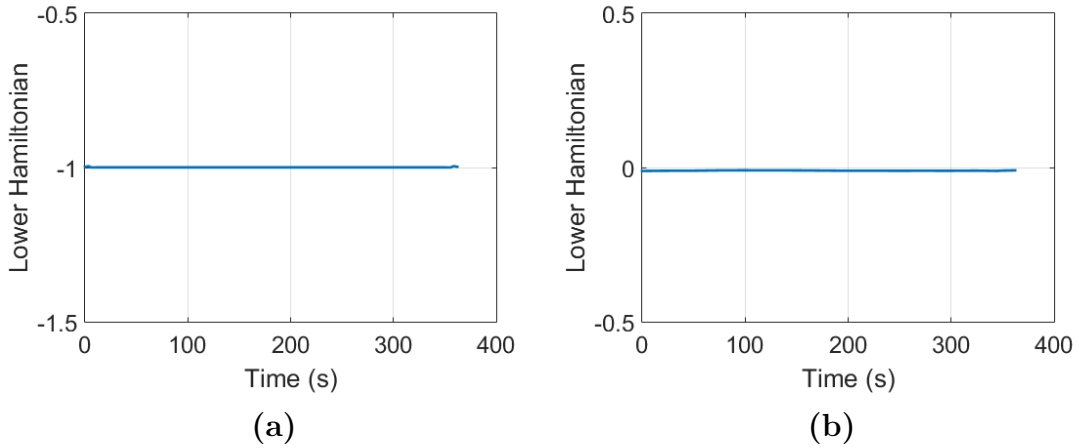

Figure 5.4: Consistency of the lower Hamiltonian for the: (a) ST-EAM ; (b) minimum energy attitude steering.

the Hamiltonian associated to the minimum energy solution is demonstrated to be constant, it is not -1; this discrepancy is due to the fact that problem A_s is solved as a *fixed-time* problem, not a *minimum-time* problem. Figure 5.5a shows the complementarity condition on the spacecraft angular rate, ω_3: The KKT multiplier associated to ω_3 is observed to vary in accordance to Eq. (5.18) which specifies that $\mu_{\omega,3} = 0$ unless the constraint upon ω_3 is active. The specifics on the other necessary conditions such as the details on transversality, the Hamiltonian value conditions, etc. while verified, have been omitted for brevity. Therefore, by passing both feasibility and the necessary conditions posed by Pontryagin's Minimum Principle, the solution obtained by solving to problem A_s may be considered an optimal solution.

5.5 Feedback Implementation

In a practical flight setting,[1,5,6,26–29] the open loop trajectories obtained from solving optimal control problems are typically most effectively implemented when tracked by a feedback controller.[15] In this section, the attitude and body rate

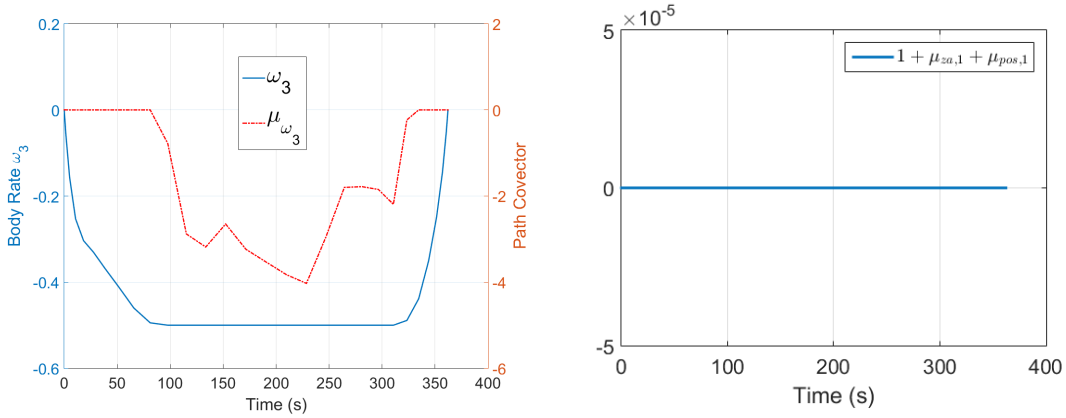

(a) **(b)**

Figure 5.5: Verification of necessary conditions to the Minimum Energy Attitude Steered 180-deg rest-to-rest slew about the spacecraft z-axis: (a) Complementarity condition for ω_3; (b) Stationary condition for $z_{a,1}$.

trajectories associated to the baseline eigenaxis maneuver and the minimum energy attitude steering used as inputs to a standard quaternion-error control-law. A block diagram of the control loop used in this section is shown in Figure 5.6: To track a commanded attitude ($q_c \in \mathbb{R}^4$) and spacecraft body velocity ($\omega_c \in \mathbb{R}^3$), the feedback law produces a body torque $\tau_{sc}^{\mathcal{B}} \in \mathbb{R}^3$. For the N_{rw} reaction wheels to produce this body torque, reaction wheel toques are allocated through a least squares allocation, where $A^+ \in \mathbb{R}^{N_{rw} \times 3}$ is the pseudoinverse of A. Figure 5.7 shows

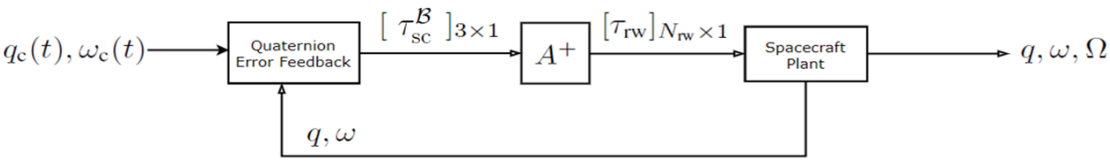

Figure 5.6: Quaternion error feedback control law for implementing minimum energy maneuvers

that the feedback controller correctly tracks the attitude and body rate of the two maneuvers. Tables 5.3 and 5.4 summarize the energy and power performance due to tracking the baseline eigenaxis maneuver, as well as the minimum energy maneuver, obtained by solving to Problem A_s. The small discrepancy in the energy

and power metrics between the open-loop and closed-loop performances for both maneuver schemes, is in part because the influence from the dynamics of the ACS were not considered in the problem formulations for either maneuver type. Even with this small discrepancy, by opting for the minimum energy maneuver over the baseline shortest time eigenaxis maneuver, the slew may be completed with 36% less energy (from 113.1 J to 72.2 J) with dissipative losses reduced by 46% (from 109.0J to 59.4 J). The minimum energy off-eigenaxis maneuver is able to drive the peak-to-average power ratio down from 81.4 to 6.5 (a reduction of 92%), completing the baseline maneuver with 95% less peak power (1.2 W as compared to 23.0 W). Figures 5.8 and 5.9 depicts the dramatically stark difference in energy and power consumption between the two maneuver schemes and demonstrate that the open-loop solutions accurately predict the closed-loop response of the feedback controller in Figure 5.6. By maneuvering off-eigenaxis, energy, dissipative losses, and peak power are dramatically reduced. Therefore, late in the mission life of a spacecraft, when diminished power profiles are more likely to occur, more slews may be feasible by opting for minimum energy maneuvering in situations where the reaction wheels can not be directly controlled.

Table 5.3: Metrics to the close-loop implementation of the baseline eigenaxis maneuver and minimum energy attitude steering in Figure 5.7 (values in parenthesis represent percentage change from tracking the baseline).

Maneuver Type	TT (s)	$\mathcal{E}$ (J)	$\mathcal{E}_{total}^{loss}$ (J)	$\mathcal{C}_{loss}$ (J)	$\mathcal{F}_{loss}$ (J)
Baseline Eigenaxis Maneuver	400.0	113.1	109.0	61.1	47.9
Minimum Energy Attitude Steering	400.0 (0.0%)	72.2 (36.2%)	59.4 (-45.5%)	8.0 (-86.9%)	51.4 (+7.3%)

Table 5.4: RWA power usage to the closed-loop the baseline eigenaxis maneuver and minimum steering (values in parenthesis represent percentage change from the closed-loop baseline).

Maneuver Type	Peak Power (W)	Average Power (W)	Peak-to-Average Power Ratio
Baseline Eigenaxis Maneuver	23.0	0.3	81.4
Minimum Energy Attitude Steering	1.2 (-94.8%)	0.2 (-33.3%)	6.5 (-92.0%)

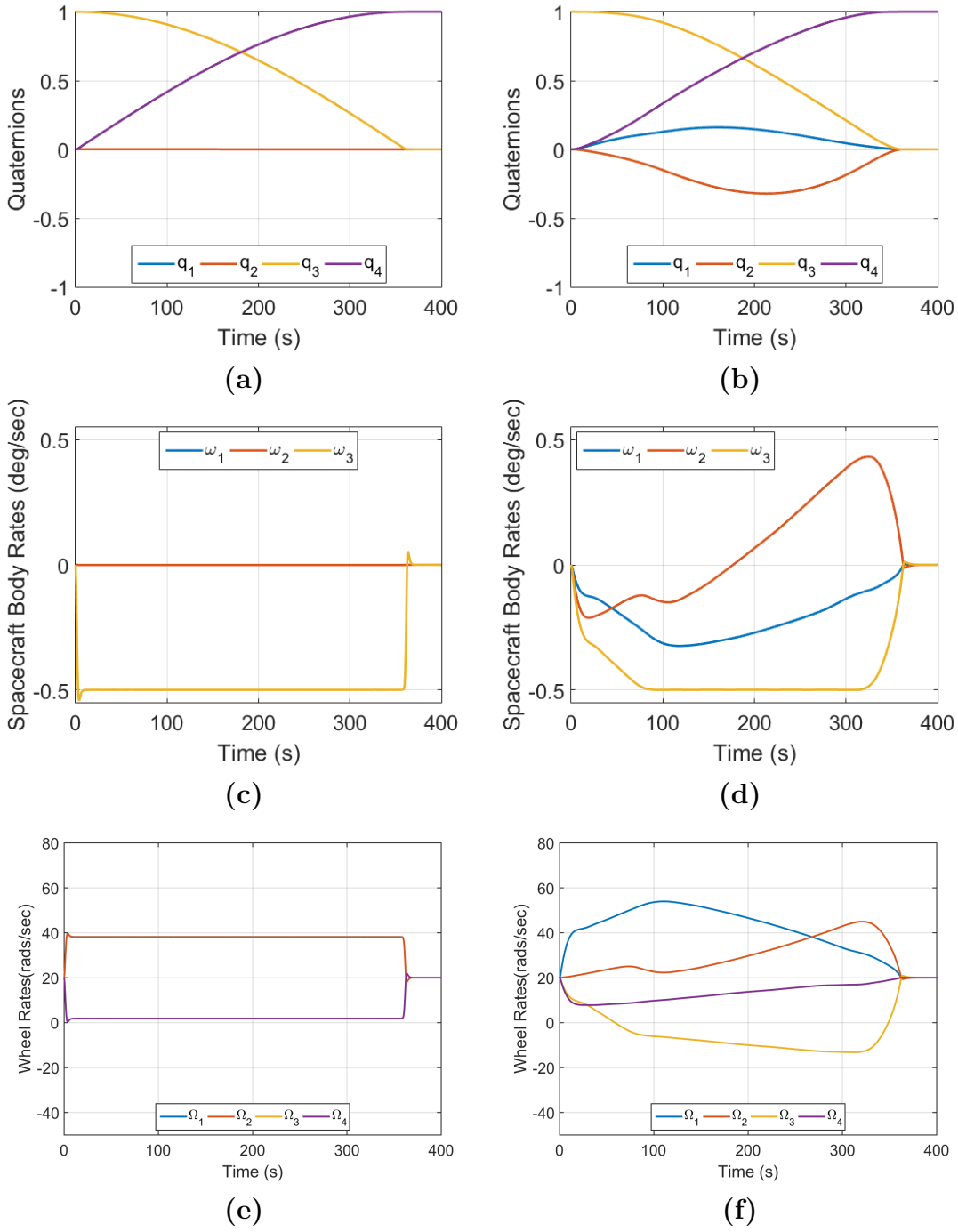

Figure 5.7: Closed-loop state profiles for the baseline eigenaxis maneuver and minimum energy attitude steering: baseline attitude and body rates in (a) and (c) ; attitude and body rates for minimum energy attitude steering in (b) and (d); (e) and (f) are the reaction wheel rates over the course of the maneuver.

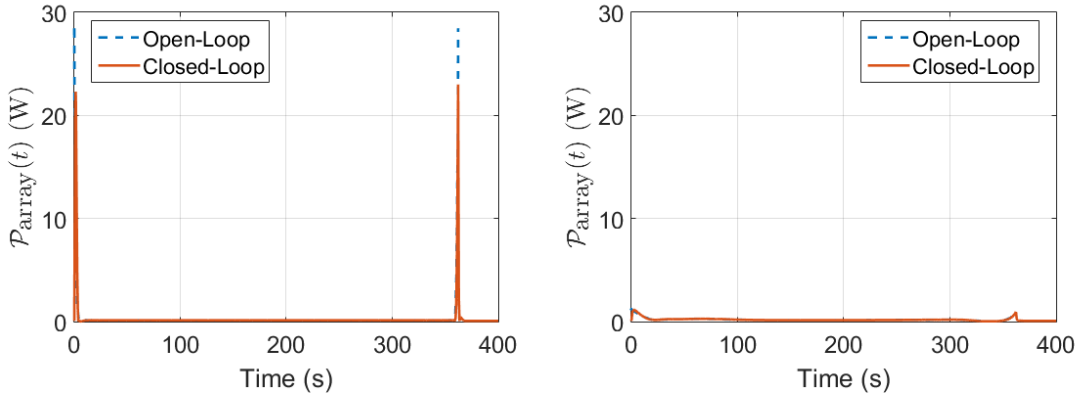

Figure 5.8: Power consumed by the reaction wheel array over the maneuver for the open-loop (dashed) and closed-loop (solid) implementation: (a) baseline eigenaxis maneuver; (b) minimum energy attitude steering.

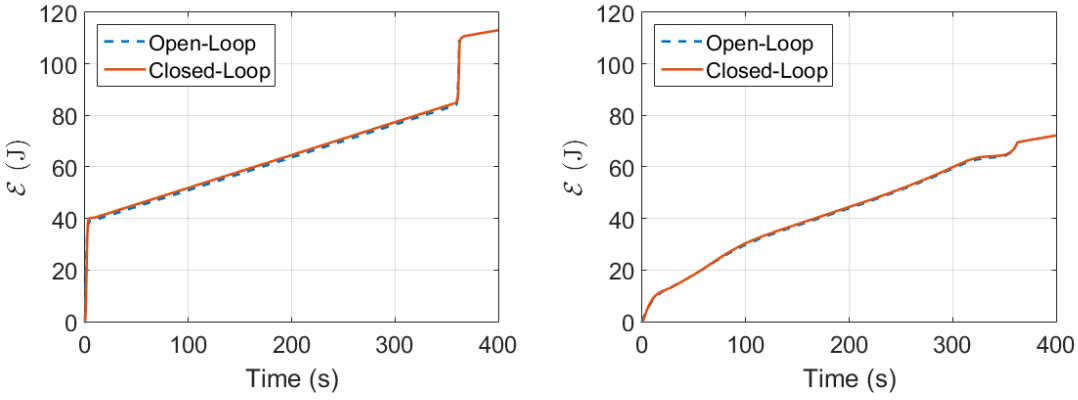

Figure 5.9: Energy for open-loop (dashed) and closed-loop (solid) implementation: (a) baseline eigenaxis maneuver; (b) minimum energy attitude steering.

5.6 Conclusions

This chapter demonstrates the existence of solutions to minimum electrical energy maneuvering in the situations *when the reaction wheels can not be directly controlled*, such as with a heritage attitude control system.The approach taken was the formulation of a family of nonlinear nonsmooth L^1, operationally relevant, optimal control problems to minimize the electrical energy the reaction wheel array to perform a slew, *solely* through steering the attitude of the spacecraft. Steering the attitude can produce maneuvers which substantially reduced electrical energy requirements as well as reduce peak power, compared to conventional eigenaxis maneuvering . Results present in this chapter demonstrate that *a significant penalty to both energy and power is incurred by enforcing eigenaxis maneuvering*. By maneuvering off-eigenaxis, energy, dissipative losses, and peak power are dramatically reduced. Therefore, late in the mission life of a spacecraft, when diminished power profiles are more likely to occur, agile slews may be feasible by opting for minimum energy maneuvering in situations where the directly controlling the reaction wheels is not possible.

Additionally it was shown that the open-loop solutions for minimum energy attitude steering can be implemented using closed-loop control. Moreover the open-loop solutions accurately predict the closed loop response. Therefore in situations where the ACS does not permit direct access to the reaction wheels, attitude steering may be utilized as a valuable tool for managing power and energy requirements. Additionally it is noted that no modification to the flight software is required to fly the new minimum energy maneuvers. Because of this, there is a great potential to effect and implement these reduced energy maneuvers on a broad class of spacecraft.

Chapter 6

Conclusions and Future Work

> "Without continual growth and progress, such words as improvement, achievement, and success have no meaning."
>
> *Albert Einstein*

Power is as necessary to the operation of a spacecraft, as breathing is to a human. Energy is a fundamentally limited resource of a spacecraft which directly effects its utility and mission life. Power profiles of the spacecraft attitude control system degrade as a spacecraft ages, which reduces the capabilities of the attitude control system and onboard sensors. Proper management of the energy and power systems of a reaction wheel attitude control system can increase the longevity of scientific collection, as well as to potentially increase the lifespan of reaction wheels. But, to properly manage the energy and power profiles, they must be understood in the context of an industry-strength flight setting.

This body of work has addressed fundamental questions in regards to minimizing the energy and reducing the power required to slew a spacecraft which uses reaction wheel momentum exchange devices for attitude control. Situations which can potentially arise in a practical flight setting were identified, motivated, addressed, and have been answered from a practical standpoint of a flight set-

ting, which consists of incorporating constraints apropos to an operational setting. These constraints were actuator constraints (associated to rate-gyros and reaction wheels) nonlinear rotational dynamics, as well the introduction of a constraint which enforced eigenaxis maneuvering. The main situations addressed and answered in this work were: (*i*) What is an appropriate metric for measuring energy of *a reaction wheel spacecraft* (*ii*) How can energy be reduced when the attitude of the spacecraft is predetermined (*iii*) How can energy be reduced when the reaction wheels can not be directly controlled and (*iv*) What is the relationship between energy and transfer time for on-and off-eigenaxis maneuvering.

An aspect of this thesis key to the results, is that *electrical* energy is minimized. This choice has allowed the development of a cost-functional which is more in line with the actual operational cost of a reaction wheel actuator, and has separated this work from the rest of literature associated to energy-optimal attitude control regarding reaction wheel spacecraft. Works up to this dissertation have minimized proxies associated to electrical energy that are either based upon mechanical energy or some measurement of control effort rather than directly minimizing electrical energy. Additionally, this dissertation developed a cost functional to minimize copper and friction dissipative losses which resulted with a naturally occurring quadratic functional.

Minimizing electrical energy slews has been shown to a problem in L^1 optimal control. To overcome the challenges posed by nonsmoothness, an augmentation method was adopted which transformed formulation to an equivalent smooth formulation by lifting the dimensionality of the problem through the addition of ancillary control variables and path constraints upon those variables. This method has allowed the problem formulation for minimum electrical energy slews to be solved without any approximation.

The relationship between transfer time and electrical energy for both conventional eigenaxis maneuvering, and unconventional off-eigenaxis maneuvering, has been identified in this dissertation under minimum dissipative losses (thereby reducing the amount of heat to reject), as well as under minimum electrical energy (thereby reducing battery draw). The nonlinear relationship between electrical energy and transfer time demonstrated that there exits a slew time interval about the shortest-time maneuver with the property that a small increase in transfer time from the time optimal slew time results with a large decrease in electrical energy. The relationship further shown that there exists a slew time, such that savings upon energy are negligible for any transfer time past this point. Additionally, the nonlinear relationship between the two maneuver types showed that there exists a tradespace between off-and on-eigenaxis maneuvering. This tradespace demonstrated that there exists agile maneuvering within energy budget of conventional eigenaxis maneuvering, thereby refuting age-old intuition that a more agile maneuver necessarily requires more control effort. The tradespace also shown that by maneuvering off-eigenaxis, energy may be greatly decreased for the same slew time budget as a conventional eigenaxis maneuver. These results upon the tradespace have shown that constraining the rotational motion of a spacecraft about an eigenaxis grossly hinders transfer time and electrical energy and peak-power, and that substantial savings upon transfer time and energy can be obtained by opting for off-eigenaxis maneuvering.

The situation where the attitude can not be changed has been motivated as a real concern in a flight setting and a reduced energy solution for this situation has been presented: It has been shown that null motions may be utilized to reduce the energy cost performing the slew. To demonstrate this a one dimensional linear optimal control problem was subsequently developed which provided (computa-

tionally) fast reduced-energy solutions, which could be implemented in real-time and also served to serves as a simple necessary condition specific for slews with minimum dissipative losses.

This dissertation demonstrated that situations exits when the reaction wheels may not be directly controlled and that, in this situation, reduced electrical energy solutions are obtainable by steering the attitude of the spacecraft through controlling the body torque of the spacecraft. These solutions also shown that the peak power and average power can dramatically be reduced by steering the spacecraft. Open loop trajectories obtained in this body of work by solving optimal control formulations were demonstrated to accurately predict closed loop behavior when tracked by feedback controllers.

Therefore, the collection of results to this body of work may be a valuable tool to mission operations for planning and budgeting purposes in an operational scenario for reduced energy slews for reaction wheel spacecraft. Results in this dissertation demonstrate that eigenaxis maneuvering significantly limits a spacecraft in terms of agility, energy, and power: Substantial reductions upon transfer time, energy, dissipative losses, and power may be realized by maneuvering off-eigenaxis.

A substantial and obvious extension to this body of research is to have an empirical study which validates the findings throughout this dissertation. This experiment, or set of experiments, could be as simple as validating minimum electrical energy shortest time maneuvers, or perhaps demonstrating the closed loop responses in the Attitude Steering material in Chapter 5. A physical example which demonstrates energy savings by applying the results in this work would be quite beneficial.

Appendix A

Simulation Parameters

"We'll meet again, we'll part once more."

James Joyce
Finnegans Wake

The parameters for the example spacecraft used throughout this work are summarized in Table A.1.

Parameter Description	Symbol	Value & Units
Number of reaction wheels	N_{rw}	4
Armature resistance	R	1.8 Ohms
Motor torque constant	K_{T}	0.0696 Nm/A
Back EMF constant	K_{V}	0.0696 V $\cdot$(rads/s)$^{-1}$
Wheel viscous friction coefficient	β_{v}	4.3×10^{-5} Nm $\cdot$(rads/s)$^{-1}$
Maximum reaction wheel speed	Ω_{max}	450.0 rads/s
Maximum motor torque	τ_{max}	0.14 Nm/s
Wheel rotor inertia	J_{rw}	0.012 kg $\cdot$ m^2
(Per) Wheel speed bias	Ω_{bias}	20.0 rads/s
Rate gyro limit	ω_{max}	0.5 degs/s – per axis
Reaction wheel projection matrix	A	$\frac{1}{\sqrt{3}}\begin{bmatrix} 1 & -1 & -1 & 1 \\ 1 & -1 & 1 & -1 \\ 1 & 1 & -1 & -1 \end{bmatrix}$
Spacecraft inertia tensor	J_{sc}	$\begin{bmatrix} 59.22 & -1.14 & -0.80 \\ -1.14 & 40.56 & 0.10 \\ -0.80 & 0.10 & 57.60 \end{bmatrix}$ kg $\cdot$ m^2

Table A.1: Spacecraft parameters [1, 3, 4] used in this work.

Appendix B

Published Works

> "The way to do research is to attack the facts at the point of greatest astonishment."
>
> *Celia Green*

This chapter presents the body of publications associated to and with the author, which have served as the foundation to this dissertation.

B.1 Journals

- Harleigh C. Marsh, Mark Karpenko, and Qi Gong. "Relationships Between Maneuver Time and Energy for Reaction Wheel Attitude Control," Journal of Guidance, Control, and Dynamics, Vol. 41, No. 2 (2018), pp. 335-348.

B.2 Conferences & Presentations

- Harleigh C. Marsh, Mark Karpenko, and Qi Gong. "Energy Constrained Shortest Time Maneuvers for Reaction Wheel Satellites,"AIAA/AAS Astrodynamics Specialist Conference, September 2016, Long Beach, CA. Paper number: AIAA 2016-5579.

- Mark Karpenko, Cornelius J. Dennehy, Harleigh C. Marsh, and Qi Gong. "Minimum power slews and the James Webb Space Telescope," The 27th AAS/AIAA Space Flight Mechanics Meeting, San Antonio, TX, February 5 to February 9 2017, Paper number: AAS 17-285.

- Harleigh C. Marsh, Mark Karpenko, and Qi Gong. "Electrical-Power Constrained Attitude Steering," AAS/AIAA Astrodynamics Specialist Conference, Stevenson, WA, August 20 to August 24 2017, Paper number: AAS-17-774.

B.3 Posters

- Graduate Research Symposium 2017: "Energy Constrained Shortest-Time Maneuvers For Reaction Wheel Satellites," University of California, Santa Cruz.
- Speed Geek 2016: "Energy Constrained Shortest-Time Maneuvers for Reaction Wheel Satellites," AIAA/AAS Astrodynamics Specialist Conference, September 2016, Long Beach, CA. Out of 500 technical presenters, Harleigh was one of ten selected to present at Speed Geek 2016. This poster was a brief on the accepted conference paper at Space 2016.
- Advanced Studies Laboratories and University Affiliated Research Center Poster Symposium: "Mission Control Technologies (MCT): Presenting a Viable Open-Source Mission-Operations Software Project to the Public," NASA Ames Research Center, August 8, 2013.

Bibliography

[1] M. Karpenko, S. Bhatt, N. Bedrossian, A. Fleming, and I. M. Ross, "First Flight Results on Time-Optimal Spacecraft Slews," *Journal of Guidance, Control, and Dynamics*, Vol. 35, No. 2, 2012, pp. 367–376.

[2] H. Schaub and J. L. Junkins, *Analytical Mechanics of Space Systems*. AIAA Education Series, AIAA, Reston, VA, Third ed., 2003.

[3] B. Bialke, "High fidelity mathematical modeling of reaction wheel performance," *21st Annual American Astronautical Society Guidance and Control Conference*, 1998, pp. 483–496.

[4] E. Ahronovich and M. Balling, "Reaction Wheel and Drive Electronics For LeoStar Class Space Vehicles," 1998.

[5] N. Bedrossian, M. Karpenko, and S. Bhatt, "Overclock My Satellite," *IEEE Spectrum*, Vol. 49, No. 11, 2012, pp. 54–62.

[6] M. Karpenko, S. Bhatt, N. Bedrossian, and I. M. Ross, "Flight implementation of shortest-time maneuvers for imaging satellites," *Journal of Guidance, Control, and Dynamics*, Vol. 37, No. 4, 2014, pp. 1069–1079.

[7] J.-F. Cordeau and G. Laporte, "Maximizing the value of an earth observation satellite orbit," *Journal of the Operational Research Society*, Vol. 56, No. 8, 2005, pp. 962–968.

[8] S. M. Krimigis and R. B. Decker, "The Voyagers' Odyssey," *American Scientist*, Vol. 103, No. 4, 2015, p. 284.

[9] G. L. Bennett and E. Skrabek, "Power performance of US space radioisotope thermoelectric generators," *Thermoelectrics, 1996., Fifteenth International Conference on*, IEEE, 1996, pp. 357–372.

[10] "Jet Propulsion Laboratory California Institude of Technology: Voyager Spacecraft, `https://voyager.jpl.nasa.gov/mission/spacecraft/`," Accessed: 2018-1-3.

[11] G. Swinerd, *How Spacecraft Fly: Spaceflight Without Formulae*. Springer Science & Business Media, 2008.

[12] S. Chesi, Q. Gong, and M. Romano, "Aerodynamic Three-Axis Attitude Stabilization of a Spacecraft by Center-of-Mass Shifting," *Journal of Guidance, Control, and Dynamics*, Vol. 40, No. 7, 2017, pp. 1613–1626.

[13] H. J. Sussmann and J. C. Willems, "300 years of optimal control: from the brachystochrone to the maximum principle," *IEEE Control Systems*, Vol. 17, No. 3, 1997, pp. 32–44.

[14] K. D. Bilimoria and B. Wie, "Time-Optimal Three-Axis Reorientation of a Rigid Spacecraft," *Journal of Guidance, Control, and Dynamics*, Vol. 16, No. 3, 1993, pp. 446–452.

[15] F. A. Leve, B. J. Hamilton, and M. A. Peck, *Spacecraft Momentum Control Systems*, Vol. 1010. Springer, 2015.

[16] "Selection of Electric Motors for Aerospace Application," http://llis.nasa.gov/lesson/893, Feb 1999. Lesson Number: 893, Lesson Date: 1999-02-01, Submitting Organization: Marshall Space Flight Center, Accessed: 2016-11-09.

[17] R. Rigger, "On stiction, limit and constraint avoidance for reaction wheel control," *SpaceOps 2010 Conference Delivering on the Dream Hosted by NASA Marshall Space Flight Center and Organized by AIAA*, 2010, p. 1931.

[18] F. L. Markley, R. G. Reynolds, F. X. Liu, and K. L. Lebsock, "Maximum torque and momentum envelopes for reaction-wheel arrays," *Journal of Guidance, Control and Dynamics*, Vol. 33, No. 5, 2010, pp. 1606–1614.

[19] C. D. Brown, *Elements of spacecraft design*. Aiaa, 2002.

[20] I. M. Ross and M. Karpenko, "A Review of Pseudospectral Optimal Control: from Theory to Flight," *Annual Reviews in Control*, Vol. 36, No. 2, 2012, pp. 182–197.

[21] B. Wie and P. M. Barba, "Quaternion Feedback for Spacecraft Large Angle Maneuvers," *Journal of Guidance, Control, and Dynamics*, Vol. 8, No. 3, 1985, pp. 360–365.

[22] B. Wie, H. Weiss, and A. Arapostathis, "Quarternion feedback regulator for spacecraft eigenaxis rotations," Vol. 12, 1989, pp. 375–380.

[23] B. Wie and J. Lu, "Feedback Control Logic for Spacecraft Eigenaxis Rotations Under Slew Rate and Control Constraints," *Journal of Guidance, Control, and Dynamics*, Vol. 18, No. 6, 1995, pp. 1372–1379.

[24] R. Blenden and H. Schaub, "Regenerative Power-Optimal Reaction Wheel Attitude Control," *Journal of Guidance, Control, and Dynamics*, Vol. 35, No. 4, 2012, pp. 1208–1217.

[25] B. Wie, *Space Vehicle Dynamics and Control*. AIAA Education Series, AIAA, Reston, VA., Second ed., 2008.

[26] N. Bedrossian, S. Bhatt, M. Lammers, L. Nguyen, and Y. Zhang, "First Ever Flight Demonstration of Zero Propellant Maneuver Attitude Control Concept," *AIAA Guidance, Navigation and Control Conference and Exhibit*, 2007, p. 6734.

[27] N. S. Bedrossian, S. Bhatt, W. Kang, and I. M. Ross, "Zero–propellant Maneuver Guidance," *IEEE Control Systems Magzine*, Vol. 29, No. 5, 2009, pp. 53–73.

[28] W. Kang and N. Bedrossian, "Pseudospectral Optimal Control Theory Makes Debut Flight — Saves NASA $1M in Under 3 hrs," *SIAM news*, Vol. 40, No. 7, 2007.

[29] S. Bhatt, N. S. Bedrossian, Longacre, and L. Nguyen, "Optimal Propellant Maneuver Flight Demonstration on ISS," *AIAA Guidance, Navigation and Control Conference*, No. AIAA 2013-5027, Boston, MA, Aug 19-22 2013.

[30] I. M. Ross, "A Historical Introduction to the Convector Mapping Principle," *Proceedings of Astrodynamics Specialists Conference*, Monterey, CA, 2005.

[31] Q. Gong, I. M. Ross, W. Kang, and F. Fahroo, "Connections between the covector mapping theorem and convergence of pseudospectral methods for optimal control," *Computational Optimization and Applications*, Vol. 41, No. 3, 2008, pp. 307–335.

[32] Q. Gong, I. M. Ross, and F. Fahroo, "Costate computation by a Chebyshev pseudospectral method," *Journal of Guidance, Control, and Dynamics*, Vol. 33, No. 2, 2010, pp. 623–628.

[33] A. V. Rao, "A survey of numerical methods for optimal control," *Advances in the Astronautical Sciences*, Vol. 135, No. 1, 2009, pp. 497–528.

[34] M. Karpenko and R. J. Proulx, "Experimental Implementation of Riemann–Stieltjes Optimal Control for Agile Imaging Satellites," *Journal of Guidance, Control, and Dynamics*, Vol. 39, No. 1, 2015, pp. 144–150.

[35] H. Schaub and V. J. Lappas, "Redundant Reaction Wheel Torque Distribution Yielding Instantaneous L2 Power-Optimal Spacecraft Attitude Control," *Journal of Guidance, Control, and Dynamics*, Vol. 32, No. 4, 2009, pp. 1269–1276.

[36] F. L. Markley, "Attitude Estimation or Quaternion Estimation?," *Journal of Astronautical Sciences*, Vol. 52, No. 1, 2004, pp. 221–238.

[37] B. Palais, R. Palais, and S. Rodi, "A Disorienting Look at Euler's Theorem on the Axis of a Rotation," *American Mathematical Monthly*, Vol. 116, No. 10, 2009, pp. 892–909.

[38] J. Sola, "Quaternion kinematics for the error-state Kalman filter," *arXiv preprint arXiv:1711.02508*, 2017.

[39] F. L. Markley and J. L. Crassidis, *Fundamentals of spacecraft attitude determination and control*, Vol. 33. Springer, 2014.

[40] W. Casaday, *Reaction wheel with brushless DC motor drive.* NASA CR – 388, 1966.

[41] R. Fulcher, "A brushless dc torquer-driven reaction wheel for spacecraft attitude control," NASA TN – D-5265, 1969.

[42] M. Yoong, Y. Gan, G. Gan, C. Leong, Z. Phuan, B. Cheah, and K. Chew, "Studies of Regenerative Braking in Electric Vehicle," *Sustainable Utilization and Development in Engineering and Technology (STUDENT), 2010 IEEE Conference on*, IEEE, 2010, pp. 40–45.

[43] X. Nian, F. Peng, and H. Zhang, "Regenerative Braking System of Electric Vehicle Driven by Brushless DC Motor," *IEEE Transactions on Industrial Electronics*, Vol. 61, No. 10, 2014, pp. 5798–5808.

[44] M. Karpenko, C. J. Dennehy, H. C. Marsh, and Q. Gong, "Minimum Power Slews and the James Webb Space Telescope," *27th AAS/AIAA Space Flight Mechanics Meeting*, No. AAS 17-285, San Antonio, TX, February 5 to February 9 2017.

[45] S. L. Scrivener and R. C. Thompson, "Survey of time-optimal attitude maneuvers," *Journal of Guidance, Control, and Dynamics*, Vol. 17, No. 2, 1994, pp. 225–233.

[46] H. Shen and P. Tsiotras, "Time-optimal control of axisymmetric rigid spacecraft using two controls," *Journal of Guidance, Control, and Dynamics*, Vol. 22, No. 5, 1999, pp. 682–694.

[47] R. Proulx and I. Ross, "Time-optimal reorientation of asymmetric rigid bodies," *Advances in the Astronautical Sciences*, Vol. 109, 2001, pp. 1207–1227.

[48] A. Fleming, "Real-time optimal slew maneuver design and control," Master's thesis, Monterey, California. Naval Postgraduate School, December 2004.

[49] A. Fleming, P. Sekhavat, and I. M. Ross, "Minimum-Time Reorientation of a Rigid Body," *Journal of Guidance, Control, and Dynamics*, Vol. 33, No. 1, 2010, pp. 160–170.

[50] A. Fleming and I. M. Ross, "Singularity-free optimal steering of control moment gyros," *Advances in the Astronautical Sciences*, Vol. 123, 2006, pp. 2681–2700.

[51] A. Fleming and I. M. Ross, "Optimal control of spinning axisymmetric spacecraft: A pseudospectral approach," *AIAA Guidance, Navigation and Control Conference and Exhibit*, No. AIAA 2008-7164, Honolulu, Hawaii, August 18 to 21 2008, 2008.

[52] A. Fleming, P. Sekhavat, and I. Michael Ross, "Constrained, minimum-time maneuvers for CMG actuated spacecraft," *Advances in the Astronautical Sciences*, Vol. 135, No. 2, 2009, pp. 1009–1027.

[53] D. Dueri, F. Leve, and B. Açıkmeşe, "Minimum error dissipative power reduction control allocation via lexicographic convex optimization for momentum control systems," *IEEE Transactions on Control Systems Technology*, Vol. 24, No. 2, 2016, pp. 678–686.

[54] W. R. Wehrend, "Minimum Energy Reaction Wheel Control for a Satellite Scanning a Small Celestial Area," NASA TN D-392, 1967.

[55] S. Skaar and L. Kraige, "Single-Axis Spacecraft Attitude Maneuvers Using an Optimal Reaction Wheel Power Criterion," *Journal of Guidance, Control, and Dynamics*, Vol. 5, No. 5, 1982, pp. 543–544.

[56] S. Skaar and L. Kraige, "Large-Angle Spacecraft Attitude Maneuvers Using an Optimal Reaction Wheel Power Criterion," *Journal of the Astronautical Sciences*, Vol. 32, No. 1, 1984, pp. 47–61.

[57] H. C. Marsh, M. Karpenko, and Q. Gong, "Energy Constrained Shortest-Time Maneuvers For Reaction Wheel Satellites," *AIAA/AAS Astrodynamics Specialist Conference*, No. AIAA 2016-5579, Long Beach, CA, September 2016.

[58] I. M. Ross, *A Primer on Pontryagin's Principle in Optimal Control, second edition.* Collegiate Publishers, San Francisco, CA, 2015.

[59] Q. Gong, I. M. Ross, W. Kang, and F. Fahroo, "Connections between the covector mapping theorem and convergence of pseudospectral methods for optimal control," *Computational Optimization and Applications*, Vol. 41, No. 3, 2008, pp. 307–335.

[60] M. Grassi and M. Pastena, "Minimum power optimum control of microsatellite attitude dynamics," *Journal of Guidance, Control, and Dynamics*, Vol. 23, No. 5, 2000, pp. 798–804.

[61] I. M. Ross, R. J. Proulx, M. Karpenko, and Q. Gong, "Relationships Between Maneuver Time and Energy for Reaction Wheel Attitude Control," *Journal of Guidance, Control, and Dynamics*, Vol. 41, No. 2, 2018, pp. 335–348.

[62] Q. Gong, W. Kang, and I. M. Ross, "A Pseudospectral Method for the Optimal Control of Constrained Feedback Linearizable Systems," *IEEE Transactions on Automatic Control*, Vol. 51, No. 7, 2006, pp. 1115–1129.

[63] I. M. Ross, "Space Trajectory Optimization and L1-Optimal Control Problems," *Modern Astrodynamics, edited by P. Gurfil, Elsevier, St. Louis, MO*, 2006, pp. 155–188, Chapter 6.

[64] J. T. Betts, *Practical methods for optimal control and estimation using nonlinear programming*. SIAM, 2010.

[65] M. Athans, "On Optimal Linear Control Systems Which Minimize the Time Integral of the Absolute Value of the Control Function (Minimum-Fuel Control)," 1962, MIT Lincoln Laboratory, Report 22G-4, Lexington, Mass.

[66] O. Hájek, "L1-optimization in linear systems with bounded controls," *Journal of Optimization Theory and Applications*, Vol. 29, No. 3, 1979, pp. 409–436.

[67] G. Vossen and H. Maurer, "On L1-minimization in optimal control and applications to robotics," *Optimal Control Applications and Methods*, Vol. 27, No. 6, 2006, pp. 301–321.

[68] N. Dennehy, "Spacecraft Hybrid Control at NASA: A Look Back, Current Initiatives, and Some Future Considerations," *Proceedings of the 37th Annual AAS Guidance and Control Conference*, No. AAS paper: AAS-14-101., Breckenridge, CO, January 31 – February 5, 2014 2015.

[69] A. Y. Lee and E. K. Wang, "In-Flight Performance of Cassini Reaction Wheel Bearing Drag in 1997âĂŞ2013," *Journal of Spacecraft and Rockets*, Vol. 52, Jan. 2015, pp. 470–480, 10.2514/1.A33047.

[70] D. J. Sahnow, H. W. Moos, S. D. Friedman, W. P. Blair, S. J. Conard, J. W. Kruk, E. M. Murphy, W. R. Oegerle, and T. B. Ake III, "Far Ultraviolet Spectroscopic Explorer: one year in orbit," *International Symposium on Optical Science and Technology*, International Society for Optics and Photonics, 2000, pp. 131–136.

[71] L. E. Bell, "Cooling, heating, generating power, and recovering waste heat with thermoelectric systems," *Science*, Vol. 321, No. 5895, 2008, pp. 1457–1461.

[72] A. Witze, "Desperately Seeking Plutonium," *Nature*, Vol. 515, No. 7528, 2014, p. 484.

[73] W. H. Larson and J. L. Wertz, *Space Mission Analysis and Design, 3rd ed.* Portland, OR: Microcosm Press, 1999.

[74] P. Tsiotras, H. Shen, and C. Hall, "Satellite Attitude Control and Power Tracking with Energy/Momentum Wheels," *Journal of Guidance, Control, and Dynamics*, Vol. 24, Jan. 2001, pp. 23–34, 10.2514/2.4705.

[75] D. A. Dueri, B. A. Acikmese, and F. A. Leve, "Reaction wheel dissipative power reduction control allocation via lexicographic optimization," *AIAA/AAS Astrodynamics Specialist Conference, AIAA SPACE Forum*, 2014.